Copyright Warning & Restrictions

The copyright law of the United States (Title 17, United States Code) governs the making of photocopies or other reproductions of copyrighted material.

Under certain conditions specified in the law, libraries and archives are authorized to furnish a photocopy or other reproduction. One of these specified conditions is that the photocopy or reproduction is not to be "used for any purpose other than private study, scholarship, or research." If a, user makes a request for, or later uses, a photocopy or reproduction for purposes in excess of "fair use" that user may be liable for copyright infringement,

This institution reserves the right to refuse to accept a copying order if, in its judgment, fulfillment of the order would involve violation of copyright law.

Please Note: The author retains the copyright while the New Jersey Institute of Technology reserves the right to distribute this thesis or dissertation

Printing note: If you do not wish to print this page, then select "Pages from: first page # to: last page #" on the print dialog screen

ABSTRACT

DEAGGLOMERATION AND MIXING VIA THE RAPID EXPANSION OF HIGH PRESSURE AND SUPERCRITICAL SUSPENSIONS

by
Daniel To

Nano-materials are the focus of many research activities due to the desirable properties imparted from their small grain size and high interfacial surface area. However, these materials are highly cohesive powders in the dry state and typically form large agglomerates, leading to a diminished surface area or even grain growth, which minimizes the effectiveness of these nanomaterials. This dissertation addresses the issue of mixing nanopowders constituents by deagglomerating them and achieving simultaneous mixing so that even after inevitable reagglomeration, the effectiveness of large interfacial surface area may be preserved.

Nano-particle mixtures were prepared using the environmentally benign dry mixing methods of Stirring in Supercritical Fluids and the Rapid Expansion of High Pressure and Supercritical Suspensions (REHPS). Stirring in Supercritical Fluids was capable of producing course scale nano-particle mixtures that were comparable to mixtures produced with more traditional liquid solvents, without the necessity of filtration and caking issues that are typically associated with them. The REHPS process was capable of producing high-quality mixtures on the sub-micron scale, and was made far superior when the nano-powders were first pre-mixed by stirring to decrease inhomogeneity of the feed. It was also shown that in general, conditions that enhanced turbulent shear stress, and thereby deagglomeration, also enhanced mixing, however this effect could be obscured by inhomogeneities introduced by the feed mixtures.

Previous authors have suggested that the primary deagglomeration mechanism is the explosive expansion of the carbon dioxide from within the agglomerate as it transitions from a high pressure to an ambient environment. In this study two other deagglomeration mechanisms were proposed, namely intense turbulent shear stress imparted by the fluid in the nozzle and impaction with the Mach disc near the exit of the nozzle. Explosive expansion was observed to have almost no effect on nozzle deagglomeration and subsequent mixing. It has been shown that the turbulent shear stress and the residence time under shear were the dominant factors related to agglomerate breakage, while impaction with the Mach disc has played a minimal role.

DEAGGLOMERATION AND MIXING VIA THE RAPID EXPANSION OF HIGH PRESSURE AND SUPERCRITICAL SUSPENSIONS

by
Daniel To

A Dissertation
Submitted to the Faculty of
New Jersey Institute of Technology
in Partial Fulfillment of the Requirement for the Degree of
Doctor of Philosophy in Chemical Engineering

Department of Chemical, Pharmaceutical and Biological Engineering

May 2011

APPROVAL PAGE

DEAGGLOMERATION AND MIXING VIA THE RAPID EXPANSION OF HIGH PRESSURE AND SUPERCRITICAL SUSPENSIONS

Daniel To

Dr. Rajesh N. Davé, Dissertation Advisor — Date
Distinguished Professor of Chemical, Pharmaceutical and Biological Engineering, NJIT

Dr. Ecevit Bilgili — Date
Assistant Professor of Chemical, Pharmaceutical and Biological Engineering, NJIT

Dr. Boris Khusid — Date
Professor of Chemical, Pharmaceutical and Biological Engineering, NJIT

Dr. Norman Loney — Date
Professor of Chemical, Pharmaceutical and Biological Engineering, NJIT

Dr. Sankaran Sundaresan — Date
Professor of Chemical, Engineering, Princeton University, NJ

BIOGRAPHICAL SKETCH

Author: Daniel To

Degree: Doctor of Philosophy

Date: May 2011

Undergraduate and Graduate Education:

- Doctor of Philosophy in Chemical Engineering,
  New Jersey Institute of Technology, Newark, NJ, 2011
- Master of Engineering in Chemical Engineering,
  Cooper Union: For the Advancement of Science and Art, New York, NY, 2006
- Bachelor of Engineering in Chemical Engineering,
  Cooper Union: For the Advancement of Science and Art, New York, NY, 2004

Major: Chemical, Pharmaceutical and Biological Engineering

Accepted Publications:

To D, Sundaresan S, Davé R. Nano-particle Mixing via Rapid Expansion of Supercritical or High-Pressure Suspensions. Journal of Nanoparticle Research. 2011. In Press

To D, Yin X, Sundaresan S, Davé R. Deagglomeration of Nano-particle Aggregates via Rapid Expansion of Supercritical or High-Pressure Suspensions. AIChE Journal. 2009;55:2807-2826

Submitted Publications:

Han X, Ghoroi C, To D, Chen Y, Davé R. Simultaneous micronization and surface modification for improvement of flow and dissolution of drug particles. International Journal of Pharmaceutics. Under Review

Presentations:

To D, Dalvi S, Sundaresan S, Davé R. Deagglomeration and Mixing of Nanopowders Using RESS Based Methods. AICHE 2009 Annual Meeting. Nashville, TN, November 10, 2009.

Han X, To D, Davé R, Steigerwald S, Foster G. Dispersion of Surface Modified Powders for Inhalation Application. AICHE 2009 Annual Meeting. Nashville, TN, November 10, 2009

To D, Yin X, Sundaresan S, Davé R. Methods for Submicron Deagglomeration and Mixing. Asian Particle Technology Symposium 2009. New Delhi, India, September 14, 2009

To D, Davli S, Ermoline A, Pancyzk M, Capece M, Davé R, Yin X, Sundaresan S. Characterization of Mixing and Deagglomeration Using RESS Based Methods. NSF CMMI Engineering Research and Innovation Conference 2009 at Honolulu, HI, June 22, 2009

To D, Dalvi S, Davé R, Sundaresan S. Formation of Mullite by Rapid expansion of High Pressure Suspension of Alumina and Silica in Supercritical CO2. AIChE 2008 Annual Meeting, November 20, 2008

Scicolone J, To D, Ermoliné A, Yin X, Sundaresan S, Davé R. Environmentally Benign Deagglomeration and Mixing of Nanoparticles. NJIT Provost Graduate Student Research Day 2008. April 9, 2008

To D, Ermoliné A, Davé R, Yin X, Sundaresan S. Deagglomeration of Nanparticle Agglomerates by Rapid Expansion of Supercritical Carbon Dioxide through a Nozzle. AIChE 2007 Annual Meeting. Salt Lake City Utah, November 8, 2007

Davé R, To D, Scicolone J, Pfeffer R. Deagglomeration and Mixing of Nanoparticles. AIChE 2006 Annual Meeting. San Francisco, Ca, November 13, 2006

To my parents, thank you for carrying me all this way.

To the Llama, you were right, you always were. I know that now.

ACKNOWLEDGMENT

I would like to acknowledge the mentorship I have received from my advisor Dr. Rajesh Davé and my committee, Dr. Ecevit Bilgili, Dr. Boris Khusid, Dr. Norman Loney and Dr. Sankaran Sundaresan. Through their teachings I have been able to understand the true definition of scientific research. And through the example of such scientists as Dr. Sameer Dalvi and Dr. Chinmay Ghoroi I have learned what it takes to be one and what I myself am capable of. I would also like to thank James Scicolone, Maxx Capece, Xi Han and the rest of our group for helping me along the way.

I would also like to acknowledge the National Science Foundation who funded this research through a NIRT grant, DMI-0506722, and financial support through an IGERT fellowship via DGE-0504497.

TABLE OF CONTENTS

TABLE OF CONTENTS
(Continued)

TABLE OF CONTENTS
(Continued)

TABLE OF CONTENTS
(Continued)

Chapter **Page**

LIST OF TABLES

LIST OF TABLES
(Continued)

LIST OF FIGURES

LIST OF FIGURES
(Continued)

LIST OF FIGURES
(Continued)

Figure **Page**

LIST OF FIGURES
(Continued)

LIST OF FIGURES
(Continued)

LIST OF SYMBOLS

A	Nozzle cross-sectional area (m^2)
D_{a1}	Measured diameter (m)
D_{a2}	Corrected aerodynamic diameter (m)
D_f	Fractal dimension
D_{Nozzle}	Nozzle diameter (m)
IOS	Intensity of Segregation
L_{Agg}	Characteristic agglomerate length (m)
L_e	Length scale of the most energetic eddies (m)
L_p	Primary particle size (m)
N	# of particles in an agglomerate
P	Pressure (Pa)
R(r)	Auto correlation function
R_1	APS correlation 1
R_2	APS correlation 2
Re	Reynold's number
R_g	Radius of gyration of an agglomerate
SOS	Scale of Segregation (m)
V	Velocity (m/s)
Δd_i	Diameter window used in agglomerate size data (m)
d_i	Diameter listed in size distribution info (m)

LIST OF SYMBOLS
(Continued)

k	Power law prefactor
f	Fanning friction factor
h	Enthalpy (J/kg)
i	Summation index
n,i	Number of occurrences
r	Distance between sites used in R(r)
t	Time (s)
v,i	Volume of agglomerates (m^3)
w	Heat flux through the nozzle wall (J/m^2-s)
x	Axial length along the nozzle (m)
$\dot{m}$	Mass flowrate (kg/s)
$\chi_{n,i}$	Relative number frequency
$\chi_{v,i}$	Relative volume frequency
ε	Energy dissipation rate (m^2/s^2)
μ	Viscosity (Pa-s)
μ_A	Mean relative concentration of alumina
μ_S	Mean relative concentration of silica
ν	Kinematic viscosity (m^2/s)
ρ_{agg}	Agglomerate density (kg/m^3)
ρ_{true}	True material density (kg/m^3)
ρ_f	Density of the fluid (kg/m^3)

LIST OF SYMBOLS
(Continued)

σ^2	Relative concentration variance
τ_t	Shear stress (Pa)
τ_e	Elongation stress (Pa)
ζ	Length scale larger than when a mixture is random (m)
$\bar{\tau}$	Time-averaged shear stress (Pa)

CHAPTER 1

INTRODUCTION

1.1 Motivation

Nanoparticles and nanocomposite materials have many unique properties owing to their small particle/grain size and large contact area between the nano-sized constituents[1-3]. A major challenge in making and handling such materials is the tendency of the nanoparticles to aggregate due to van der Waal forces and form large fractal structures tens or hundreds of microns in size[4-8]. Composite materials made by simply mixing agglomerates of the constituent nanoparticles will invariably have much smaller contact area between constituents than is theoretically possible and will therefore lack the potential advantages that nanocomposites can offer. The full potential of a nanocomposite material can only be achieved when the constituent nanoparticles are properly dispersed and mixed – preferably at a nano-scale – and the agglomeration between particles is well controlled. Unfortunately, conventional methods for powder mixing tend to be homogeneous only above the scale of tens of microns because they fail to break the primary aggregates[9-12]. Therefore there is a need for innovative approaches to achieve efficient nano-scale deagglomeration and mixing[13-17], as well as elucidation of the various deagglomeration mechanisms.

In addition to mixing, deagglomeration of nanopowders can also be desirable in other contexts such as controlling the light scattering efficiency[18], the suspension viscosity[19, 20], and the bulk density of materials[21-23]. For example, several researchers have found that reducing agglomerate size led to an increase in the relative density (ratio of compact

bulk density to the true density) of dry powder compacts, which upon sintering led to improved bulk properties and product uniformity[19-21].

1.2 Objective

The Rapid Expansion of High Pressure and Supercritical Suspensions (REHPS) has previously been shown to produce high quality mixtures on the sub-micron scale via an environmentally benign method, however little was understood about the deagglomeration efficiency or mechanisms resulting from this process[14-17]. In the REHPS process, *insoluble* nanopowders are stirred and then expanded through a fine capillary nozzle. It was concluded in previous studies[16, 17] that a high degree of mixing occurred due to the rapid expansion of the suspension and not because of simply stirring in supercritical carbon dioxide prior to the expansion. These mixing experiments offer indirect proof that effective deagglomeration of the original agglomerates has taken place in the REHPS process. The objective of this study is to demonstrate that the REHPS process is an effective means of both deagglomeration and mixing as well as developing methods of characterization that can accurately discern the deagglomeration mechanism.

1.3 Background

1.3.1 Nano-materials

Nano-sized materials have become of significant importance due to the high percentage of surface molecules resulting from their small grain size. This leads to a high interfacial surface area and therefore increased solid state interactions such as reactions[21, 24], increased solubility rates[25, 26] and increased effective diffusion rates[27-29]. In addition,

the individual domains on the nano-scale often have different properties from the bulk material.

These properties have offered significant benefits to a variety of applications. One such application is the production of nano-composite materials by mixing two or more constituents together on the nano-scale where the individual constituents are used to reinforce each other and produce enhanced bulk materials[30, 31]. This is often the only path available when two constituents cannot be produced simultaneously in a mixed state, and the composites need to be prepared by mixing two or more nanopowders (i.e. powders composed entirely of nanoparticles) together and then pressing and sintering the resulting mixture to ensure high densities and material continuity. The major difficulty in utilizing this approach, however, is that the individual nano-constituents tend to cluster together, due to inter-particulate cohesion, to form aggregates and agglomerates, which may be 100's or 1000's of times larger than the individual particles[5, 32-34]. This decreases the available surface area and ultimately limits the interaction between the constituents, resulting in low quality composites[24, 35]. For further discussion on the importance of achieving high quality mixtures and the associated problems may be found in a recent paper[35].

1.3.2 Agglomeration of Nanoparticles

The nano-particle agglomerates are typically formed through a diffusion limited process and their structure is commonly represented by a power law model[4]. Such agglomerates assume self-similarity seen in fractal patterns, where the growth of the mass or the number of particles in an agglomerate, N, with respect to its radius of gyration, R_g, is defined by the fractal dimension, D_f, as shown by equation 1.1, where k is a prefactor

(defined as the ratio of agglomerate to primary particle diameter) and *a* is the radius of the primary particle [5, 36, 37]. The fractal dimension ranges from 1 – 3 and as equation (1.1) shows, a slight increase in its value can result in a significant increase in the number of particles in the agglomerate with the same radius of gyration. This could lead to highly variable porosities and intra-agglomerate particle contacts depending on the fractal dimension.

$$N = k\left(\frac{R_g}{a}\right)^{D_f} \tag{1.1}$$

1.3.3 Deagglomeration

Nanoparticle agglomerates are commonly broken down and dispersed using a variety of wet methods that use either high shear or ultrasonic cavitation, in conjunction with organic solvents, surfactant or pH modifiers[19, 20, 38-41]. High-shear devices employ viscous drag and the high energy dissipation rates during formation in turbulent flow to break nanoparticle agglomerates. Examples include high-pressure homogenization (throttling a liquid suspension through a fine capillary nozzle) or high-speed/high-shear stirring. Using a motionless high-pressure homogenizer for individual suspensions of zirconia (12 nm), silica (7, 12, 20, 30 nm) and titania (21 nm) in an ethylene glycol aqueous solution, Seekkuarchchi et al.[19] showed that nanoparticle agglomerates could be broken down below 100 nm. Ultrasonic devices, on the other hand, focus acoustic energy to very small length scales to produce cavitation, micro-jets and large pressure gradients[38] to facilitate deagglomeration[20]. Although wet methods are effective means to produce stable suspensions of mixed and deagglomerated nanopowders, they require the use of organic (or aqueous) solvents, surfactants, or other interfacial agents;

furthermore, producing dry powder from suspensions is often a slow and energy-intensive process in which many difficult issues may arise, such as density based stratification, electrostatic separations and caking during drying. Therefore, there is a need for simpler approaches for deagglomeration and mixing of nanopowders that minimize the use of environmentally hazardous solvents, surface agents, and suspensions.

Deagglomeration of cohesive powders via rapid depressurization has been the subject of several other investigations[28, 29, 42, 43]. These studies have generally looked at the deagglomeration of particles whose size is in the range of 1-50 μm. Weimer, et al.[29] showed that the conversion of 15μm Al particles to AlN reached almost 90% when the particles were completely deagglomerated, as opposed to 49% when the particles were in the form of aggregates. Kobayashi[28] showed that the equivalent diffusion coefficient of SO_2 to agglomerated limestone powders, generally a size independent parameter, increased with increasing limestone agglomerate sizes due to the inability of SO_2 in penetrating the aggregate structure. Kousaka et al. performed limited studies to show that rapid depressurization was indeed capable of dispersion sub-micron particles[44], however only low gas pressures and sub-sonic expansion velocities were considered.

The Rapid Expansion of High Pressure and Supercritical Suspensions (REHPS) process is similar in principle to high pressure homogenization, with the one major deviation being that a gaseous or supercritical medium is utilized, which results in drastically different experimental practices. In both methods a suspending fluid carry nano-particle agglomerates is throttled through a fine capillary nozzle on the order of 100 μm. The utilization of high pressure/supercritical CO_2 takes advantage of its liquid-like densities and the gas-like viscosities in the homogenization process. The 3 major benefits

of the gaseous or supercritical mediums are (1) pressures lower than 100 bar are commonly used in the REHPS process, while pressures >> 500 bar are generally used in high pressure liquid homogenization; (2) at the exit of the nozzle a shockwave forms, which is a pressure, density and velocity discontinuity; (3) the powder can be collected from aerosol or if a mixture, a high quality mixture can be directly collected without the potential for drying based segregation.

In REHPS, the high shear stress in the nozzle can cause deagglomeration; furthermore, passing through the Mach disc in the freely expanding jet, if formed, can be another means for agglomerate breakup. Brandt et al.[45] investigated the effect of shock waves on deagglomeration of nano-powder agglomerates in a shock-tube filled with argon. Two types of nanopowders, Degussa Aerosil OX50 and Aerosil TT600 (both silica powders, d_p = 40 nm, but with different bonding surface energy levels), were studied and the agglomerate sizes were measured by in-situ laser scattering. It was observed that as the agglomerates passed through the shock, their (count mean) diameters were reduced to about 200 nm for OX50 and about 400 nm for TT600.

It has also been shown by many authors that the scale of deagglomeration can be correlated to the high energy dissipation rates during eddy formation in highly turbulent liquid flow[46-48]. For example the hydrodynamic conditions in the homogenizer are characterized by the value of ε, which is a key parameter in the theoretical models of the emulsification process in turbulent flow[49]. It therefore makes sense that this could be very important for the REHPS process as well. The eddies commonly range in size from the scale of the pipe diameter to the Kolmogorov length scale. Generally however, the eddies on the extreme edges of the spectrum have significantly lower local dissipative

energy than the maximum energy eddies and will therefore not break agglomerates as readily. The maximum energy eddy length scale is generally 1 – 2 orders of magnitude larger than the Kolmogorov scale (the length scale where viscous forces dominate)[50] and will coincide with a length scale where deagglomeration is likely to occur. The size of the maximum energy eddy in pipe flow is described by equation 1.2[51].

$$L_e = 0.05 D_{nozzle} \, \mathrm{Re}^{-1/8} \tag{1.2}$$

While there has been significant effort devoted to understanding the agglomerate break up mechanisms in turbulent liquid flows, little has been devoted to systems, such as one studied in the REHPS process, as they do not form stable suspensions and can therefore be difficult to analyze. It is expected that analysis of mixing followed by deagglomeration can offer some insights into the effectiveness of the deagglomeration process.

1.3.4 Mixing

A major obstacle in effectively mixing nanopowders is that cohesive forces (van der Waals and electrostatic attractions) dominate over the individual primary particle's own inertial forces so that the particles would rather form large hierarchical assemblies or agglomerates with fractal structures than follow their own inertia. As previously mentioned, these assemblies can be several orders of magnitude larger than the original particle. Conventional dry powder mixing methods are unable to mix nanopowders below the agglomerate scale due to the inability to break up the agglomerate structure, which results in mixture qualities being limited to the scale of the agglomerate. This is especially true for materials like carbon nanotubes as the high aspect ratio results in a

higher number of inter-particle contacts per individual nanotube. While, there are various wet methods currently available to mix nanopowders on the sub-agglomerate scale, which include ultrasonication, high shear stirring and high pressure homogenization, however these methods may suffer the same difficulties previously mentioned, including the use of potentially hazardous solvents and surface modifiers as well as the segregation and caking during the drying process.

In recent years, a variety of methods have been developed using different mechanisms to promote nanopowder mixing[17, 32, 35, 52, 53] including: Magnetically Assisted Impact Mixing (MAIM) [53], Ultrasonication in Supercritical Fluids [52], the Rapid Expansion of High Pressure and Supercritical Suspensions [17, 32, 35]. The present study focuses on the use of Rapid Expansion of High Pressure and Supercritical Suspensions (REHPS), where nanopowders suspended in high pressure and supercritical carbon dioxide are expanded through a fine capillary nozzle. This method is based on the RESS (Rapid Expansion of Supercritical Solutions) process which is known for particle formation during the expansion process due to the rapid changes in CO_2 properties. Similarly, the REHPS process takes advantage of the high density and viscosity at pre-expansion conditions, and the rapid change in properties during expansion to simultaneously deagglomerate and mix the nanopowders.

1.3.5 REHPS: RESS-based Mixing and Deagglomeration

The Rapid Expansion of High Pressure or Supercritical Suspension (REHPS) is a process of simultaneous deagglomeration and mixing which can achieve high quality mixtures on the sub-micron scale. It is a RESS-based mixing method which takes advantage of the liquid-like densities and viscosities of high pressure carbon dioxide, while still retaining

the gas-like diffusivities and velocities. The feasibility of the REHPS process for deagglomeration and mixing of nano-powders has been reported in the literature [16, 17, 35]. Wei et al. presented a single experiment on Rapid Expansion of High Pressure and Supercritical Suspensions (REHPS) mixing and thus established the proof-of-concept. The authors suggested that primary mechanism of deagglomeration and subsequent mixing was explosive expansion of the carbon dioxide from within the agglomerate as it transitions from a high pressure to an ambient environment. Yang et al. showed that the REHPS process was capable of mixing nano-powders on the sub-micron scale, however only limited experimental conditions were investigated. In those studies [16, 17], constant pressure was not maintained during expansion, allowing the reactor pressure to decrease by nearly 30%. In Yang et al., the mixing quality was characterized by comparing a characteristic elemental ratio at 20 random points from a single loose powder sample via Energy Dispersive X-ray Spectroscopy (EDS), which is limited in scope. In contrast, characterization of the mixing quality in the present study is more rigorous through analyzing the intensity and scale of segregation proposed by Danckwerts [54]. Further, to differentiate between multiple high quality mixtures a more sensitive characterization method has been employed, which involves sampling of 400 random points on the smooth surface of a tableted powder sample with EDS to determine the intensity of segregation [35, 55, 56]. Coarse scale mixtures were characterized by the scale of segregation of EDS based maps on elemental concentration with respect to spatial locations, which is a novel addition to the analysis of nano-powders mixtures.

In this study REHPS deagglomeration and mixing experiments, coupled with modeling, were performed in parallel to elucidate the primary deagglomeration

mechanism. Two possible deagglomeration mechanisms were explored: (1) impaction with a Mach disc that forms at the exit of the nozzle and (2) turbulent shear imparted by the high pressure or supercritical fluids within the nozzle. It will be shown that the intense turbulent shear imparted by the fluid have the most significant effect on the deagglomeration and mixing processes, while impaction with the Mach disc only offered minimal improvement. In general it was shown that by increasing the turbulent shear and the residence time under shear, and therefore enhanced deagglomeration resulted in higher quality mixtures, however this could be convoluted by poor mixing in the feed powder resulting in large scale inhomogeneities resulting from poor axial mixing and subsequently non-simultaneous deagglomeration and mixing.

CHAPTER 2

REHPS DEAGGLOMERATION

2.1 Introduction

In this Chapter, deagglomeration of nanopowders by REHPS is investigated via experiments of the rapid expansion process. The experimental REHPS system, which will be introduced in more detail in the below, closely resembles the well-known RESS (Rapid Expansion of Supercritical Solutions) process used mainly for rapid precipitation of solubles to form very fine powders. The deagglomeration experiments involved two different types of nanoparticle agglomerates (alumina and titania), and were carried out under several different operating conditions. The resulting particle size distributions were characterized using multiple experimental techniques.

In the REHPS process, *insoluble* nanopowders are stirred and then expanded through a fine capillary nozzle. It was concluded in previous studies[16, 17] that a high degree of mixing occurred due to the rapid expansion of the suspension and not because of the simple stirring in supercritical carbon dioxide prior to the expansion, because the stirred mixture was of a rather poor quality. These mixing experiments offer indirect proof that effective deagglomeration of the original agglomerates has taken place in the RESS/REHPS process. In this study, various experimental techniques will be employed to provide direct evidences that REHPS is an effective means for deagglomeration of nanopowders.

2.2 Experimental Apparatus

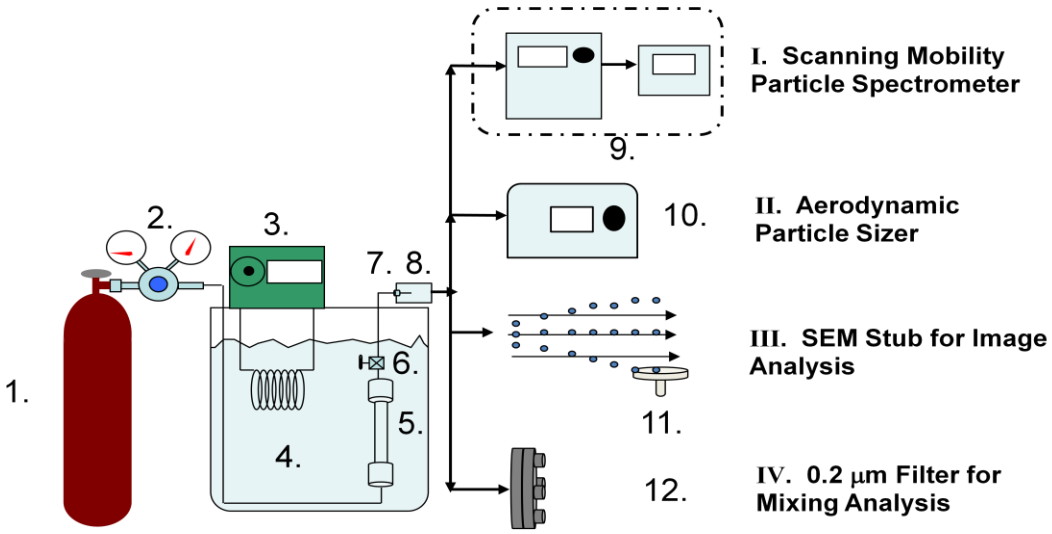

1. CO_2 supply, 2. One-stage reducing regulator, 3. Immersion heater and water bath, 4. Heat exchange coil, 5. High pressure mixing vessle, 6. On/Off valve, 7. Capillary nozzle, 8. Expansion tube, 9. SMPS, 10. APS, 11. SEM stub for image analysis, 12. 0.22 mm nozzle.

Figure 2.1 The schematic for the REHPS apparatus. Part I shows analysis via the SMPS. Part II shows analysis via the APS. Part III shows collection for offline characterization via electron microscopy and image analysis. Part IV shows powder collection for offline mixing analysis via electron microscopy in conjunction with energy dispersive X-ray spectroscopy (EDS).

The deagglomeration experimental apparatus is shown in Figure 2.1 (parts I, II, and III), where 0.1 g of the powder to be deagglomerated alumina Alu C (d_p = 13 nm), silica R972 (d_p = 16nm) or titania P25 (d_p = 21 nm) nanopowders supplied by Evonik Degussa GmbH, was charged into a 24-mL vessel (Figure 2.1 part I, unit 5). The vessel was pressurized with 99.9% pure carbon dioxide (Welco Gas) to the desired operating pressure using a one-stage reducing regulator (unit 2), which ranged from 1.72 to 7.93 MPa. Prior to entering the vessel the CO_2 was passed through a 2 m x 0.762 mm ID stainless steel heat exchange coil (unit 4) submerged in a warm water bath and immersion heater (unit 3) to transition the CO_2 into the gaseous or supercritical region in addition to

regulating the operating temperature. More extreme conditions (i.e. pressures above and 7.93 MPa and temperatures below the supercritical point) were not investigated as carbon dioxide condensation would dominate during the gas expansion, which may lead to unrepresentative size distributions resulting from the precipitation of dry ice[35].

The powders were expanded to the atmosphere through a capillary nozzle (unit 7) to allow for collection from an aerosolized state, which was initiated by turning the On/Off valve (unit 6). The expanded CO_2 stream was then directed into a 26.7 cm (length) expansion tube (unit 8). Expansion tubes of different diameters were used for different upstream pressures to ensure that the linear velocity of the suspension upon exiting the expansion tube was roughly constant (3.2 m/s) to facilitate iso-kinetic sampling for size distribution determination. The inner surface of the expansion tube was coated with vacuum grease to ensure that agglomerates that collide with the tube will mostly be trapped, thus mitigating their interference with the measurements. The aerosol stream was characterized by the SMPS (unit 9) 100 seconds after initiation for three consecutive 60 second windows. The SMPS can be operated in either (A) a non-scanning mode that monitors the concentration of agglomerates of a chosen diameter as a function of time, or (B) a scanning mode that determines the size distribution by scanning over a range of diameters. The data presented here were obtained using the scanning mode. As a scan typically requires 60 seconds, it was necessary to ensure that during this time the concentration of aerosols for each size was roughly constant. Therefore, a number of REHPS experiments were performed employing the non-scanning mode of the SMPS to examine how aerosol concentration changed with time at various chosen diameters. These experiments revealed that concentrations became nearly steady between 90 and

300 seconds after the initiation of the REHPS experiment. Therefore, when the scanning mode of the SMPS was used to determine the size distribution, data was only collected after 100 seconds after initiating the REHPS experiment; three successive measurements were made for each experiment and each of them lasted 60 seconds: 100–160, 160–220 and 220–280 seconds. The experiment was repeated three times, thus generating 9 size distribution data sets for each operating condition. REHPS experiments were also conducted using compressed nitrogen at 1.72 and 7.93 MPa (and alumina nanopowders) to examine the possibility of using other gases for deagglomeration. In those experiments, the SMPS was used and followed similar steps to determine the agglomerate size distributions.

Additionally a scanning electron microscope was used to image the deagglomerated powders, which were collected by diffusion on a silicon substrate placed in the centerline of the aerosol stream, 6 inches away from the nozzle, and oriented parallel to its flow. The parallel orientation of the silicon substrate avoids significant disruption of the aerosol flow, while also preventing agglomerate fragmentation by collision with the silicon substrate. In general approximately 1000 agglomerates were sized by image analysis within the range of 40 to 3,000 nm. For a complete description of the operating procedures of deagglomeration and characterization of nanopowders please refer to To et al.[35]

The SMPS uses the different mobilities of the agglomerates to determine their sizes and determine the size distribution; the SMPS unit is rated to measure particle sizes in the range of 19 to 572.5 nm. The expanded aerosol suspension was drawn into the SMPS at 0.27 L/min through a 60 cm long, 0.64 cm ID hose. The sheath air was set at

2.7 L/min to achieve the optimum sheath flow to aerosol flow ratio of 10 to 1. Two correction algorithms offered by the SMPS were applied to account for potential errors: the Diffusion Loss Correction was applied to account for the loss of agglomerates below 100 nm within the SMPS, and the Multiple Charge Correction prevents under sizing due to the occurrence of multiple charges on agglomerates larger than 100 nm.

The APS is rated to measure particle sizes in the range of 0.5 to 20.0 μm. The aerosol suspension from the expansion chamber was drawn through a hose (0.64 cm ID, 60 cm long) and delivered to the detector at a flowrate of 1 L/min. Additionally, sheath air was drawn in at 4 L/min. Data were also recorded at the same time windows as in the SMPS measurements (100 –160, 160–220 and 220–280 seconds) and the experiments were repeated in triplicate to produce a total of 9 size distribution data sets for each operating condition.

An off-line method based on Scanning Electron Microscopy (SEM) was also used to determine the size of the agglomerates after the expansion, as shown in Figure 2.1 Part III. Samples of agglomerates were collected from the expanded aerosol stream by Brownian diffusion on a smooth silicon chip mounted on a 13 mm aluminum stub. The chip was placed at the centerline of the stream, 6 inches away from the exit of the nozzle, and the surface of the chip was held *parallel* to the direction of the aerosol flow, minimizing its influence on the aerosol stream. This parallel configuration of the collecting surface also reduced the possibility of agglomerate fragmentation due to collisions between the agglomerates and the surface. The SEM images of the agglomerates were analyzed using ImageJ®, where a brightness threshold was set to convert the SEM images into binary images, making the background (chip surface) white

and the foreground (agglomerates) black. The size of the agglomerate (the diameter of a circle enclosing the same projected area as the agglomerate) can then be determined. In general, approximately 1000 agglomerates were sized using this method for each experiment.

2.3 Experimental Results on Deagglomeration

The SMPS, APS and SEM imaging were used to characterize the sizes of the agglomerates after expansion from different mixing chamber pressures. Each experiment was performed in triplicate, with three sets of data per experiment as explained earlier. The nine data sets were averaged to determine size distribution statistics. In this manner, the number- and volume- weighted mode diameters were obtained for each mixing vessel pressure P_0. In what follows, the size distributions are reported as relative number frequency, χ_n, and relative volume frequency, χ_v, as functions of diameter.

$$\chi_{n,i} = n_i / \Sigma_j n_j \qquad \chi_{v,i} = n_i v_i / \Sigma_j n_j v_j \qquad (2.1)$$

Here, n_i and v_i denote the number of occurrences and volume of agglomerates whose diameters lie in the region d_i and $d_i + \Delta d_i$, where Δd_i is the diameter window used to classify the agglomerate size data. It is understood that *diameter* henceforth refers to mobility diameter (SMPS), aerodynamic diameter (APS) or projected area diameter (SEM).

2.3.1 SMPS size analysis

As mentioned earlier, for each experiment, size distribution data was collected over three time windows: 100-160 seconds, 160-220 seconds and 220-280 seconds after initiating

the experiment. Figure 2.2 shows a typical measurement: the three size distributions obtained by the SMPS over the three time windows are very similar, indicating that there is no significant change in the agglomerate size distribution over time from 100 to 280 seconds.

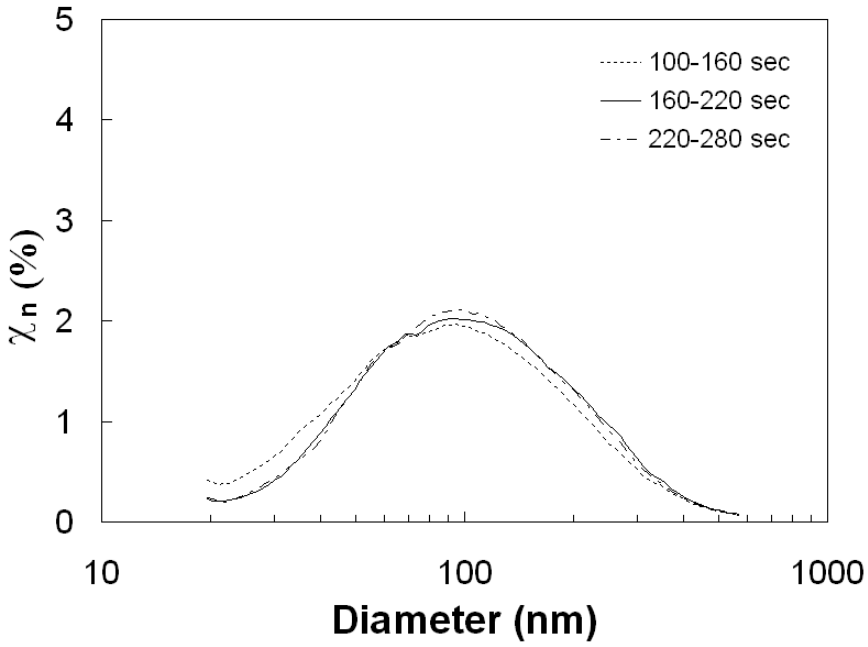

Figure 2.2 A typical measurement of three SMPS size distributions over three consecutive time windows, which show a constant size distribution over the length of the experiment.

Although not shown, similar control experiments were performed where only carbon dioxide was expanded through the nozzle. At the lower mixing vessel pressures of 1.72 to 5.86 MPa, the SMPS did not detect any particles, suggesting that there was neither condensation of CO_2, nor condensation of potential dissolved impurities. At the highest pressure (7.93 MPa), small amount of aerosol particles were detected at times greater than 220 seconds from the initiation of the experiment. These particles, assumed to be dry ice, were at a concentration of about 10^5 counts/cm^3 and a mode size below 25

nm. This concentration is one to two orders of magnitude smaller than the counts obtained in the deagglomeration experiments, indicating that condensation of CO_2, even at the highest pressure of 7.93 MPa, does not interfere significantly with the measurements of agglomerate size distribution.

Table 2.1 Number- and Volume-weighted Mode Mobility Diameters for Alumina, Silica and Titania Nanopowders Expanded Through a 254 μm ID x 10 cm Long Nozzle and Extracted From the SMPS

Pressure (MPa)	Alumina		Silica		Titania	
	Number Weighted (nm)	Volume Weighted (nm)	Number Weighted (nm)	Volume Weighted (nm)	Number Weighted (nm)	Volume Weighted (nm)
1.72	85	532	66	551	79	>572.5
3.79	69	372	132	524	69	346
5.86	91	346	116	501	62	358
7.93	35	346	95	504	37	260

The number- and volume- weighted mode diameters of expanded alumina, silica, and titania measured by the SMPS, listed in Table 2.1, show that the nanopowders were significantly deagglomerated by the REHPS process. Representative number and volume weighted size distributions are shown in Figures A.1 – A.3 in Appendix A. The number-weighted mode diameters were all below 100 nm. The measured size distributions were all very wide (the standard deviations are significant when compared to the mode diameters). For alumina and silica powders, there was no clear trend indicating whether the agglomerate size increased or decreased with pressure at the lower pressures (1.72-

5.86 MPa) in the number weighted mode diameters; for titania powders, the agglomerate size appeared to decrease with increasing pressure, but the dependence was weak. It was only at the highest pressure that a significant reduction in the number-weighted mode diameters was observed. The volume-weighted mode diameters decreased with increasing pressure. However, the fact that some of the volume-weighted mode diameters were close to the SMPS measurement upper limit of 572.5 nm indicated that agglomerates larger than 572.5 nm were likely to be present. The trend observed in the REHPS experiments using nitrogen as the suspending medium was similar: when the pressure decreased from 7.93 to 1.72 MPa, the number-weighted agglomerate size increased from 66 nm to 71 nm, and the volume-weighted agglomerate size increased from 219 nm to 288 nm.

2.3.2 APS size analysis

The APS determined the agglomerate velocity by measuring the time required for it to pass a distance of 90 μm, from which the aerodynamic diameter of the agglomerate was determined. Classically, the aerodynamic diameter should be calculated based on results obtained in a stagnant gas. When determined in the presence of gas flow (outside of the Stoke regime, $N_{Re} > 0.5$) it can be affected by the agglomerate density. The APS uses a recursive algorithm referred to as the Stokes correction[57] to determine the corrected aerodynamic diameter D_{a2} from the measured diameter D_{a1}, the gas density ρ_a, gas viscosity μ, the relative velocity of the agglomerate to the gas flow ($U - \overline{V}$), the true agglomerate density ρ_2 and a calibration standard with a density of ρ_1(1000 kg/m^3):

$$D_{a2} = D_{a1}\left[\frac{6+R_2^{2/3}}{6+R_1^{2/3}}\right]^{1/2}; \qquad R_1 = \frac{\rho_a\left(U-\overline{V}\right)D_{a1}}{\mu\sqrt{\rho_1}}; \qquad R_2 = \frac{\rho_a\left(U-\overline{V}\right)D_{a2}}{\mu\sqrt{\rho_2}} \qquad (2.2)$$

Because of the Stokes correction, the density for the agglomerate affects the estimate of the aerodynamic diameter. This system is further complicated by the fractal nature of the agglomerates, resulting in size-dependent agglomerate density. The fractal pattern, which follows a quasi-power-law equation, relates the number of particles in an agglomerate, *N*, to the ratio of the diameters of the agglomerate and the primary particle, (L_{agg}/L_p):

$$N = k\left[\frac{L_{agg}}{L_p}\right]^{D_f} \qquad (2.3)$$

where *k* is a constant and D_f is the fractal dimension. It then follows that the agglomerate density is given by

$$\rho_{app} \approx \rho_{true}\left[\frac{L_{agg}}{L_p}\right]^{D_f-3} \qquad (2.4)$$

Agglomerates of nanoparticles tend to have fractal dimensions close to 2.5 corresponding to the diffusion-limited aggregation case[4, 5, 34]. Although the fractal dimension is often treated as a constant independent of the agglomerate size, it has been shown that the agglomerates composed of natural kaolinite particles were better represented by a variable fractal dimension[58-60]. Such variable fractal dimension would further complicate the estimate for agglomerate density. As information on the variation of the agglomerate density with agglomerate size is unavailable for these powders, definitive Stokes correction is not possible. Consequently, the influence of different choices for the agglomerate density on the corrected aerodynamic diameter distribution

extracted from the APS data was tested. Figures 2.3a and 2.3b show the number- and volume-weighted distributions obtained in one experiment involving titania powder for various assumed values of the density. Included are the results for true density (4290 kg/m^3), the bulk density of the agglomerate sample as obtained (125 kg/m^3), the density at the mode agglomerate size assuming a fractal dimension of 2.5 (568 kg/m^3) and the density at the mode agglomerate size assuming a fractal dimension of 1.8 (20 kg/m^3).

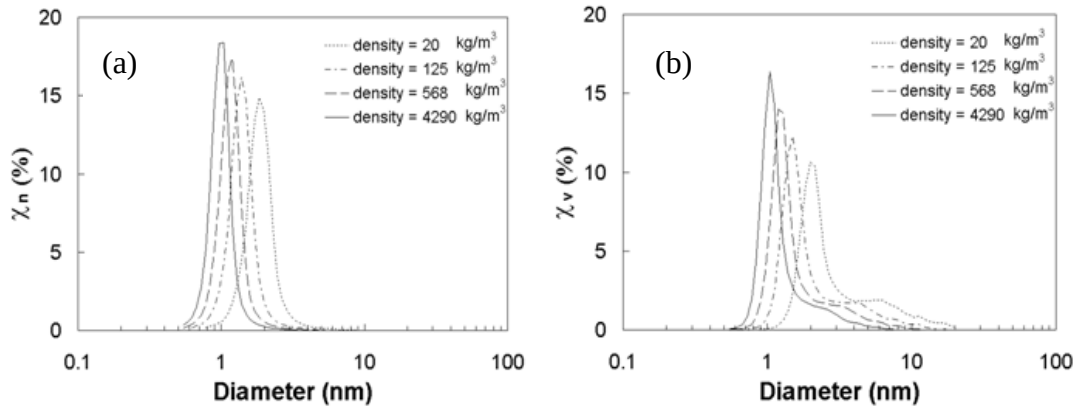

Figure 2.3 (a) Number and (b) volume weighted distributions of titania nanopowders expanded at 5.86 MPa through a 254 μm x 10 cm nozzle; measured by the APS. The Stokes Correction of size with respect to density was used at 4290, 568, 125, 20 kg/m^3.

It is clear from Figures 2.3a-b that the size distributions become wider, with the mode diameter increasing with decreasing agglomerate density. It should be noted that even though the density was varied over two orders of magnitude, the number- and volume-weighted mode diameters were relatively stable: the number-weighted mode diameter varied between 0.97 and 1.84 μm, and the volume-weighted mode diameter varied between 1.04 and 1.98 μm. Thus, the uncertainty in agglomerate density does not affect the typical order of magnitude of APS size measurements. In what follows, it has been

assumed that the agglomerate densities were the same as their respective bulk densities in the APS analysis (125 kg/m^3 for titania, 48 kg/m^3 for alumina and 50 kg/m^3 for silica).

Table 2.2 Number- and Volume-Weighted Mode Aerodynamic Diameters for Alumina, Silica and Titania Nanopowders Expanded Through a 254 μm ID x 10 cm Long Nozzle and Extracted From the APS

Pressure (MPa)	Alumina		Silica		Titania	
	Number Weighted (μm)	Volume Weighted (μm)	Number Weighted (μm)	Volume Weighted (μm)	Number Weighted (μm)	Volume Weighted (μm)
1.72	1.98	1.98	1.34	2.64	1.49	1.60
3.79	1.84	2.13	1.49	1.98	1.49	1.60
5.86	1.98	2.13	1.53	2.01	1.49	1.60
7.93	1.98	2.13	1.47	2.48	1.49	1.60

The number- and volume-weighted mode diameters of the expanded alumina and titania nanopowders, measured by the APS, are listed in Table 2.2. The number- and volume- weighted mode diameters were similar, suggesting that the size distributions were relatively narrow. Indeed, size distributions suggest that the vast majority of the agglomerates had diameters between 1 and 3 μm, which are shown in Figure A.3 in Appendix A.

The agglomerate size data listed in Tables 2.1 and 2.2 are very different – this is expected because SMPS and APS cover different size ranges, with practically no overlap. If the agglomerates entering SMPS/APS had a narrow, unimodal size distribution, then either SMPS or APS would detect a peak, but not both. The fact that both SMPS and APS measurements detected peaks in their respective sizing ranges suggests that: (a) The

size distribution of the agglomerates was wide and not unimodal, and/or (b) reagglomeration might have occurred in the expansion tube and the hose leading to SMPS/APS units, producing large agglomerates that were detected by the APS. It was expected that reagglomeration would not affect the SMPS very much, because the large agglomerates formed by reagglomeration would fall out of the sizing range of the SMPS. Through the mixing experiments, discussed in detail in Chapter 3, it was confirmed that the larger agglomerates detected by the APS indeed came from reagglomeration after the expansion, and that the sizes reported by the SMPS were more indicative of the actual sizes of the agglomerates immediately after the expansion.

2.3.3 Diffusion Collection and SEM Image Analysis

Table 2.3 Number- and Volume- Weighted Mode Projected Area Mobility Diameters for Alumina, Silica and Titania Nanopowders Expanded Through a 254 μm ID x 10 cm Long Nozzle and Extracted From Image Analysis Results

Pressure (MPa)	Alumina		Silica		Titania	
	Number Weighted (nm)	Volume Weighted (nm)	Number Weighted (nm)	Volume Weighted (nm)	Number Weighted (nm)	Volume Weighted (nm)
1.72	61	945	314	1409	96	1576
3.79	243	710	145	1327	77	609
5.86	108	774	87	1167	83	864
7.93	193	718	116	922	49	411

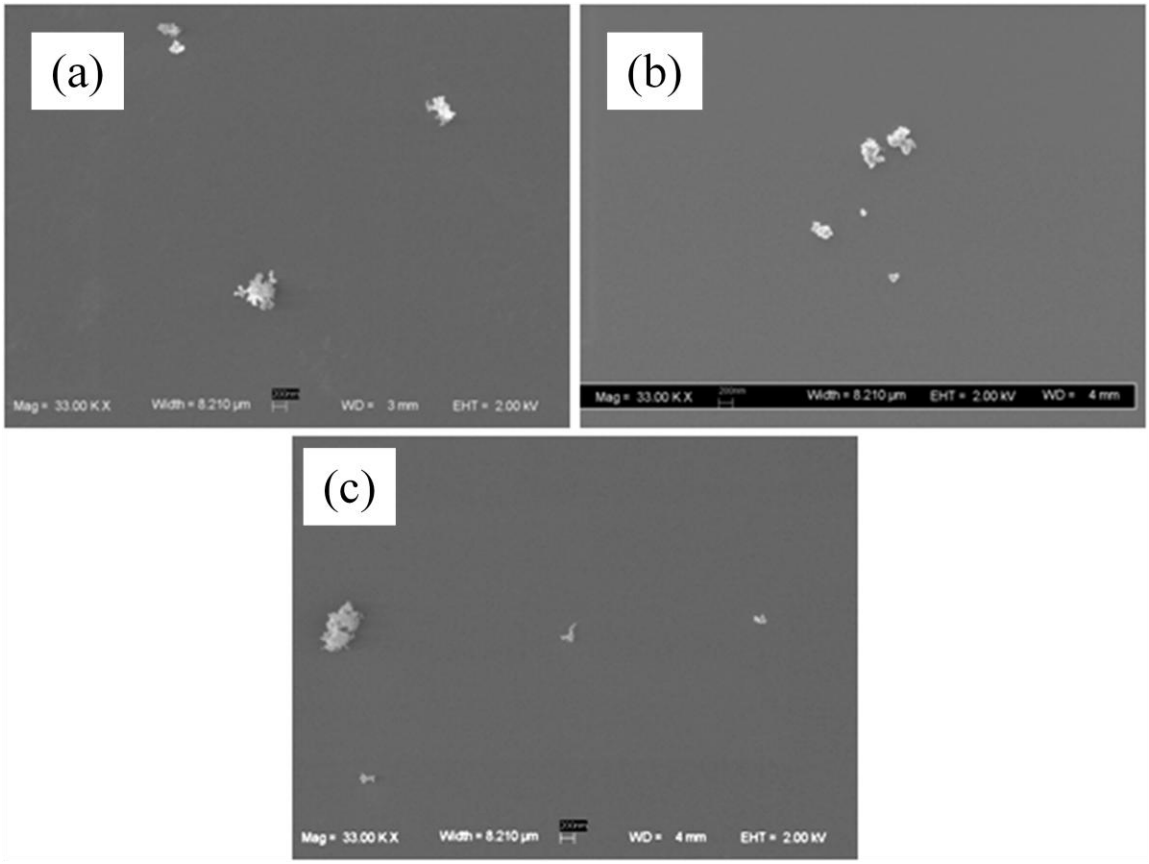

Figure 2.4 Typical micrograph of (a) alumina, (b) silica and (c) titania nanopowders expanded through a 254 μm x 10 cm nozzle.

The number- and volume-weighted mode diameters of the agglomerates collected on the surface of silicon chips, measured by SEM imaging, are listed in Table 2.3. Typical images of alumina, silica and titania nanopowders collected on the chip are shown in Figures 2.4a-c. The number-weighted mode diameters for alumina were all below 400 nm. Similar to the SMPS data (c.f. Table 2.1), there was no clear trend indicating the effect of pressure on the final agglomerate size. For titania powders, the average agglomerate sizes were below 100 nm, and the size decreased with increasing pressure just like in the SMPS data. Although there was significant variability in the volume-weighted mode diameters, there was a general trend of decreasing size with

increasing pressure. The abundance of sub-micron agglomerates identified by SEM image analysis agreed with the mixing length-scale observed in alumina and silica mixtures (discussed later in the Chapter 3 for mixing experiments). It should be noted, though, that SEM imaging analysis could also be biased by reagglomeration on the silicon chip surface and the fact that larger agglomerates, due to their inertia, would not diffuse to the chip surface and also could not stay there as easily as the smaller agglomerates.

2.4 Discussion

Deagglomeration of suspensions of nanoparticle aggregates via rapid expansion of supercritical or high-pressure suspensions has been investigated experimentally. The size distribution of fragmented nanopowders exiting the nozzle attached to a pressure vessel was characterized via online SMPS and APS and off-line SEM imaging.

The number- and volume- weighted mode diameters of expanded alumina, silica and titania measured by the SMPS, listed in Table 2.1, show that the nanopowders are significantly deagglomerated by the REHPS process. The number-weighted mode diameters were all below 100 nm, and the effect of pressure was rather weak; at the highest pressure, the number-weighted mode diameters of alumina and titania fragments were 35 nm and 37 nm, respectively. The SMPS was designed to characterize the fine fraction. The volume-weighted size distributions indicate that although agglomerates larger than the SMPS measurement size limit of 572.5 nm were indeed likely to be present, however a significant amount of the agglomerates are below 500 nm. At the higher pressures, from 3.79 to 7.93 MPa, there was a trend of decreasing fragment size

with increasing pressure. Thus the SMPS results clearly indicated that most of the fragments resulting from the REHPS process (on a volume basis) were below half micron in size, while the majority of them were under 100 nm in size; as some reagglomeration could have occurred during the SMPS sampling, the actual sizes could have been even smaller than these values. Selected REHPS experiments done using nitrogen instead of CO_2 indicate that the results are comparable and hence alternate gases may be used for the purpose of deagglomeration.

The APS measurements showed that most of the agglomerates had aerodynamic diameters between 1 and 3 μm; furthermore, since the number- and volume- weighted modes were similar, the agglomerate size distribution was not wide. It was also shown that while there is an uncertainty regarding the value of the agglomerate density, the APS results are not too sensitive to its assumed value.

The deagglomeration results from SEM analysis indicated that number-weighted mode diameters for alumina were all below 400 nm, while those for titania were below 100 nm. The volume-weighted mode diameter appeared to decrease with increasing mixing chamber pressure. For alumina, the volume-weighted mode at the higher pressures were all between 700 and 800 nm, while, for titania, they showed a more drastic change with increasing pressure, as the value went down to about 400 nm at the highest pressure. While there was a significant amount of variability in this data, the results were closer to the SMPS results than to the APS results, and were also comparable to the scale of mixing discussed in Chapter 3.

On the basis of the overall deagglomeration results it can be concluded that REHPS led to fragments which were at the sub-micron scale, and more likely to be less

than 0.5 μm in size. The higher values reported by the APS are indicative of re-agglomeration during sampling.

Overall, the results from the deagglomeration in the REHPS process considered here are comparable to or better than those in Brandt et al.[45], where the reduction in agglomerate size was correlated to the pressure drop across the normal shock. It is noted that in their studies, the agglomerates consisting of 40 nm SiO_2 primary particles (in contrast to the particles considered here, which are about 20 nm) were fragmented to a number (or count) average size of 400-500 nm when the pressure drop across the normal shock was about 0.1 MPa. The number-average was significantly below that range and typically smaller than 100 nm.

As dry nanoparticles are invariably present as large fractal agglomerates that are tens or hundreds of microns in size, dry mixing of the individual nanoparticle constituents at the sub-micron scale is not easily achieved unless an effective deagglomeration step is included in the process. The REHPS process discussed in this Chapter achieves such fragmentation and is therefore of value in mixing nanoparticle agglomerates, which can subsequently be processed to make nanocomposites of superior properties than feasible otherwise.

CHAPTER 3

REHPS MIXING

3.1 Introduction

In Chapter 2 detailed studies on deagglomeration of alumina, silica and titania nano-powders were performed and a systematic effect of pressure on deagglomeration efficiency was observed. Modeling the REHPS deagglomeration process (Appendix B) suggested that there are two important deagglomeration mechanisms; shearing in the nozzle and passing through the Mach disc at the exit of the nozzle [35]. It was suggested that agglomerate sizes resulting from shearing inside the nozzle should follow a square root dependence with nozzle diameter [35], while the influence of the Mach disc will result in agglomerate sizes that will decrease with increasing pressure, but will be unaffected by nozzle size. However the suggested models have not been validated.

Composites containing complex materials such as carbon nanotubes, which have not been previously explored through the REHPS process, are considered. Here, the ability of REHPS to not only deagglomerate carbon nanotube bundles but also mix them at sub-micron scale with nano-powders of alumina, silica and titania was investigated.

3.2 Experimental

REHPS mixing is based on the process of simultaneous deagglomeration and mixing of nanopowders suspended in high pressure and supercritical carbon dioxide upon expansion through a fine nozzle on the order of 100s of microns. The REHPS mixing apparatus is similar to the REHPS deagglomeration apparatus and is shown in Figure 2.1

Part IV. Instead of collection of the for size analysis, the powders were collected on a 0.22 mm filter (Figure 2.1, unit 8). 0.75 g of premixed alumina and silica nanopowders was charged into the 24-mL tubular mixing vessel (unit 5) at weight ratios of 1:1 and 71.8:28.2 (mullite stoichiometry, Al_2O_3/SiO_2). The operating pressure of the vessel was controlled using a one-stage reducing regulator (unit 2) when investigating pressures between 1.72 and 7.93 MPa. Pressures above 7.93 MPa were achieved using a liquid carbon dioxide Thar Technologies pump. The effect of the different phases (liquid, gas, supercritical) of the suspending fluid on the quality of mixing was investigated by adjusting both temperature and pressure of the CO_2 to achieve sub-critical and supercritical conditions. The gas conditions ranged from 1.72 to 5.51 MPa and 45^oC; the supercritical conditions ranged from 7.93 to 13.79 MPa and 45^oC; the liquid condition was at 8.27 MPa and 28^oC.

The mixture was prepared by turning the On/Off valve (unit 6) and expanding the nano-powder suspension through a capillary nozzle (254 μm ID and 10 cm long, unit 7) and collected on the filter. Three replicates were prepared for each experiment and mixtures qualities in the form of intensities of segregations were averaged.

To determine the effect of the premixed state of the nanopowders before the REHPS process nanopowders were stirred in supercritical CO_2 and then feed to into the REHPS mixing apparatus as described above. For a complete description of the stirring in supercritical CO_2, please refer to Appendix D.

3.2.1 2-pass mixing

The effect of the initial mixing condition was investigated by passing the powder through the REHPS process a second time. A sample (0.75 g) from 1-pass product collected from multiple experiments performed at the same pressure, was charged into the high pressure vessel as the "premixed" powder for the second pass of REHPS at the same operating pressure. The investigated pressures were 1.72, 7.93 and 13.79 MPa at a temperature of 45^{o}C. A liquid condition of 8.27 MPa and 28^{o}C was also investigated. Experiments were performed in triplicate and IOS values were averaged.

3.2.2 Effect of Nozzle Diameter

The effect of nozzle diameter was investigated for 1-pass mullite mixtures by comparing the mixing quality of alumina and silica powders expanded through 254 μm nozzle to powders expanded through 508 and 1524 μm nozzle.

3.2.3 Applications of REHPS Mixing with CNT and Mullite

Multi-walled carbon nanotubes (CNT) were deagglomerated via the REHPS process by expansion from 7.93 MPa and 45^{o}C. Due to the high aspect ratio nanotube agglomerates could be sized via image analysis of SEM micrographs where the Feret diameter was measured, which is the largest end to end length of the CNT agglomerate. The CNT agglomerates were collected by diffusion in a similar fashion to the silica nanopowders. Approximately 2000 agglomerates were sized. Additionally individual mixtures of CNT and alumina, silica and titania nanopowders were prepared via the REHPS process. Mixtures were prepared at weight ratios of 50% CNT in the oxide material and were

expanded from 7.93 MPa and 45^{o}C. Mixtures were analyzed qualitatively via SEM imaging.

3.3 Mixture Quality Analysis

The 0.2 g of powder was collected from the various different mixing methods were pressed into a 13 mm tablet at 600 MPa. The quality of the mixture was characterized using scanning electron microscopy in conjunction with energy dispersive x-ray spectroscopy (SEM-EDS), which was used to determine the elemental concentrations at spatial locations with resolutions of approximately 1 μm [(52)]. This method was used in two ways: (1) a scanning mode was used to produce elemental mappings to develop a qualitative ranking of mixtures on the scale of approximately 75 x 50 μm (the dimensions of the scan); (2) the elemental concentrations at 400 spots, which were used to determine the intensity of segregation (IOS) and scale of segregation (SOS) and were initially proposed by Danckwerts [(54)]. A more in depth description of this process can be seen in To etal [(35)]. The intensity of segregation is a measure of concentration homogeneity (comparable to molecular diffusion), represented by the normalized variance as shown in equation (3.1), where σ^2 is the sample variance, μ_A and μ_S are the mean concentrations by weight of alumina and silica, respectively. The intensity of segregation ranges from 0 to 1, representing the completely homogeneous state and the completely segregated state, respectively.

$$IOS = \frac{\sigma^2}{\mu_A \mu_S} \tag{3.1}$$

The scale of segregation uses the auto correlation function to determine the characteristic size of the segregated regions and is described by equations (3.2) and (3.3). The auto correlation function, $R(r)$ shown in equation (3.2), evaluates the similarity of concentrations between spatial locations of known distance r. The scale of segregation is the integral of $R(r)$ with respect to r and defines the scale at which a pattern in the mixture composition with respect to spatial locations can be discerned. Above this scale, the mixture can be considered random. The agglomerate size cannot be directly measured by the scale of segregation, however a change in agglomerate size will correspond to a similar change in SOS.

$$R(r) = \sum_{i}^{N} \frac{\overline{\left(a_i - \bar{a}\right)\left(a_{i+r} - \bar{a}\right)}}{\left(a_i - \bar{a}\right)^2} \tag{3.2}$$

The scale of segregation is considered to be integral of the auto-correlation function between a distance of $r = 0$, where there is complete correlation and ζ, a length scale that is much greater than the scale at which the mixture is considered random and $R(r) \sim 0$.

$$SOS = \int_0^{\infty} R(r)\,dr \approx \int_0^{\zeta} R(r)\,dr \tag{3.3}$$

3.4 Results

3.4.1 1-pass REHPS Mixing

The intensities of segregations of alumina and silica nano-powder mixtures at weight ratios of 1:1 and 72:28 (mullite stoichiometry) are listed in Table 3.1, which includes hand premixes, stirred premixes (see Appendix D), 1-pass and 2-pass REHPS mixtures.

These results are also shown graphically in Figure 3.1, which depicts the intensity of segregation values averaged over different expansion conditions for each of the three mixing methods and two mixture concentrations. This shows that 1-pass REHPS mixing offers a significant improvement over hand mixing. When comparing the average intensity of segregation values of the premixed powders (i.e. before REHPS mixing) including the hand premixed at 1:1 and 72:28 and the stirred premix at 1:1, which are 0.1592, 0.3220 and 0.1610, it is clear that stirring offers only a slight improvement to the mixing quality, however it offers a significant improvement in the variability of the powders. The scale of segregation values were also determined from the hand and stirred premixes from their respective EDS elemental mappings taken at a magnification of 5000x. The SOS values were 15 μm, 18 μm and 5 μm for the 1:1 and 72:28 hand premixes and 1:1 stirred premix. The REHPS mixed powders, however offer mixtures with IOS values one to two orders of magnitude lower, where increases in IOS imply poorer mixtures. The hand premixed IOS values range from 0.0038 – 0.0128, while the stirred premix showed further improvement and ranged from 0.0016 – 0.0040.

The hand pre-mixed 72:28 powder mixture that exited the vessel during expansion, but did not pass through the nozzle (i.e. remained in the connecting tubing between the vessel and the nozzle) was also analyzed and its intensity of segregation was measured to be high, 0.215. This shows that flow through the tubing is not as effective as the expansion step in REHPS mixing.

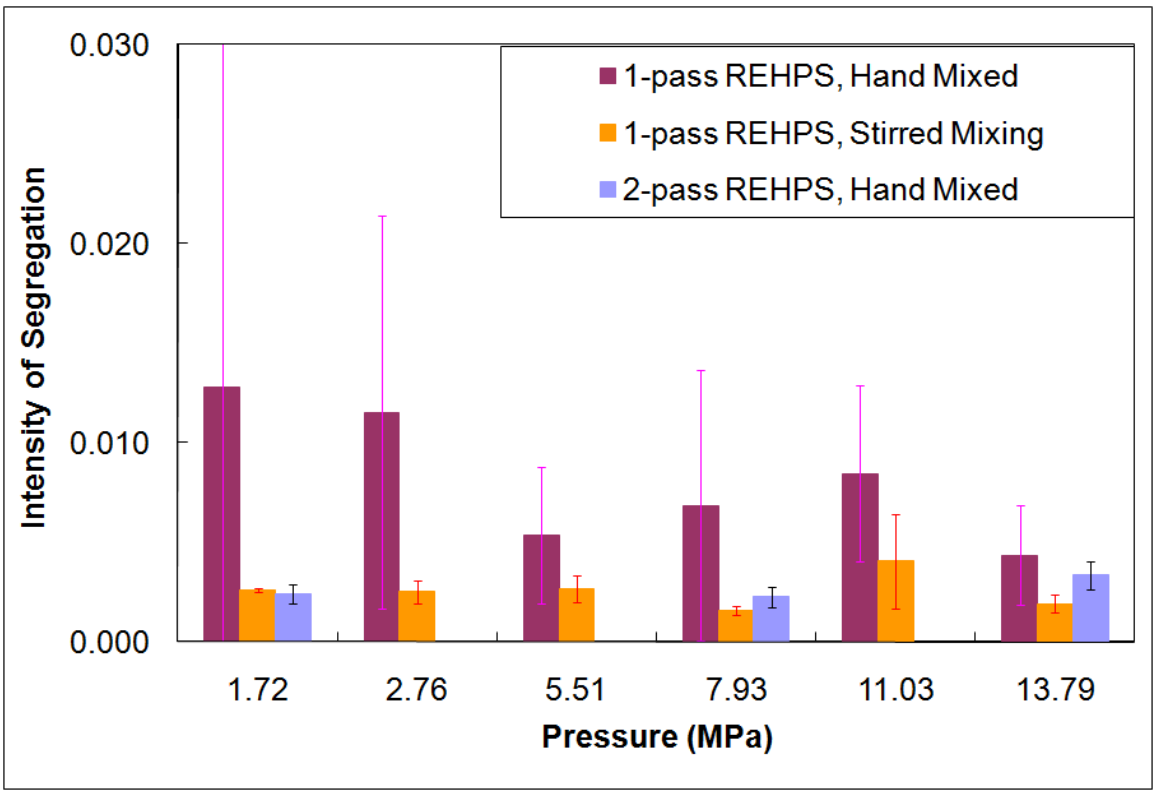

Figure 3.1 IOS valves for hand premixed 1 – pass, 2 – pass and stirred premix 1-pass REHPS mixtures at 50 wt % alumina. IOS for REHPS mixtures were averaged over different pressures and expanded through 254 μm nozzle.

It can be seen that the REHPS process produced highly variable results as shown by the large 95% confidence intervals shown in Table 3.1. It is believed that this high variability is indicative of poor pre-mixing and therefore poor axial mixing into the REHPS process, which would be manifested in non-simultaneous deagglomeration and mixing. It can be observed that when the premix is improved via stirring premixing the variability of the mixture qualities significantly decreases. As a result of this high variability it is difficult to elucidate a definitive trend between mixing quality and the expansion pressure, however there seems to be a general trend of decreasing intensity of segregation and decreasing confidence intervals with increasing expansion pressures. It

Table 3.1 Intensity of Segregation ($x10^{-3}$) of 1-pass and 2-pass REHPS Mixtures Expanded From Various Mixing Pressure and Temperatures

Mixing Condition	Pressure (MPa)	Temp (^{o}C)	1-pass			2-pass	
			50:50 Hand mixed	50:50 Stirred Mixed	72:28 Hand Mixed	50:50	72:28
Pre-mix	--	--	322.0 ± 91.6	157.3 ± 14.9	159.2 ± 79.2	--	--
Gas	1.72	45	12.8 ± 17.3	2.6 ± 0.1	5.5 ± 6.2	2.4 ± 0.5	2.4 ± 1.1
	2.76		11.5 ± 9.8	2.25 ± 0.5	4.5 ± 2.2	--	--
	5.51		5.4 ± 3.4	2.7 ±0.6	8.7 ± 6.7	--	--
Supercritical	7.93		6.8 ± 6.8	1.6 ± 0.2	3.8 ± 1.5	2.3 ± 0.5	1.9 ± 1.2
	11.03		8.5 ± 4.4	4.0 ± 2.0	8.3 ± 8.1	--	--
	13.79		4.3 ± 2.5	1.9 ± 0.4	10.2 ± 9.3	3.3 ± 0.7	2.9 ± 0.4
Liquid	8.27	28	4.2 ± 2.0	3.7 ± 2.0	3.9 ± 0.7	2.1 ± 0.7	1.9 ± 0.6

is believed that the deviation of the 72:28 hand premixed 1-pass REHPS mixtures results from content uniformity issues, which are more difficult to control as mixtures become significantly different from 1:1. Also, the liquid CO_2 mixing condition showed significantly less variation than the gas or supercritical conditions. Regardless of the expansion pressure, however, the average IOS value at each condition was below 0.0128, implying homogeneity on the scale of few microns or better.

3.4.2 2-pass Mixtures

In an attempt to further improve product mixture quality 2-pass REHPS mixing was used, where the feed mixture was the product form the hand premixed 1-pass REHPS experiments. The resulting intensity of segregation values were reduced to 0.0019 to 0.0033, which are comparable to the stirred premix. This clearly shows that a minimum level of premixing is required to achieve high quality mixtures with reasonably high reproducibility. The intensities of segregations for the hand premixed 2-pass REHPS mixtures are also shown in Table 3.1. The values are all an order of magnitude reduction in intensities of segregation values in compared to the hand premixed 1-pass REHPS mixtures. At the highest pressure there was a slight decrease in mixing quality, which is believed to result from the condensation of carbon dioxide during the nearly adiabatic expansion from pressures above 7.93 MPa, resulting in precipitation of dry ice around the agglomerates, preventing their break-up and therefore limit the mixing quality. At the liquid condition of 8.27 MPa and 28^{o}C, an average IOS value comparable to that of the REHPS experiments performed at the pressure of 7.93 MPa was observed.

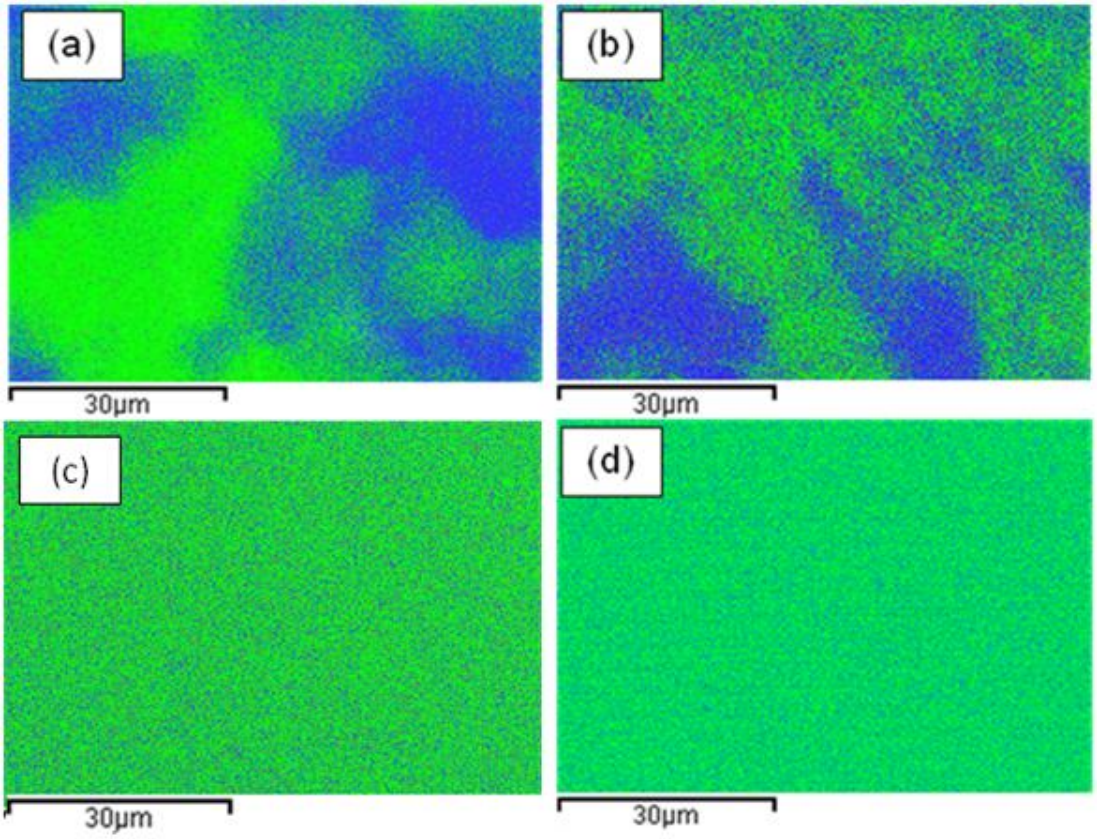

Figure 3.2 Superimposed EDS scans of elemental Al (green) and Si (blue) of (a) hand mixed powders before the REHPS process, (b) the hand mixed powders that remained in the connecting tubing between the high pressure vessel and the expansion nozzle (c) 1-pass and (d) 2-pass REHPS mixed powders at the 72:28 ratio, expanded at 7.93 MPa.

Figure 3.2 shows the EDS scans of the 72:28 mixtures before and after the REHPS mixing process, which shows the superimposed elemental scans of aluminum (green) and silicon (blue). Greener areas represent an abundance of alumina while bluer areas represent the presence of silica. It can be observed that the hand premixed powders and the premixed powders remaining in the connecting tubing shown in Figure 3.2a – b have silica regions in the range of several 10s of microns, implying similar levels of homogeneity. The poor mixing of the premixed powders within the connective tubing shows the necessity of expansion through the nozzle for significant improvement in

mixing. The 1-pass REHPS mixed powders expanded at 7.93 MPa, shown in Figure 3.2c having a more constant brightness across the scan suggests a significant improvement in mixing quality and homogeneity. Figure 3.2d shows that the EDS scan of the 2-pass REHPS was comparable to the scan for the 1-pass mixture. It is believed that the resolution of the mixing was on a smaller scale than that of the scan, and the IOS values are indicative of mixture quality.

Nozzles with larger inner diameters, 508 and 1524 mm, were used to determine their effects on the mixing quality of REHPS mixtures of 72:28 hand mixed powders expanded at a pressure of 7.93 MPa and a temperature of 45^{o}C. This pressure and mixture concentration was chosen as it gave both high quality mixtures and high reproducibility. Figures 3.3a-b show the Al elemental maps for the REHPS mixtures produced with the 508 and 1524 μm nozzle, respectively. When comparing these elemental maps to those produced by expansion through a 254 mm nozzle, shown in Figure 3.2c, it is clear that level of homogeneity has significantly decreased by increasing the nozzle diameter. The effect of the nozzle is shown in Table 3.2, which depicts that an increase in nozzle diameter results in an increase in the length scale of the maximum energy eddy, as calculated from equation (1.2). These eddy length scales were calculated using data from the National Institute of Standards and Technology[(61)], and choked flow conditions representing the stagnation point in one-dimensional compressible flow for a perfect gas[(62)].

3.4.3 The Effect of Nozzle Diameter

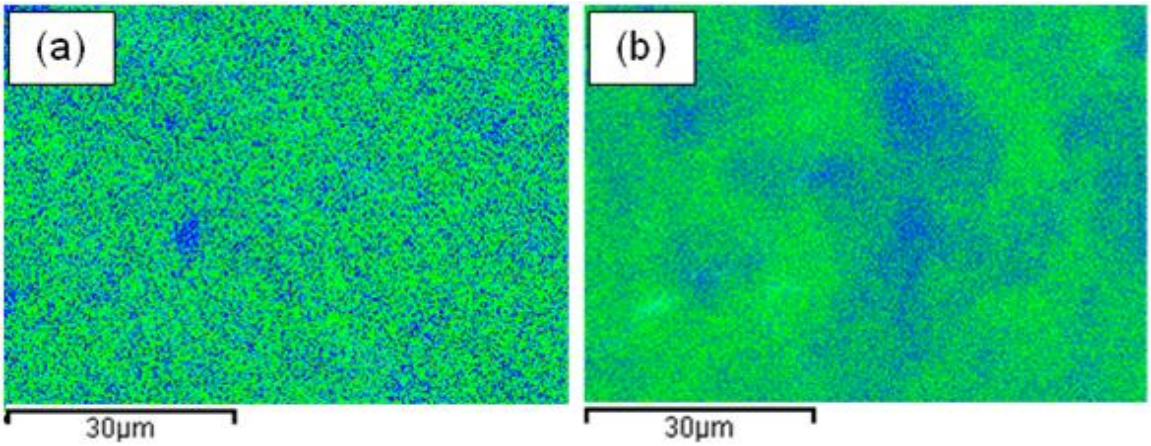

Figure 3.3 Superimposed EDS scans of elemental Al (green) and Si (blue) for 72:28 alumina: silica mixtures expanded from a pressure of 7.93 MPa through nozzles with differing diameters of (a) 508 µm and (b) 1524 µm. The EDS elemental scan for the 254 µm nozzle diameter is shown in Figure 6c.

This also coincides with an increase in both intensity of segregation and scale of segregation. It can be seen that the intensity of segregation increases with a nearly quadratic dependence on nozzle diameter indicating a significant decrease in mixture quality that is expected from the increase in nozzle diameter. The scale of segregation shows a nearly linear dependence on the nozzle diameter. Due to the limited resolution, the EDS method could not produce scales of segregation below 2 µm. This indicates a scale of segregation on the order of 1 µm or below for REHPS expansions through a 254 µm nozzle, which coincides with the deagglomeration results previously shown.

Table 3.2 Intensity of Segregation and Scale of Segregation of Mullite Mixtures Expanded From 7.93 MPa and the Associated Length Scale of the Maximum Energy Eddies During Flow Through the REHPS Process

Nozzle ID (μm)	Average	Scale of Segregation (μm)	Max Energy Eddy length (μm)
254	0.0038	< 2	2.2
508	0.0152	4.3	4.1
1524	0.1405	10.9	10.6

3.4.4 Deagglomeration and Mixing of Carbon Nanotubes

As opposed to the other nanopowders investigated in this study, the high aspect ratio of the CNT make them particularly difficult to deagglomerate, which offers a significant challenge for the REHPS process. One benefit of the high aspect ratio is the ease of identification between the string-like CNT and the spherical ceramic nano-materials, which therefore makes it a good candidate for quickly determining the mixing quality of the CNT and nano-ceramic mixtures by imaging and without the use of elemental analysis such as EDS. Figures 3.4a-b show SEM images of carbon nanotube agglomerates before and after REHPS deagglomeration from a pressure of 7.93 MPa and a temperature of 45 ^{o}C. It can be seen that the unprocessed CNT form large agglomerates generally on the order of 10 μm or larger, while the REHPS deagglomerated CNT have been reduced to smaller, less compact agglomerates and in some cases single nanotubes. Figure 3.5 shows the size distribution in terms of Feret diameter for the REHPS deagglomerated CNT, which are in predominately sub-micron sizes. The REHPS process has also been used to mix CNT with various ceramic nanopowders including silica, alumina and titania is shown in Figure 3.6.

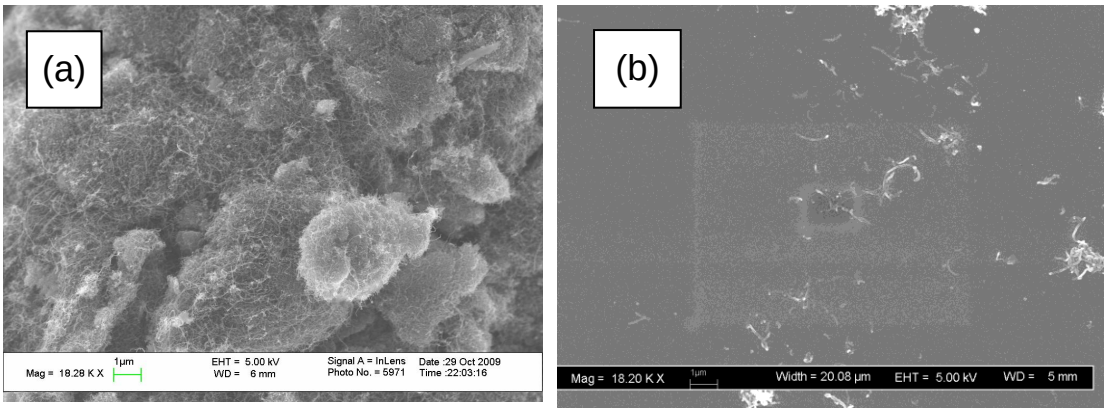

Figure 3.4 SEM images of multi-walled carbon nanotubes (a) before and (b) after deagglomeration via the REHPS process, expanded from 7.93 MPa.

Unlike the nanopowders discussed so far, the high aspect ratio of the CNT allows for its easy identification from the other ceramic constituents as can be seen in Figures 3.6 a-c. Additionally the large aspect ratio of the CNT makes their agglomerates particularly difficult to disperse, because of the high inter-molecular contact area, however as Figure 3.6 a-c clearly shows that the REHPS process was capable of mixing the CNT and the ceramics were capable of being mixed on the sub-micron scale. Figure 10a shows that the silica agglomerates on the order of a couple hundred nanometers are integrated into the micron-sized CNT agglomerates. Figure 3.6 b shows a REHPS mixture of CNT and titania, where it can be seen that several nano-sized agglomerates were integrated into the larger CNT agglomerates. Unmixed regions on the micron-scale can be attributed to the poor ability to disperse the CNT. A similar phenomenon has occurred for the CNT alumina mixture, shown in 3.6c. These results seem contrary to the deagglomeration results, which show that the silica agglomerates are more difficult to disperse than the alumina or titania powders. This discrepancy can be explained by the interaction potential between the different constituents. The CNT and the silica (silane

coated) are both hydrophobic, while the titania and alumina are both hydrophilic, which would make the CNT and silica more amenable to mixing. Additionally it is believed that this strong interaction between the CNT and silica would promote coating and continued dispersion of the smaller silica particles on the larger individual CNT. Since the titania and alumina are hydrophilic they are less likely to coat the individual CNT and are likely closer to the true size of the deagglomerated powders.

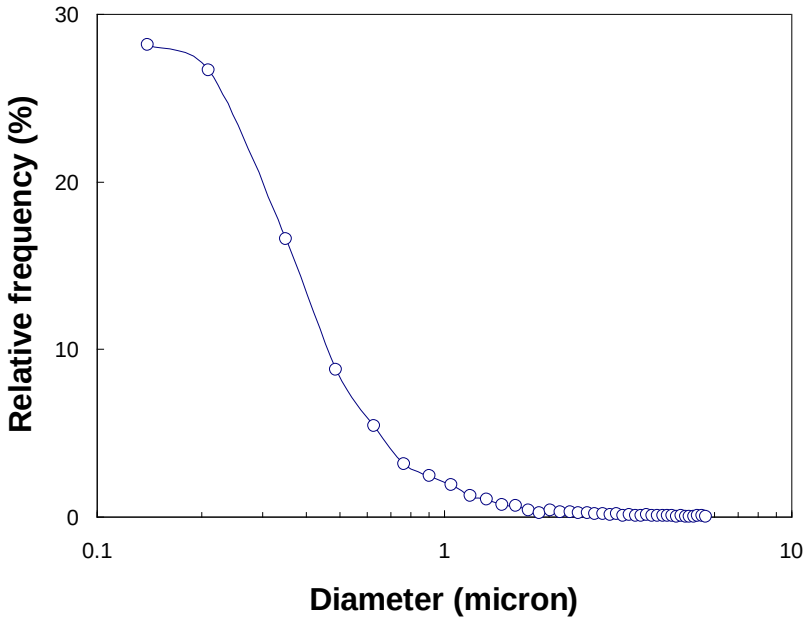

Figure 3.5 Size analysis of image analysis of REHPS deagglomerated CNT.

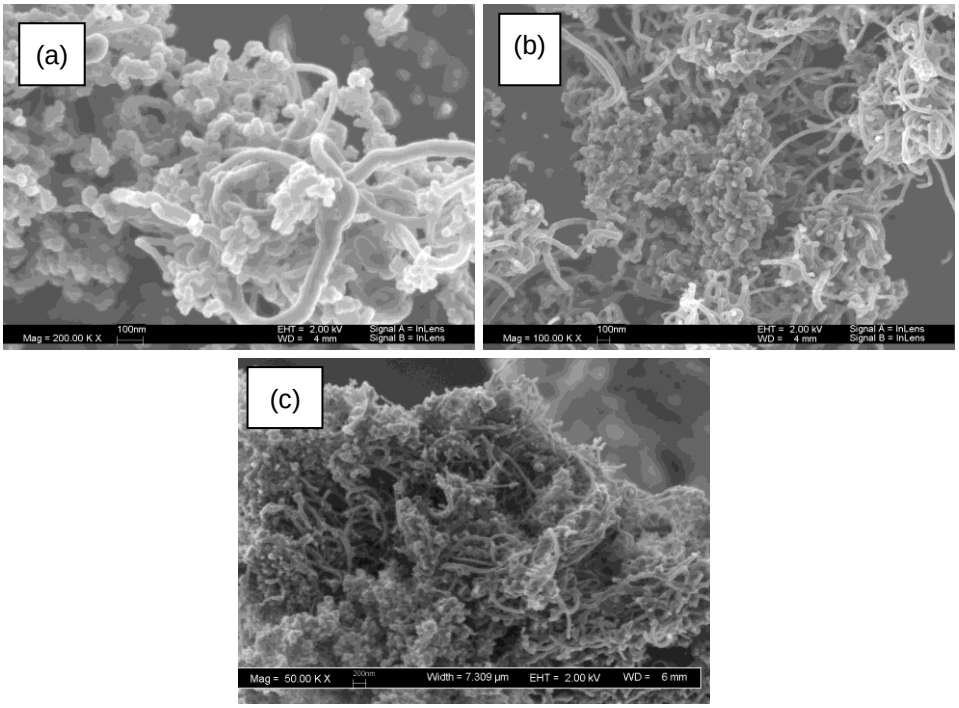

Figure 3.6 Multi-walled carbon nanotubes were mixed with (a) silica, (b) titania, (c) alumina nanopowders via the REHPS process, expanded from 7.93 MPa and 45^{o}C. CNT-nano-powder mixing clearly indicates that the mixing occurs on the nano-scale (notice the SEM scale bars which are 100 nm, 100nm and 200 nm for image a, b and c respectively).

3.5 Discussion of Results

3.5.1 REHPS Deagglomeration and Mixing

Results shown in Table 3.1 and Figure 3.1 indicate that the 1-pass REHPS mixing process was subject to a high degree of variability resulting in a wide range of mixing qualities at the same conditions, quantified by the IOS. The one exception to this was the liquid mixing condition. As a result it was difficult to discern an observable trend with respect to pressure. It was believed that this variability was due to a poor pre-mixing condition where the different constituents would exit the nozzle individually and then re-agglomerate with like fragments without mixing, as opposed to the intended goal of the

REHPS process, which is that the agglomerates would be simultaneously deagglomerated and mixed in aerosol. Additionally mixtures deviating far from a one to one weight ratios are more likely to suffer.

In an attempt to improve the mixing quality of the REHPS mixtures two modification were employed. The first was stirring premixing, which showed nearly an order of magnitude improvement on mixing quality. The second was 2-pass REHPS mixing which showed a similar improvement. This clearly shows that premix quality and therefore axial mixing into the REHPS process has a profound effect on the mixing quality of the product mixture. It should be noted that the observed increase in mixing quality in the 2-pass REHPS mixtures was believed to result from an improved pre-mixing condition. It is believed that the powders deagglomerated by the REHPS process could only be reduced to the size of the primary aggregate (where solid bridges between primary particles dominate), so successive passes through the REHPS process would not improve the deagglomeration efficiency; however it would improve the likelihood for simultaneous deagglomeration and mixing.

The mixing quality of REHPS mixtures performed at the liquid condition showed comparable intensities of segregation to those performed at the higher temperature. This suggests that temperature has little effect on the mixing quality. Additionally, it was believed that the liquid mixing condition did not encounter dry ice precipitation that was observed at the higher expansion pressures (>11 MPa) because the Joule-Thompson coefficient is significantly reduced for liquids.

3.5.2 Effect of Nozzle Diameter

The intensities of segregation results shown in Table 3.2 describe that mixtures expanded through larger nozzles have lower mixing qualities. Based on these results, as well as the elemental scans shown in Figure 3.2c and 3.3a – b, it can be seen that there is a linear dependence with nozzle size. This shows the same dependence on nozzle diameter as the size of the maximum energy containing eddies, as shown in equation (2). It is intuitive that as the most energy intensive mixing motions (i.e. the maximum energy eddies) increase in size, the scale of mixing should also increase in size. Additionally, the maximum energy containing eddies is indicative of a maximum size that agglomerate breakage is likely to occur. Further size reduction is also expected from smaller eddies, however the largest agglomerates will dominate in volume averaged size distributions and EDS mappings.

It should be noted that this does not exclude the impaction based deagglomeration mechanism as it is believed that only 50 % of the agglomerates will pass through the mach disk. For a volume based analysis technique such as EDS, which will emphasize larger agglomerates over smaller ones, the sub-micron sized agglomerates resulting from this mechanism will be over shadowed by the several micron-sized agglomerates that do not pass through the Mach disk.

3.5.3 Deagglomeration and Mixing with Carbon Nanotubes

Because of their high aspect ratio and strong intermolecular forces CNT and their agglomerates are very difficult to break up, especially in the dry state. Sanganwar has previously shown that ultrasonic mixing in supercritical fluids, although highly capable of mixing spherical nanopowders together, it was unable to loosen the tight CNT

bundles[52]. Figures 3.4, 3.5 and 3.6 have shown that the REHPS method was capable of reducing the size of the agglomerates below the micron-scale, while simultaneously mixing with ceramic powders.

3.6 Conclusions

Rapid expansion of high pressure and supercritical suspensions (REHPS), an environmentally benign approach that produces dry powders, was studied for producing mixtures of nano-powders with a scale of segregation on the order of a few microns or smaller. In the present study, two characterization methods having better resolution capabilities were used to analyze the mixing quality of the REHPS samples. First, the constituent concentration was determined at 400 sites on the surface of pressed pellet using EDS-SEM to determine the intensity of segregation. Next, an elemental mapping of alumina was obtained through EDS-SEM analysis to determine the scale of segregation, which can be correlated to agglomerate size, and thus an improvement over the elemental ratio reported in previous studies[16, 17] that does not provide any physical interpretation of the mixing quality. Employing more rigorous mixing characterization and experimental protocols than those used in previous studies[16, 17], this paper examined the influence of the expansion nozzle size, condition of the mixing quality of the premix, and pre-expansion pressure, which was held constant during the experiments. The premix quality was examined by introducing nano-powders that were either hand mixed, stirred in a supercritical fluid, or previously REHPS mixed to the REHPS mixing process. The quality of mixing of the agglomerates of the individual constituents prior to transport through the nozzle had a measurable influence on the intensity of segregation and scale of segregation observed with REHPS processed mixtures. The most important observation

was that while deagglomeration results show that agglomerate sizes decrease with increasing pressure, similar to those previously observed (To et al. 2009), the mixing results show little effect of pressure. This phenomenon is explained by the variability introduced by the premix, which leads to non-simultaneous deagglomeration and mixing and therefore a slight heterogeneity. An increase in nozzle size was shown to result in poorer mixing quality as indicated by a nearly linear decrease in scale of segregation and a nearly quadratic decrease in intensity of segregation. This correlates well with the length scale of the maximum energy eddies and proves that shear forces inside the nozzle do play an important part in the deagglomeration of the nanopowders, thus suggesting that the shear based deagglomeration mechanism previously proposed is valid. These results suggest the agglomerate sizes follow a linear correlation with nozzle diameter, however, the previously proposed shear based model suggested a square root dependence with nozzle diameter and therefore may not completely explain the shear based deagglomeration mechanism. The results indicated that single-pass processing of stirred mixtures produced mixing quality values that were as good as the two-pass processing of hand mixed samples, suggesting that improved pre-mixing via stirring in the supercritical reactor before expansion through nozzle can eliminate the need for a second REHPS pass.

The study also presented preliminary results for two practical applications of REHPS for creating nano-composites. Results for the use of REHPS for formation of mullite, an aluminosilicate valued for its refractory properties, indicate that the mixing quality has direct effect on degree of mullite formation. Second, composites containing complex materials such as carbon nanotubes, which have not been previously explored

with the REHPS process, were considered and it was shown that REHPS can not only deagglomerate carbon nanotube bundles but also mix them at sub-micron scale with nano-powders of alumina, silica and titania.

Overall, the results presented indicate that conditions that lead to better deagglomeration via REHPS also lead to better mixing, although there are important nuances as summarized above. Thus in summary, this Chapter builds on the findings of previous deagglomeration and mixing studies and adds two very important contributions to the field: (1) It provides experimental verification for the two previously proposed deagglomeration mechanisms (To et al. 2009), and through an investigation of the influence of the nozzle diameter, it establishes that the shear based deagglomeration mechanism is important. (2) The REHPS mixing process is significantly improved by improving the mixing quality of the premix, which also explains the discrepancy found in the previously reported mixing and deagglomeration results.

CHAPTER 4

EFFECT OF NOZZLE GEOMETRY ON THE REHPS PROCESS

4.1 Introduction

It has previously been suggested in this thesis that two deagglomeration mechanism are responsible for the breakage of nano-particle agglomerates (Chapter 1.3.3, 2.3 and Appendix B). The first mechanism suggested that agglomerate breakage resulted from interactions with shearing forces in the nozzle, assuming laminar flow, due to the high velocities (as the fluid approaches the speed of sound) and the high densities and viscosities of high pressure and supercritical carbon dioxide. The second mechanism suggested that impaction with the much stronger Mach disc will also break up agglomerates. However only a small portion of the material will actually pass through the Mach disc and the rest of the material follows the streamline of the fluid and flows around it. Based on a simple force balance model described in Appendix B the shear forces in the nozzle should decrease with an increase in nozzle diameter and decreasing pressure resulting in larger agglomerates, while the strength of the Mach disc is increased by increasing by expansion pressure. The effect of the nozzle diameter on agglomerate size has already been superficially explored in Chapter 3.4.3.

All of these mechanisms are likely to contribute to the breakage of the agglomerates, however it until this point it has been unclear what role each of these mechanisms play during the REHPS process. Additionally the influence of turbulent shear and elongation stresses has yet to be addressed. In this Chapter modifications will be made to the nozzle geometry to decouple deagglomeration mechanisms and identify

their importance as will be characterized through deagglomeration and mixing studies. To test the effect of the shear induced deagglomeration mechanisms on agglomerate breakage, the nozzle diameter and the contraction ratio at the entrance will be varied. A reduction in nozzle diameter is expected to result in an increase in the turbulent shearing forces in the nozzle and thereby increase the likelihood of agglomerate breakage. By decreasing the contraction ratio at the entrance to the nozzle (i.e. by increasing the diameter of the inlet tube) the acceleration of the fluid entering the nozzle will increase and therefore apply stronger elongation stresses at the entrance. By varying both the nozzle diameter and the contraction ratio between the inlet and the nozzle their individual contributions can be determined. A converging – diverging nozzle will be used to test the effect of impaction with the Mach disc. In a converging – diverging nozzle, otherwise known as a de Laval nozzle, nearly all of the flow passes through the Mach disc because it is contained within the nozzle[62]. By ensuring that the apex of the converging section is sufficiently large the agglomerate breakage due to shearing can be minimized and the effect of the Mach disc can be observed. To understand the effect of the turbulent shear stress imparted onto agglomerates it will be estimated from simulated centerline fluid properties for each of the nozzle configurations.

4.2 Experimental Apparatus

The REHPS deagglomeration and mixing studies performed in this Chapter are similar to the experiments described in Chapter 2.1 and 3.2. The experimental apparatus is similar to that shown in Figure 2.1, with the one major exception being that the nozzle geometry (Figure 2.1, unit 7) was varied to identify the importance of the various deagglomeration mechanisms. REHPS deagglomeration experiments were performed with silica R972

nanopowders, where the SMPS and SEM in conjunction with image analysis were used to characterize the effect of nozzle geometry on the deagglomerated powder. The REHPS mixing experiments were performed with a mixture of silica R972 and alumina Alu C. The nanopowders were first premixed by stirring in supercritical carbon dioxide at a pressure of 14.8 MPa and a temperature of 35 ^{o}C at an impeller speed of 2000 RPM, to minimize inhomogeneity resulting from non-simultaneous deagglomeration in the REHPS apparatus and subsequent reagglomeration with like nanoparticles. A detailed description of the stirring process can be seen in Appendix D. All REHPS experiments were performed at expansion conditions of 5.86 MPa and 45 ^{o}C. These conditions were previously shown to produce an intense Mach disc, without resulting in carbon dioxide condensation (Appendix B), which was previously been shown to be deleterious to the deagglomeration process (Chapter 3)

Two general nozzle configurations were investigated: (1) a capillary nozzle where the nozzle diameter, nozzle length, and the inlet diameter were varied depicted in Figure 4.1a and (2) a converging – diverging or de Laval nozzle depicted in Figure 4.1b. Figure 4.1a depicts the nozzle configurations used to understand the effect of the shear forces in the nozzle. The diameter of the expansion nozzle, D_{Nozzle}, was varied between 508 μm – 1524 μm, the diameter of the inlet to the nozzle, D_{Inlet}, was varied between 762 – 3175 μm, and the nozzle length, Len_{Nozzle}, was varied between 3 and 10 cm. REHPS deagglomeration and mixing experiments were performed with various combinations of D_{Nozzle} and D_{Inlet} such that the nozzle diameter could be varied while the ratio between the diameter of inlet to the diameter of the nozzle, $R_{I\text{-}N} = D_{Nozzle} / D_{Inlet}$, can be kept constant. Similarly $R_{I\text{-}N}$ was varied while D_{Nozzle} could be kept constant. The specific nozzle

configurations are listed in Table 4.1, where "X" indicates that the experiment was performed.

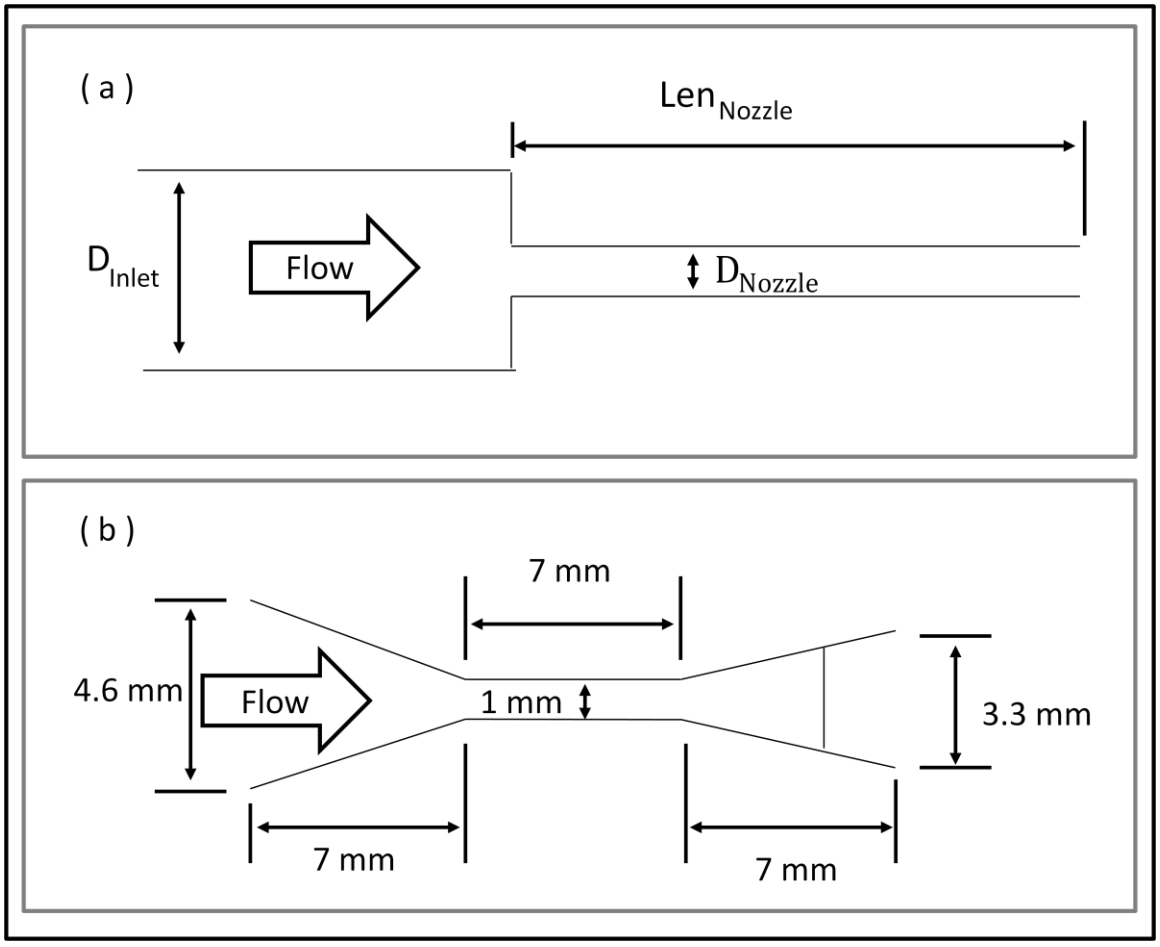

Figure 4.1 The nozzle configurations used to identify the importance of the deagglomeration mechanisms include (a) a capillary nozzle with and (b) a de Laval nozzle.

The dimensions of the de Laval nozzle, constructed from aluminum, are depicted in Figure 4.1b. It can be seen that a straight tube, with a 1 mm diameter, connects the converging and diverging sections. This wide diameter tube is expected to impart low

shearing forces onto the agglomerates and is comparable to one of the capillary nozzles (1013 μm) described in Figure 4.1a and Table 4.1.

Table 4.1 List of 3 and 10 cm Nozzle Configurations Exploring the Role of Various Deagglomeration Mechanisms on the REHPS Process

	D_{Nozzle} (μm)			
D_{Inlet} (μm)	508	762	1013	1524
762	X	-	-	-
1524	X	X	X	-
3175	X	-	X	X

4.3 Results and Discussion

4.3.1 REHPS Mixing

It should be noted that the mixing state of the alumina and silica nanopowders prior to the REHPS process was achieved via supercritical stirring to minimize inhomogeneity resulting from non-simultaneous deagglomeration and mixing. It has also been shown in Chapter 3.2 that premixing by supercritical stirring significantly improves the resulting mixing quality. When comparing these results to the intensity and scale of segregation presented in Chapter 3.2 it should be noted that similar operating conditions may yield significantly different results due to the difference in the premixing condition.

The effect of nozzle geometry on the REHPS mixing process was characterized using the scale of segregation (SOS) and intensity of segregation (IOS), which was determined via EDS analysis. The effect on nozzle length, diameter and the inlet diameter on the scale of segregation are listed in Tables 4.2 and 4.3. The corresponding intensity of segregation values (SOS) are shown in Tables 4.4 and 4.5. Typical EDS elemental scans for each of the nozzle configurations are shown in Figures 4.2 and 4.3. It should be recalled that the scale of segregation does not directly represent the agglomerate size, however as the agglomerate sizes increases the scale of segregation should also increase. From Table 4.2 and 4.3 it can be seen that the scale of segregation increases nearly linearly with nozzle diameter, which indicates a decrease in mixing quality and coincides with the EDS maps shown in Figure 4.2. These results agree with the mixing results already discussed in Chapter 3.4.3. The REHPS mixed nanopowders expanded through the 508 μm diameter nozzle show that the scale of segregation slightly increases, with inlet diameter, which coincides with the EDS images shown in Figure 4.3. While it is clear that the ratio of the inlet to the nozzle diameter has an impact on mixing quality, these results suggest that the nozzle diameter, and thereby shear induced deagglomeration dominates in the capillary nozzle geometry. When comparing the values in Table 4.2 to those in Table 4.3 it is clear that a reduction in the nozzle length generally leads to an increase in the scale of segregation.

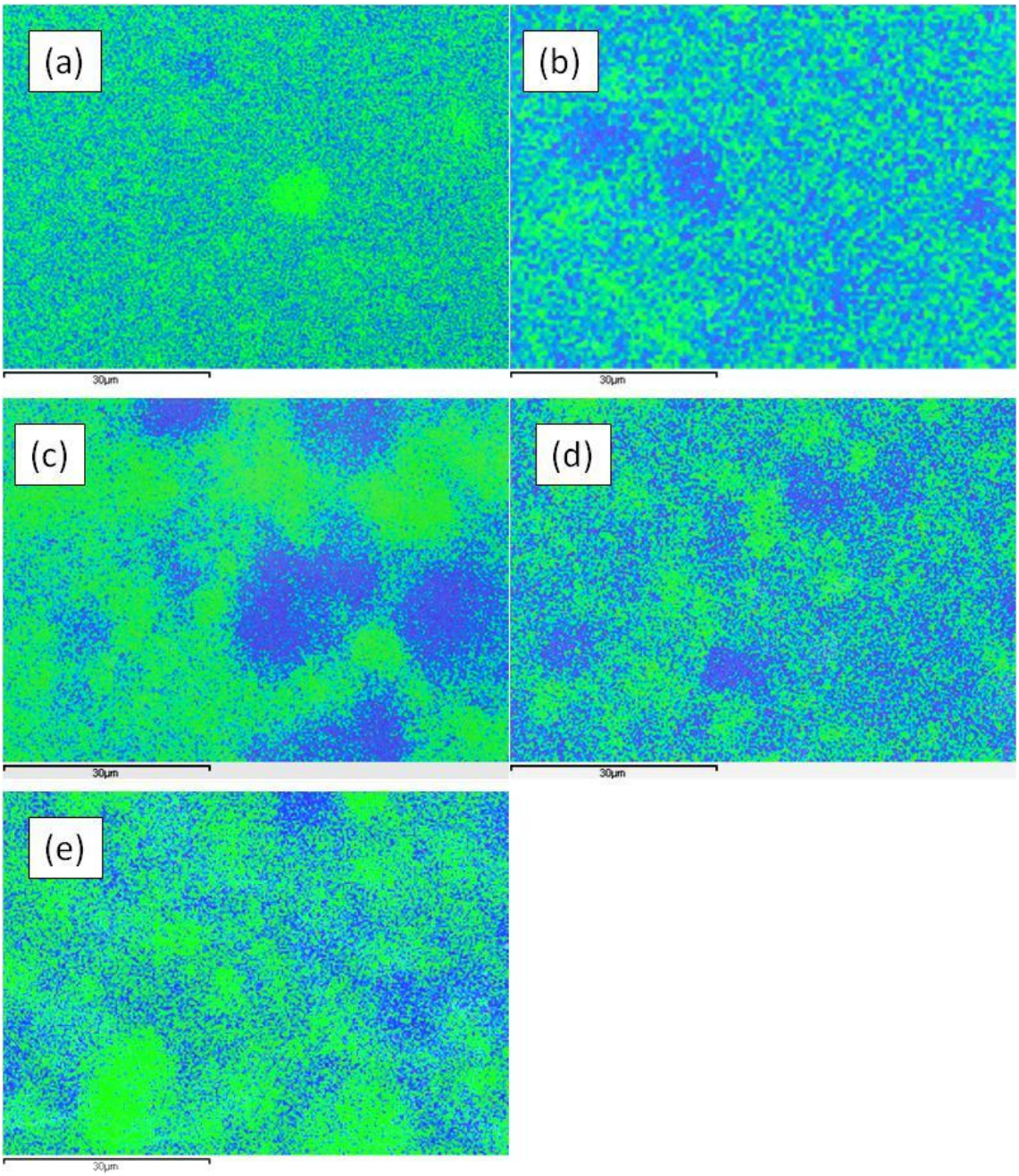

Figure 4.2 EDS scans of alumina (green) and silica (blue) of mixtures REHPS mixed through a capillary nozzle geometry consisting of inlet tube and a 10 cm long nozzle. The nozzle configurations are (a) 1524 inlet:762 nozzle, (b) 3175 inlet:1013 nozzle, (c) 3175 inlet:1524 nozzle, (d) de Laval nozzle with carbon dioxide (e) de Laval nozzle with nitrogen.

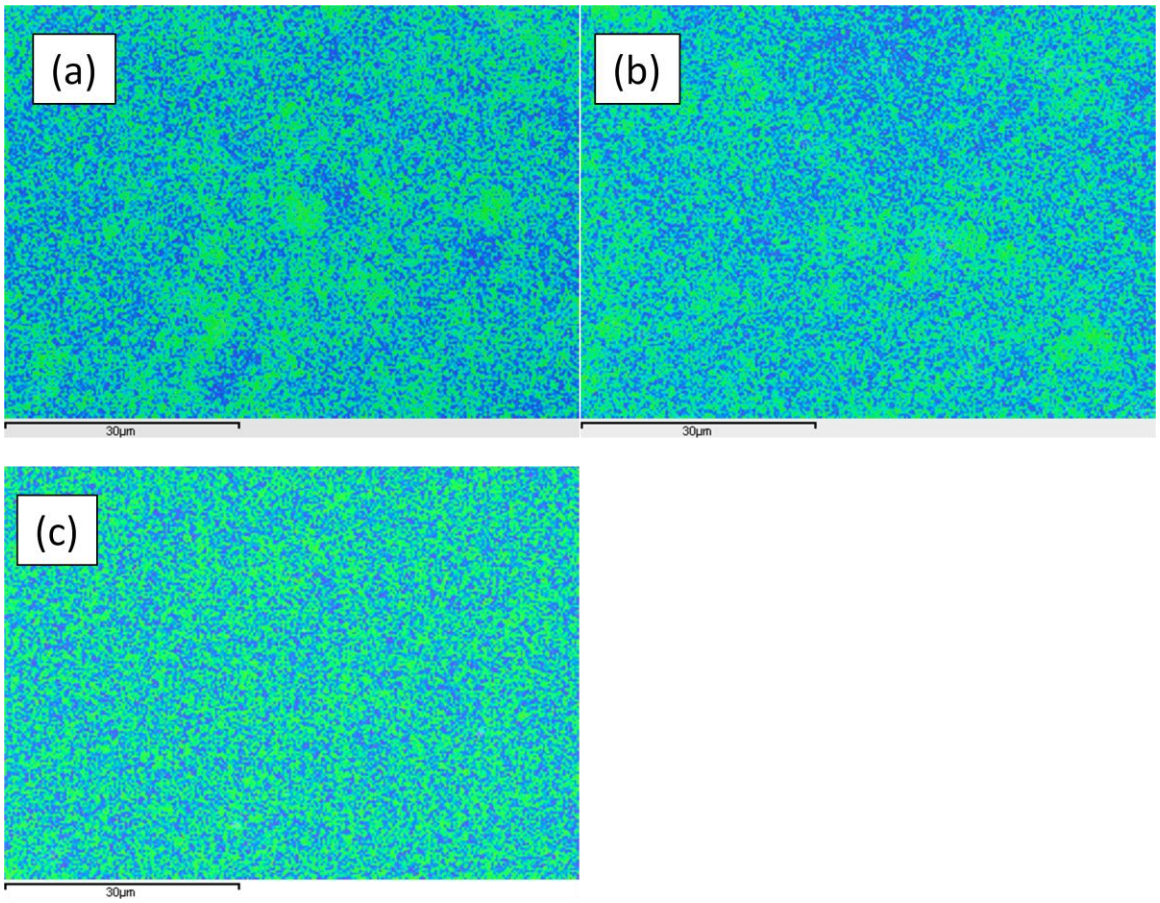

Figure 4.3 EDS scans of alumina (green) and silica (blue) of mixtures REHPS mixed through a capillary nozzle geometry consisting of a 10 cm long 508 µm nozzle and an inlet tube diameter of (a) 762, (b) 1524, (c) 3175 µm.

Table 4.2 Scale of Segregation of REHPS Mixed Powders Through 10 cm Long Nozzles

Len_{Nozzle} 10 cm	D_{Nozzle} (µm)			
D_{Inlet} (µm)	508	762	1013	1524
762	1.7 (± 0.4)	-	-	-
1524	1.6 (± 0.4)	1.7 (± 0.4)	-	-
3175	1.5 (± 0.2)	-	2.3 (± 1.1)	3.5 (± 2.2)

Table 4.3 Scale of Segregation of REHPS Mixed Powders Through 3 cm Long Nozzles

Len_{Nozzle} 3 cm	D_{Nozzle} (μm)			
D_{Inlet} (μm)	508	762	1013	1524
762	2.2 (± 1.2)	-	-	-
1524	2.0 (± 0.4)	2.3 (± 0.3)	-	-
3175	1.6 (± 0.1)	-	2.4 (± 0.5)	3.2 (± 3.2)

Nanopowders were also mixed via the REHPS process using the de Laval nozzle described in Figure 4.1b. The representative EDS image shown in Figure 4.2d indicates a fairly poor mixture, which is supported by a scale of segregation value of 2.1 (± 1.2), which is comparable to the values for the powder expanded through the 2 cm long capillary nozzle, listed in Table 4.3. The SOS value of the powder expanded through the de Laval nozzle is slightly lower than the comparably sized capillary nozzle (D_{Inlet} = 3175 μm, D_{Nozzle} = 1013 μm, L_{Nozzle} = 3 cm). Considering that lower mixing qualities are associated with shorter nozzle lengths and straight section in the de Laval nozzle is comparably smaller any of the capillary nozzle configurations, it can be assumed that the supersonic flow and impaction with the Mach disc contribute to the deagglomeration and mixing of the nanopowders, however it is likely that the shear induced deagglomeration is dominant.

Dry ice precipitation was observed to occur during expansion, which has previously been shown to introduce more inhomogeneity into the REHPS mixtures. To ensure this was not confounding the mixing results, high pressure nitrogen gas (P = 3.8

MPa, T = 20^{o}C) was used in a REHPS mixing experiment, so that carbon dioxide precipitation could be avoided (critical temperature: 126.19 K, triple temperature = 63.14 K)[63]. The EDS scan of the mixed powder can be seen in Figure 4.2e. The corresponding scale of segregation and intensity of segregation are 7.5 (± 5.4) and 56 (± 55)(10^{-3}), respectively. This indicates that dry ice formation is not confounding the mixing results during the flow and subsequent expansion through the nozzle and supports the finding that the shockwave does not have a significant effect on nanopowder mixing in the de Laval nozzle.

The deviation between the results presented in this study and those that were previously presented by Brandt et al.[45] can be explained based on two notable differences. The first is that the experiments in the previous studies were performed within a shock tube capable of producing significantly stronger shockwaves than within those presented here in the de Laval nozzle (~1.1 bar). The nanopowders with the high specific surface area (200 m^2/g, comparable to those investigated in this study, 130 m^2/g) could not be deagglomerated at this shock strength. Significant deagglomeration did not occur until the strength of the shockwave approached 3 bar. Unfortunately this shock strength is unattainable with carbon dioxide in the REHPS apparatus, as attempts to increase the shock strength (i.e. increasing upstream pressure) leads to dry ice precipitation. The second difference is that the sizes of the deagglomerated agglomerates were listed as count weighted median radius, which gives little weight to the larger agglomerate sizes that will dominate EDS elemental maps and the volume weighted size distributions described Chapters 4.3.1 and 4.3.2, respectively. While the shockwave may indeed be capable of deagglomeration nanopowders, the shock strength created in the

REHPS process is not powerful enough to significantly enhance the deagglomeration and mixing.

Table 4.4 Intensity of Segregation of REHPS Mixed Powders Through 10 cm Capillary Nozzles

Len_{Nozzle} 10 cm	D_{Nozzle} (μm)			
D_{Inlet} (μm)	508	762	1013	1524
762	3.4 (± 0.7)(10^{-3})	-	-	-
1524	2.9 (± 0.8)(10^{-3})	2.7 (± 0.7)(10^{-3})	-	-
3175	3.1 (± 0.9)(10^{-3})	-	4.6 (± 4.1)(10^{-3})	9.0 (± 2.9)(10^{-3})

Table 4.5 Intensity of Segregation of REHPS Mixed Powders Through 3 cm Capillary Nozzles

Len_{Nozzle} 3 cm	D_{Nozzle} (μm)			
D_{Inlet} (μm)	508	762	1013	1524
762	3.6 (± 1.0)(10^{-3})	-	-	-
1524	2.4 (± 0.3)(10^{-3})	4.3 (± 0.2)(10^{-3})	-	-
3175	2.5 (± 0.6)(10^{-3})	-	8.6 (± 0.1)(10^{-3})	49 (± 37)(10^{-3})

The intensity of segregation of the REHPS mixed nanopowders, shown in Tables 4.4 and Table 4.5, indicate similar trends to those described for the SOS. Specifically the intensity of segregation tends to increase with decreasing inlet diameter, increasing nozzle size and decreasing nozzle length. It should be noted that the IOS values limited

information about agglomerate size scale and have significantly more variability than the scale of segregation values described above, especially for poor mixtures (i.e. at higher IOS values)[64]. The scale of segregation, on the other hand, incorporates information about the concentration as well as the spatial location and therefore yields a highly detailed description of the mixing quality and characteristic agglomerate size. At larger nozzle diameters the intensity of segregation for the 3 cm long nozzle becomes significantly larger than that of the 10 cm long nozzle (i.e. as the mixture quality decrease).

The intensity of segregation of the nanopowders expanded through the de Laval nozzle was 8.3 (± 1.0)(10^{-3}). This high IOS values is comparable to the powders expanded through the 2 cm long capillary nozzle with a diameter of 1013 μm and an inlet diameter of 3175 μm. This coincides with the observations made for the scale of segregation, which again suggests that the Mach disc may not have a significant effect on the deagglomeration and mixing process.

4.3.2 REHPS Deagglomeration

Table 4.6 Median Volume Weighted Size of Silica R972 Expanded Through 10 cm Capillary Nozzles Measured via SMPS

Len_{Nozzle} 10 cm	D_{Nozzle} (μm)			
D_{Inlet} (μm)	508	762	1013	1524
762	231	-	-	-
1524	211	270	-	-
3175	224	-	282	290

Table 4.7 Median Volume Weighted Size of Silica R972 Expanded Through 3 cm Capillary Nozzles Measured via SMPS

Len_{Nozzle} 3cm	D_{Nozzle} (μm)			
D_{Inlet} (μm)	508	762	1013	1524
762	246	-	-	-
1524	254	280	-	-
3175	249	-	288	288

Deagglomeration studies were performed on silica R972 using the Scanning Mobility Particle Spectrometer (SMPS) equipped with the Nanoparticle Aggregate Module and SEM imaging in conjunction with image analysis to explore the effect of the nozzle geometry on the expanded agglomerate size. The median agglomerate sizes, measured by the SMPS, are listed in Table 4.6 and Table 4.7 for powders expanded through 10 cm and 3 cm long nozzles, respectively. It should be noted that the SMPS was used to measure the fine fraction of the agglomerate size distribution with a measurement range between 33 and 752 nm. It can be seen that the listed sizes generally agree with the observed trends for the scale and intensity of segregation results that were discussed in Chapter 4.3.1, specifically that the agglomerate size decreases with increasing inlet diameter, decreasing nozzle diameter and increasing nozzle length. The median agglomerate size of the nanopowders expanded from the de Laval nozzle, as extracted from the SMPS, was 338 nm. This agreement between agglomerate size and mixing quality supports the hypothesis that an improvement in the deagglomeration efficiency also leads to an improvement in the mixing quality (i.e. lower IOS and lower SOS).

Additional sizing experiments were performed by collecting the silica agglomerates by diffusion onto silicon chips. The agglomerates were then imaged by electron microscopy and subsequently sized via image analysis. The resulting size distributions are plotted in Figures 4.4-4.6. The effect of the nozzle diameter is explored in Figure 4.4 by varying the nozzle diameter while keeping the inlet diameter constant. It can be seen that as the nozzle diameter increases the cumulative size distribution shifts to the right and therefore towards larger agglomerate sizes. The size distributions shown here describes much larger median sizes than those extracted from the SMPS representing the fine fraction of the agglomerates listed in Tables 4.6 and 4.7, however it can be seen that these results show a similar trend to the size results presented in Table 4.6 and the scale of segregation results presented in Table 4.2. The effect of the inlet diameter is explored in Figure 4.5 where the nozzle diameter was kept constant while the inlet diameter was varied. There is a slight trend of increasing size distribution with decreasing inlet diameter. The increase in inlet diameter has a less significant effect on the agglomerate size than the nozzle diameter. The effect of nozzle length was investigated in Figure 4.6. The results show that as the nozzle length decreased the expanded agglomerate sizes slightly increased. These agglomerates produced from the capillary nozzle were comparable to those produced from the de Laval nozzle, which confirms the results discussed in Chapter 4.3.1.

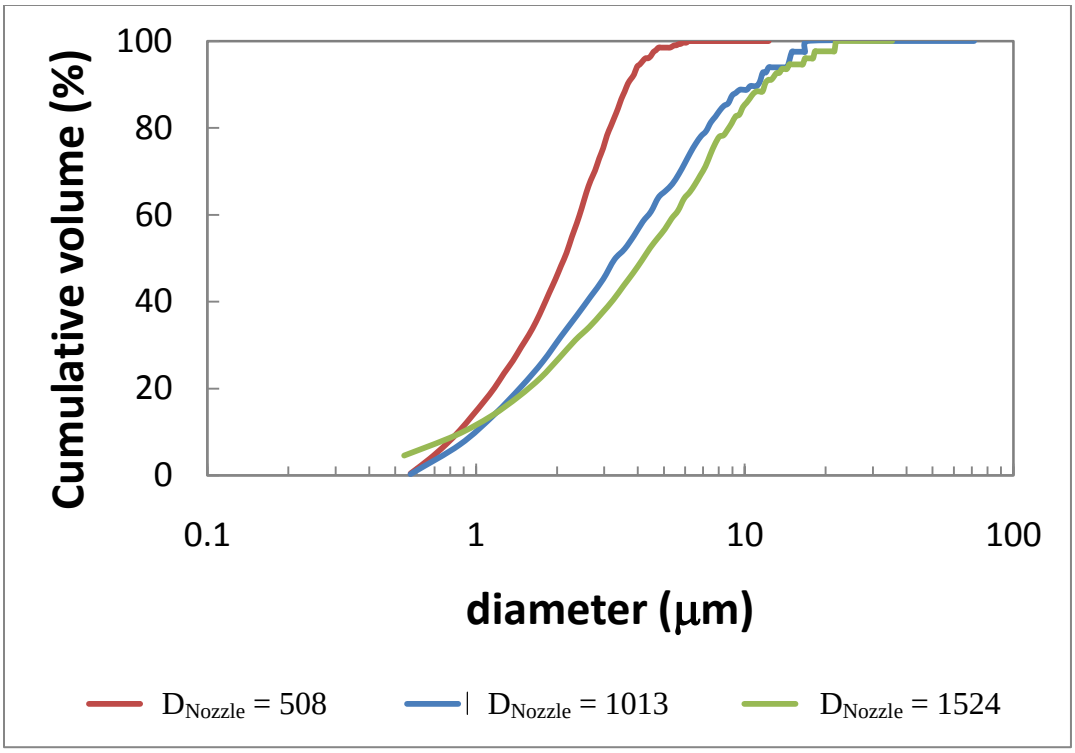

Figure 4.4 Cumulative size distributions of silica R972 nanopowders passing through a nozzle geometry consisting of a 3175 μm inlet and 10 cm long nozzles with a varying diameter.

These results coincide with the work of Kousaka et al.[44], who dispersed sub-micron particles of $CaCO_3$ and Fe_2O_3 powders through both capillary and venturi nozzles. These results indicated that capillary nozzles produce similar agglomerate sizes to a venturi nozzle with the same apex diameter. While it should be noted the agglomerates did not pass through supersonic conditions or a Mach disc however the results are qualitatively similar. These results also correspond well with the findings of Zumaeta et al.[47] who showed that longer nozzles enhanced agglomerate breakage, gradual contraction from an inlet to the nozzle diminishes agglomerate breakage.

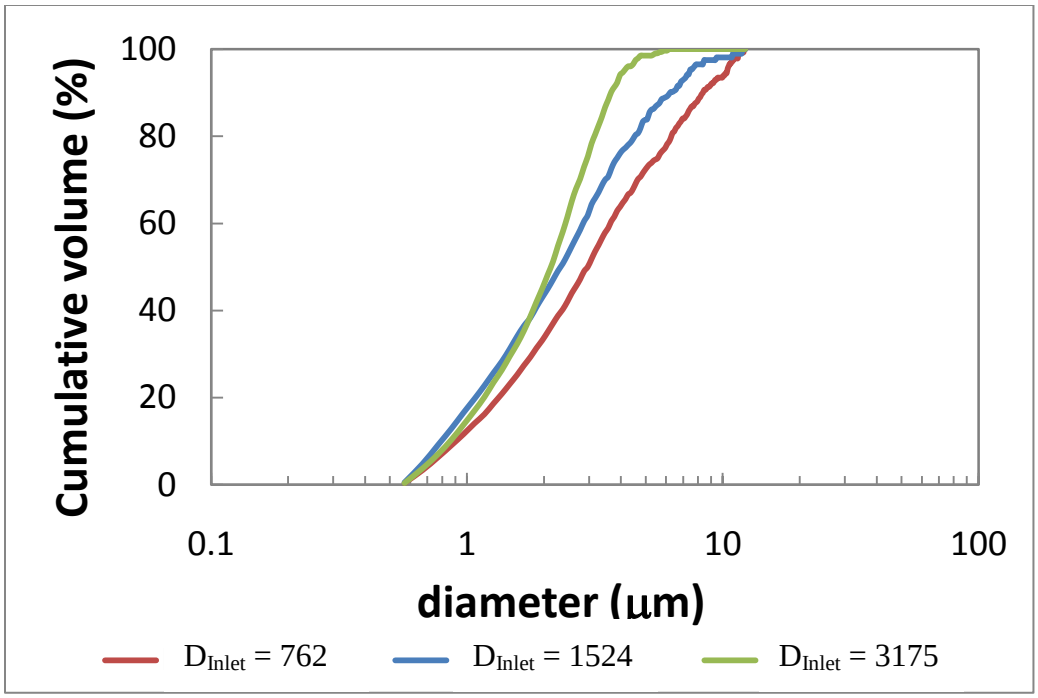

Figure 4.5 Cumulative size distributions of silica R972 nanopowders passing through a nozzle geometry consisting of inlets of varying diameters and a 10 cm long nozzle with a diameter of 508 μm.

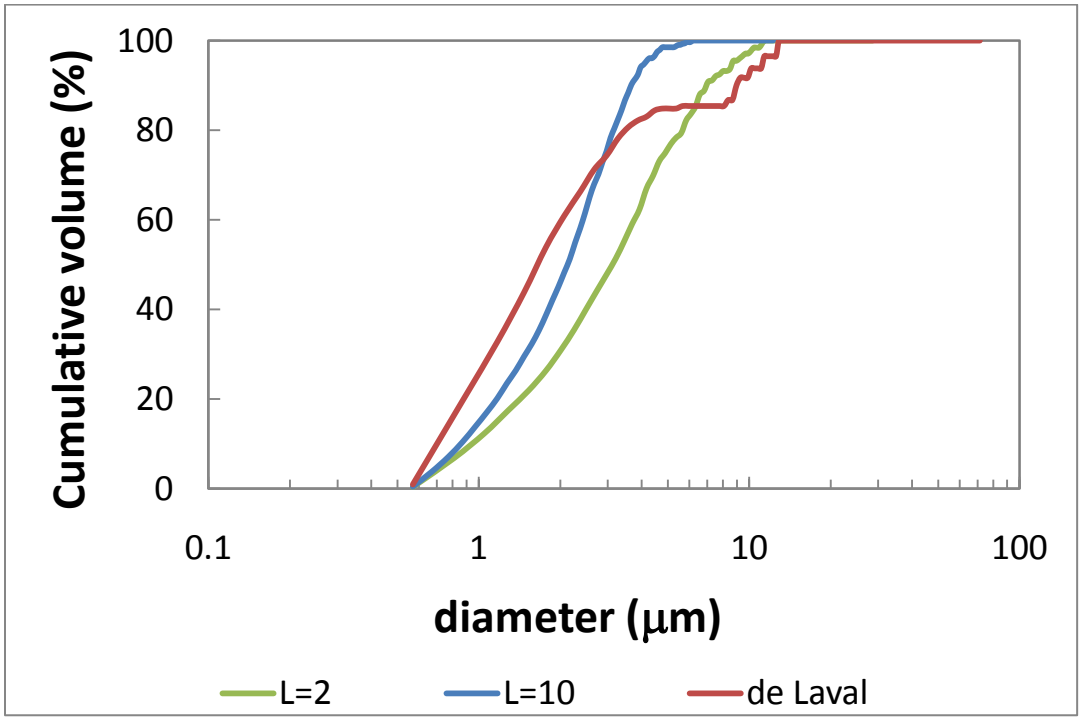

Figure 4.6 Cumulative size distributions of silica R972 nanopowders passing through either a capillary nozzle geometry consisting of 3175 μm inlet and a 508 μm nozzle with varying lengths or a de Laval nozzle.

4.3.3 Stresses in the REHPS Process

In this Chapter the various potential deagglomeration mechanisms (elongation and turbulent shear stress) will be explored through a simple stress analysis. The centerline gas pressure, temperature, density and Mach number were calculated using the one-dimensional mass and energy conservation equations shown in equations 4.1-3, which is identical to that in Weber and Thies,[65, 66]. The centerline properties were calculated with the Span and Wagner equation of state[67]. An example of the centerline properties are depicted in Figure 4.7, which represents the flow of carbon dioxide from a 3175 μm inlet tube and through a 10 cm long capillary nozzle with a diameter of 508 μm. At the interface between the inlet tube and the capillary nozzle it was assumed that a contraction from the inlet diameter to the nozzle diameter occurs over a length of 1 cm. A friction factor of 0.005 was assumed in the straight section of the nozzle. The flow inside the inlet tube was not modeled because the flow inside the inlet tube has a near zero Mach number resulting in nearly incompressible flow and a sufficiently low velocity that friction will not be significant.

$$\frac{d\rho}{\rho}+\frac{1}{2}\frac{dV^2}{V^2}=-\frac{1}{A}\frac{dA}{dx}dx \tag{4.1}$$

$$\frac{dP}{\rho V^2}+\frac{1}{2}\frac{dV^2}{V^2}=-\frac{2f}{D_{Nozzle}}dx \tag{4.2}$$

$$dh+\frac{1}{2}dV^2=\frac{w\pi D_{Nozzle}}{\dot{m}}dx \tag{4.3}$$

It can be seen that at the entrance of the nozzle there is a drastic decrease in centerline pressure, temperature and density due to the contraction in the diameter as the flow transitions from the inlet tube to the nozzle. The conservation of momentum also leads to a rapid increase in velocity, as described by the rapid change in the Mach number, which

is defined as the ratio of the velocity and the speed of sound. As the fluid proceeds along the length of the nozzle, the velocity increases towards the speed of sound. The effect of the nozzle geometry on the centerline properties are explored in Figures 4.6-4.10. When entering from a smaller inlet, as shown in Figure 4.8, the reduced contraction at the entrance resulted in reduced pressure and density losses and increased temperature and Mach numbers. As the fluid moves further into the nozzle the fluid properties nearly converge. It should be noted that while the Mach numbers are nearly identical the slightly lower temperature and slightly higher pressure and density lead to overall lower speed of sound values and therefore lower real velocities.

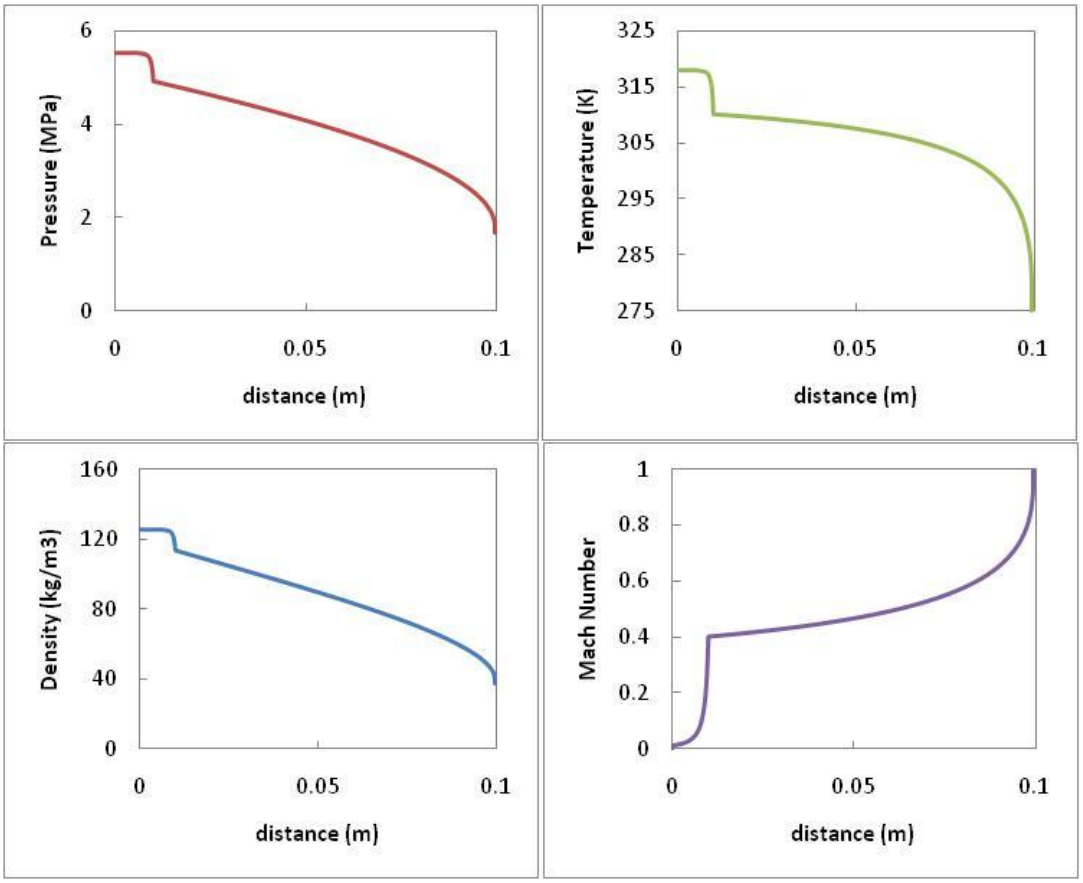

Figure 4.7 The centerline pressure, temperature, density and Mach number of the carbon dioxide flow through a capillary nozzle geometry consisting of a 3175 μm inlet and a 10 cm long 508 μm nozzle.

The high velocities and expected to produce turbulent shear stresses that will also result in agglomerate breakage. At the entrance and exit of the nozzle, where there are significant velocity gradients, elongation forces are also expected to result in deagglomeration. These stresses have been calculated from the centerline properties, like those shown in Figure 4.7 and will be discussed in more detail below.

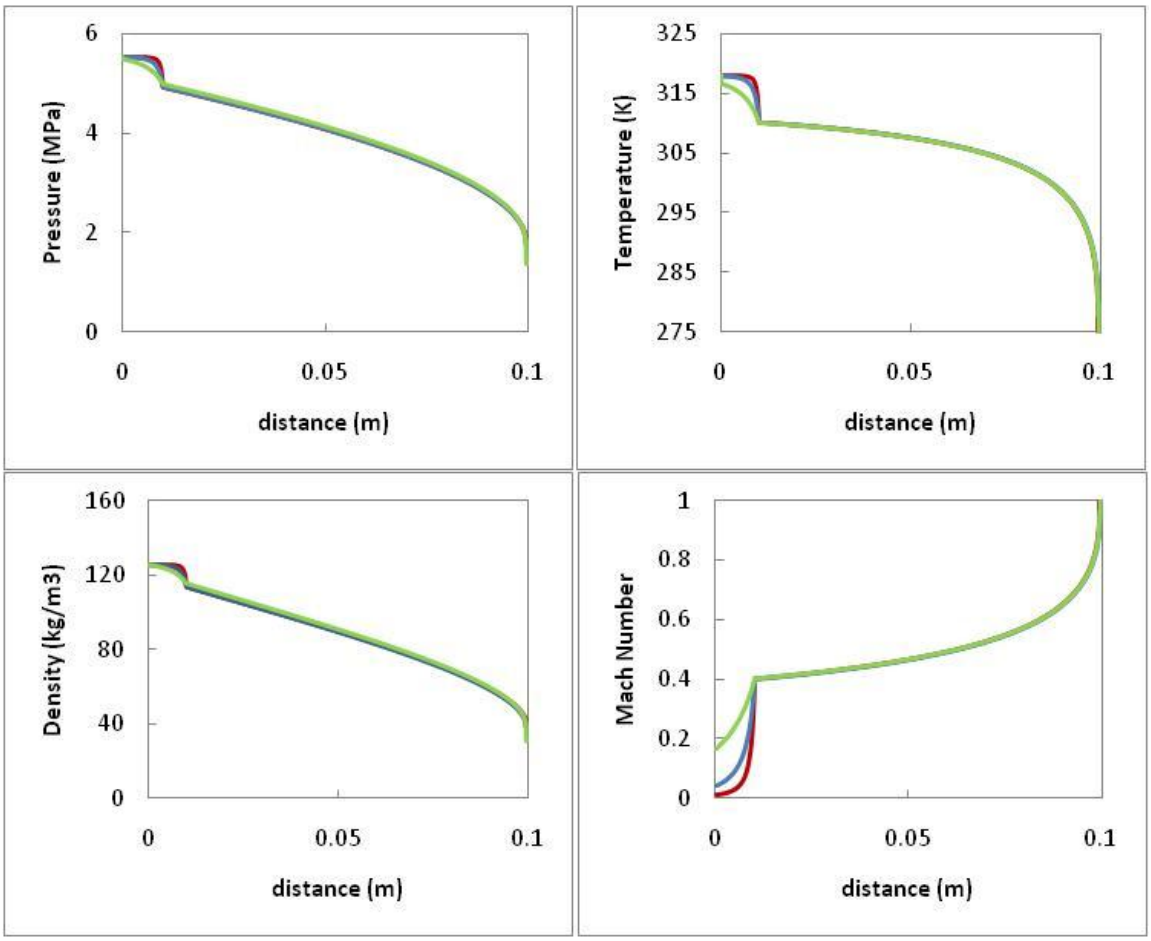

Figure 4.8 The centerline pressure, temperature, density and Mach number of the carbon dioxide flow through a capillary nozzle geometry consisting of a 10 cm long 508 μm nozzle and a varying inlet diameters: 3175 μm (red), 1524 μm (blue), 762 μm (green).

Figure 4.9 shows the effect of the nozzle diameter on the fluid properties inside of the nozzle. As the nozzle diameter increases a decrease in the pressure and density can

be observed due to the smaller contraction in the nozzle diameter (i.e. compaction of the fluid at the entrance). As the fluid proceeds down the nozzle the pressure and density increases in comparison to smaller nozzles because of the lower heat loss due to friction. It can also be seen that larger nozzle diameters have lower temperatures and higher overall Mach numbers along the length of the nozzle. Again, the actual speed of sound is larger at higher temperatures and lower pressures and densities, which coincides with smaller nozzle sizes.

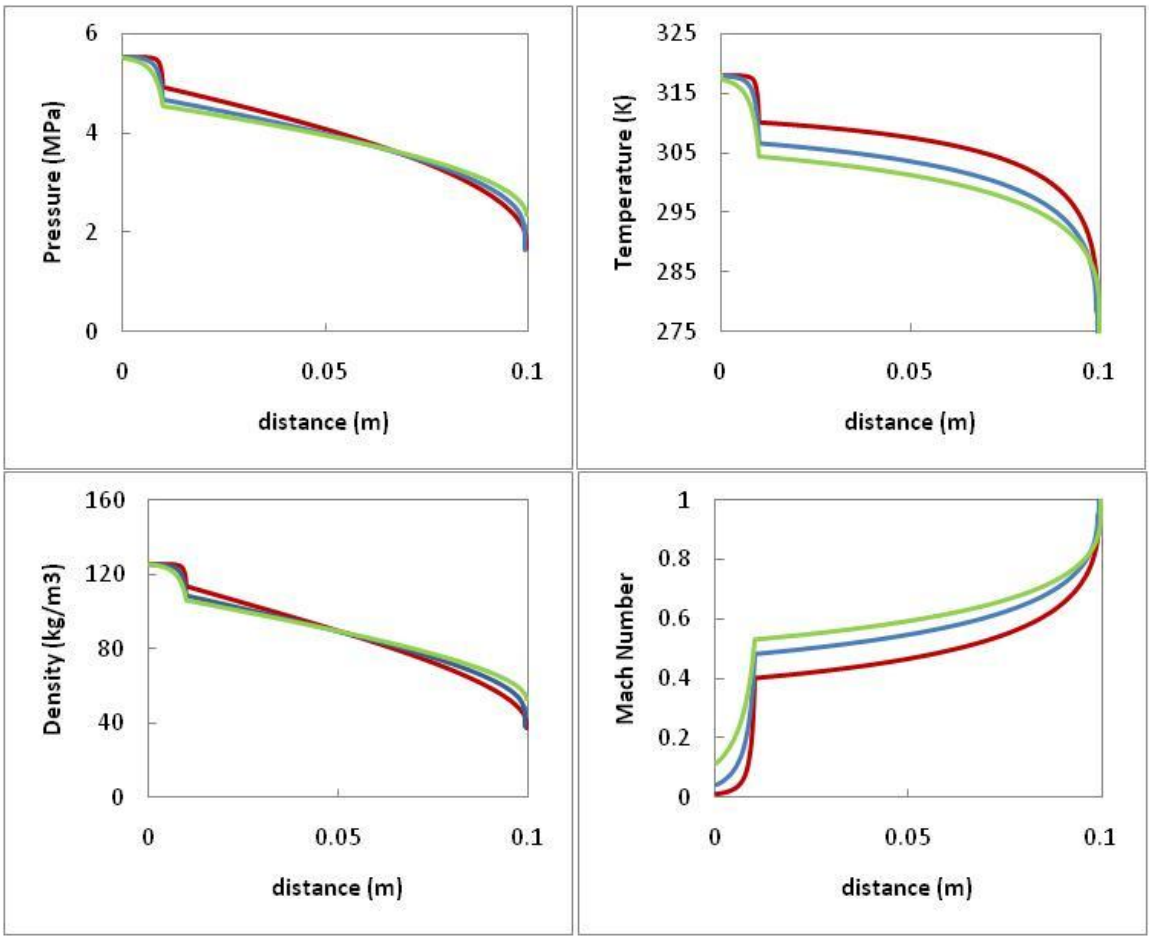

Figure 4.9 The centerline pressure, temperature, density and Mach number of the carbon dioxide flow through a capillary nozzle geometry consisting of a 3175 μm inlet tube and a 10 cm long nozzle of varying diameters: 508 μm (red), 1013 μm (blue), 1524 μm (green).

Investigation of the turbulent shear stresses imparted by the fluid onto the agglomerate can help to understand the effect of the nozzle geometry on the agglomerate breakage. The turbulent shear stress, τ_t, was calculated using equations 4.4-4.5, using the centerline properties depicted in Figures 4.8-4.9.

$$\varepsilon = \frac{fV^3}{D_{Nozzle}} \tag{4.4}$$

$$\tau_t = 0.49\rho_f \left(\frac{\varepsilon^3}{\nu}\right)^{0.25} L_{agg} \tag{4.5}$$

During the calculation of the turbulent shear stress it was assumed that the agglomerate size (L_{agg}) was on the scale of 1 μm for all nozzle geometries as indicated by SEM size analysis. The elongation stresses, τ_e, were also calculated, using equation 4.6. Equation 4.4 describes the energy dissipation rate of steady state flow through a straight pipe[51]. Equations 4.5 and 4.6 are similar to those described in Weiler et al.[68] and Wengeler et al. [69], respectively.

$$\tau_e = \mu \frac{dV}{dx} V \tag{4.6}$$

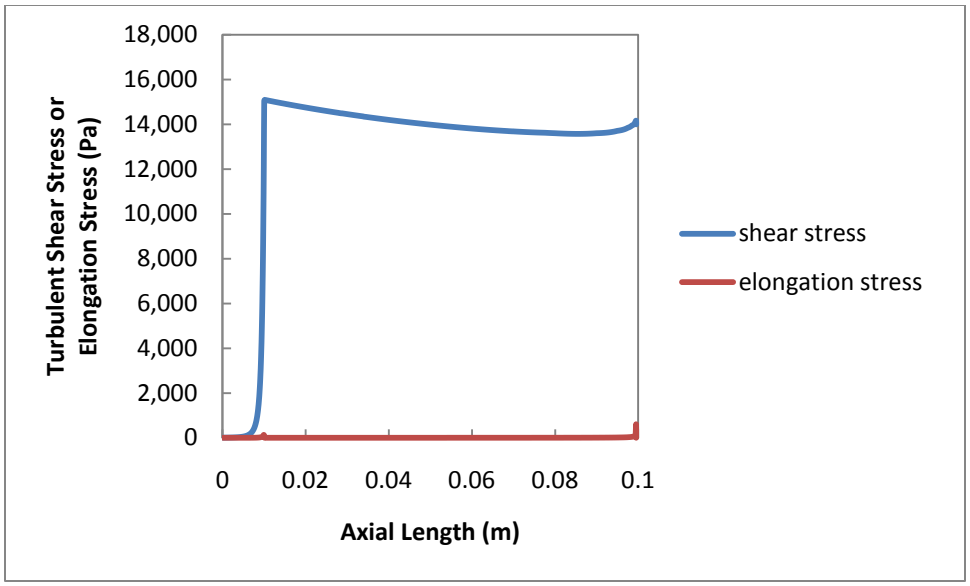

Figure 4.10 The turbulent shear stress and Elongation stress plotted as a function of axial length.

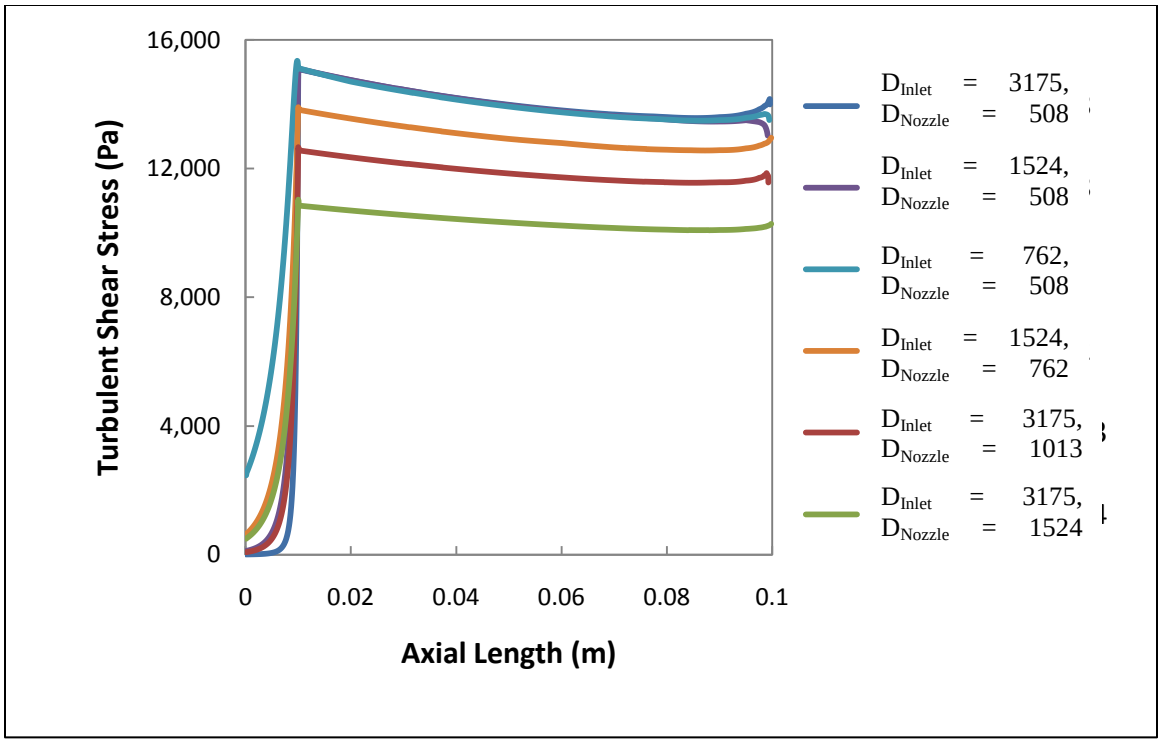

Figure 4.11 The turbulent shear stress plotted as a function of axial length.

The turbulent shear stress and the elongation stress are plotted as function of axial location along the length of the nozzle in Figures 4.10. When comparing the turbulent shear stress and the elongation stress it can be seen that the maximum turbulent shear stress is nearly two orders of magnitude larger than the maximum elongation stress. As a result it is believed that the elongation stresses do not play a significant role in the deagglomeration. It can be seen that the turbulent shear stress increases from nearly zero at the entrance to its maximum value in the nozzle, which coincides with the sharp increase in the Mach number (and thereby velocity) due to the contraction from the inlet to the nozzle. As the fluid progresses down the length of the nozzle, the turbulent shear stress decreases, even as the Mach number increases, due to the significant decrease in density and viscosity. The maximum turbulent shear stress decreases as the nozzle diameter decreases, due to a reduction in the energy dissipation rate, ε, described in equation 4.4. This coincides with the results deagglomeration and mixing results described in Chapter 4.3.1 and 4.3.2. When comparing the turbulent shear stress of the fluid flow through the 508 μm nozzles from different inlet tubes it can be seen that values decrease slightly for smaller inlet tubes, due to lower speed of sound values (at higher fluid pressures and densities) and therefore lower overall velocities. While application of the maximum shear stress is important in the breakage of agglomerates[69], it has been established that the residence time under shear is also important in agglomerate breakage[47, 70-73]. The effect of the residence time is explored by weighting the shear stress by the residence time ($\Delta t=\Delta x/\Delta V$), as described by equation 4.7. It was assumed that the small shear stress values, near the entrance of the nozzle were neglected during the time weighting process as they were expected yield insignificant breakage. Only the

shear stress on the same scale as the maximum value was (i.e. at nozzle lengths between 0.01 m – 0.1 m). These values are listed in Table 4.8.

$$\bar{\tau}_t = \frac{\sum \tau_{ti} \times (t_{i+1} - t_i)}{residence\ time} \tag{4.7}$$

It can be seen that the shear stress*time values liste in Table 4.8 correlate well with the deagglomeration and mixing results presented in Chapter 4.3.1 and 4.3.2. The idea of coupling shearing forces with residence time has been explored in homogenization studies by investigating the effect of multiple passes through high pressure homogenizers[47, 70, 72] or homogenization time in rotor stators systems[71, 73]. In this system the residence time was varied by decreasing the nozzle length. It should be noted that agglomerate nozzle configuration are not assumed to be at steady state. Therefore longer residence times will be assumed to produce more breakage. In Figure 4.11, it can be seen that the pressure and density and temperature decrease more rapidly and the Mach number increases more rapidly in the 3 cm nozzle in comparison to the 10 cm nozzle. It can also be seen that the final pressure and density are higher in the smaller nozzle than the larger nozzles due to the smaller frictional. The differences in the shear stress can be explained by the coupled shear stress*time parameters listed in Table 4.8. This indicates that longer residence times enhance agglomerate breakage. It can be not4ed that the coupled (shear stress)*time values for the 3 cm and 10 cm nozzles do not correspond well with each other. This can be explained by the difference in the maximum shear stress between similar nozzle configurations with different lengths. Larger maximum shear stress values are expected yield more significant deagglomeration.

Table 4.8 Time Averaged Turbulent Shear Stress on Agglomerates and the Residence Time in 3 and 10 cm Nozzles

Configuration		Len_{Nozzle} 10 cm		Len_{Nozzle} 3 cm	
Inlet Diameter (μm)	Nozzle Diameter (μm)	Time-Averaged Turbulent Stress (Pa x 10^3)	Residence time (ms)	Time-Averaged Turbulent Stress (Pa x 10^3)	Residence time (ms)
3175	508	14.1	0.76	26.4	0.13
1524	508	14.0	0.76	26.6	0.13
762	508	14.0	0.76	27.1	0.13
1524	762	13.0	0.70	22.0	0.12
3175	1013	11.9	0.65	18.6	0.12
3175	1524	10.4	0.62	14.8	0.11

The Span and Wagner equation of state could not be used to estimate the centerline properties of the flow through the diverging section of the de Laval nozzle as dry ice formation was observed to occur during expansion. In an attempt to estimate the centerline fluid properties in the de Laval nozzle, the properties in the converging and straight sections were first calculated using the Span and Wagner equation of state. The fluid properties in the diverging section were estimated using the ideal gas law. The strength of Mach disc was calculated using normal shock tables[74].

The maximum shear stress and (shear stress)*time in the straight section of the de Laval nozzle was estimated to be 7.3 (10^4) Pa and 2.7 Pa-s, respectively. The maximum shear stress value is comparable to the maximum shear stress for the 1013 μm nozzle with a length of 3 cm, which qualitatively agrees with and the size and mixing results that were previously shown. It should be noted that the (shear stress)*time is significantly smaller than that of the 1013 μm x 3 cm capillary nozzle due to the significantly smaller residence time in the straight section. Deagglomeration and mixing experimental results produced by rapid expansion through the de Laval nozzle indicate considerably different trends from those predicted by the impaction induced model describing interactions with the Mach disc (see Table B.4 in Appendix B) and therefore suggests that turbulent shear stress (not impaction with the Mach disc) dominates in the de Laval nozzle.

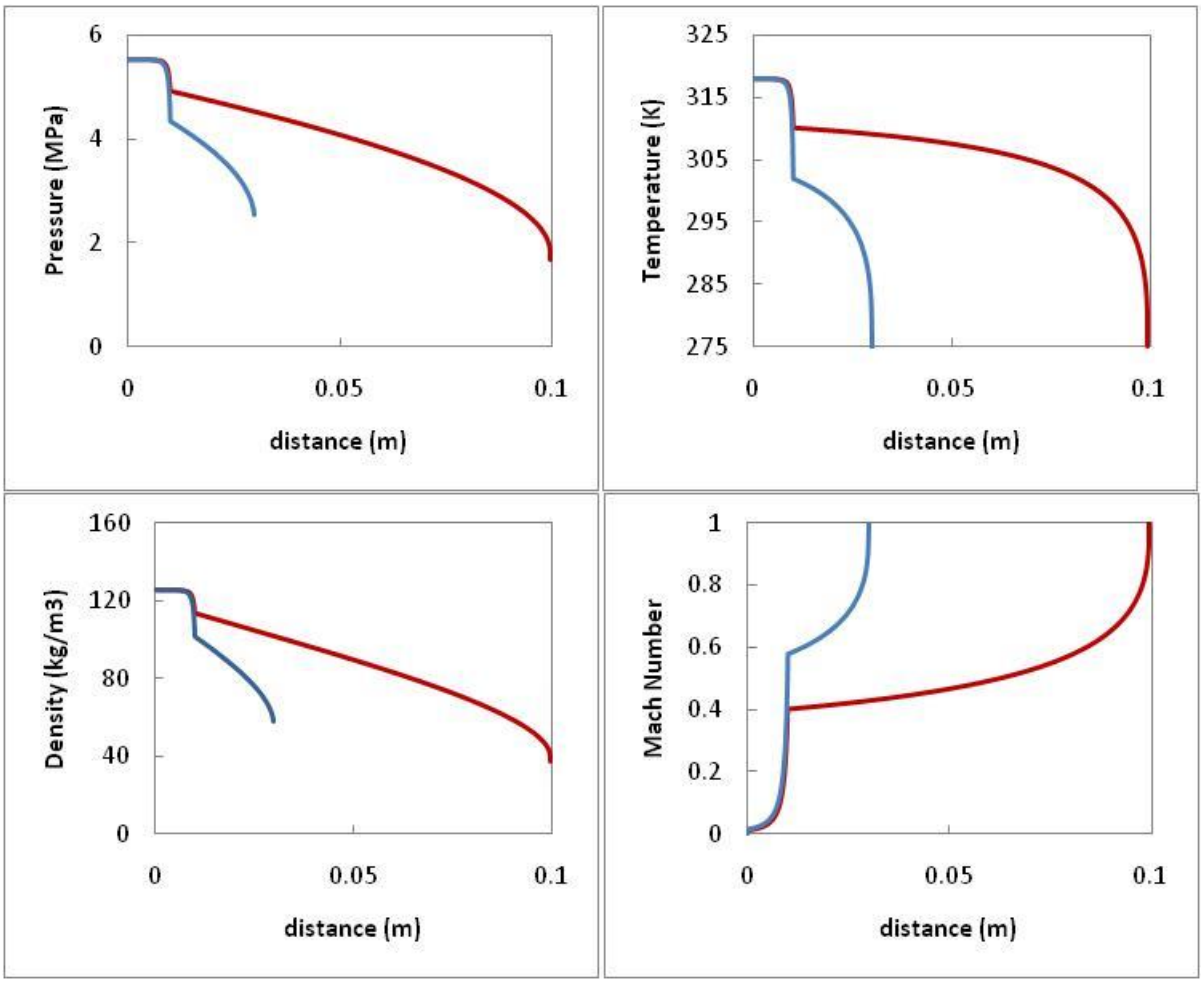

Figure 4.12 The centerline pressure, temperature, density and Mach number of the carbon dioxide flow through a capillary nozzle geometry consisting of a 3175 μm inlet tube and a 508 μm nozzle of varying lengths: 10 cm (red), 3 cm (blue).

The length scale of the maximum energy dissipation rate, as described by equation 1.2 is listed in Table 4.9. It can be seen that this length scale increases nearly linearly with increasing nozzle size. When comparing this length scale to the SOS values described in Tables 4.2 and 4.3, it can be seen that the SOS also increases nearly linearly with the maximum energy eddies, similar to the results shown in Chapter 3.4.3. This again suggests that the turbulent shear stress imparted by the fluids may be significant in the breakage of the agglomerates. The length scale of the maximum energy eddies for

the shorter nozzles are comparable to but slightly smaller than those of the larger nozzles, which suggests enhanced deagglomeration and contradicts the experimental results. It is possible that the shorter residence times, described in Table 4.9, lead to incomplete deagglomeration and that longer residence times are required to completely deagglomerate these nanopowders.

Table 4.9 Length Scale of the Maximum Energy Eddies for Each Nozzle Configuration

Inlet Diameter (μm)	Nozzle Diameter (μm)	Max Energy Eddy length for 10 cm nozzle (μm)	Max Energy Eddy length for 3 cm nozzle (μm)
3175	508	5.2	4.9
1524	508	5.1	4.9
762	508	5.2	5.0
1524	762	7.3	7.1
3175	1013	9.3	9.1
3175	1524	13.0	12.7

4.4 Conclusions

The Rapid Expansion of High Pressure and Supercritical Suspensions (REHPS), an environmentally benign method to efficiently deagglomerate and mix nanoparticles agglomerates was studied to elucidate the primary deagglomeration mechanism. This was accomplished by performing REHPS deagglomeration and mixing experiments through various capillary nozzle geometries (specifically geometries with varying length,

diameter and inlet sizes) and a de Laval configuration that were able to emphasize specific deagglomeration mechanisms. The centerline fluid properties through the different nozzle geometries were estimated using a one-dimensional flow model. The mixing quality and the deagglomeration efficiency were shown to qualitatively agree with the length scale of the maximum energy eddies, estimated by the simulated flow properties. This was shown by the nearly linear agreement between scale of segregation and the eddy length scale. It was also shown that residence time under shear is likely to play a significant role in the breakage of the agglomerates. The turbulent shear stress was also estimated from the centerline properties and shown to qualitatively agree with the eddy length scale results. These results suggest that turbulent shear stress in the nozzle is likely to be the dominant deagglomeration mechanism. Finally it was shown that the Mach disc did not have a significant influence on the REHPS process, as opposed to what was previously suggested; the shock wave developed in the REHPS process is not powerful enough to efficiently break up the nanoparticles agglomerates.

CHAPTER 5

CONCLUSIONS

The environmentally benign mixing method of the Rapid Expansion of High Pressure and Supercritical Suspensions (REHPS) was investigated to understand the production of high quality mixtures of nano-powders. This present study differs from previous REHPS studies for two significant reasons, such as: (1) improvements in the experimental methods were introduced into the REHPS process while improved characterization methods capable made distinguishing between different high quality mixtures, were used; (2) REHPS deagglomeration experiments were performed in parallel to mixing experiments to develop a better understanding of the REHPS process, determining the effect of the processing parameters (i.e. pressure, nozzle diameter, nozzle length and inlet tube diameter) and ultimately to elucidate the primary deagglomeration mechanisms.

In the present study, two characterization methods having better resolution capabilities were used to analyze the mixing quality of the REHPS samples. In the previous REHPS mixing study, the quality of the mixtures were determined by comparing a characteristic elemental ratio at 20 random points via Energy Dispersive X-ray Spectroscopy (EDS) of a loose powder sample. Additionally, constant pressure was not maintained during expansion, allowing the reactor pressure to decrease by nearly 30%. This consideration led to the present study where REHPS mixed powders were characterized by two more sensitive characterization methods capable of differentiating between multiple high quality mixtures. First, the constituent concentration was measured at 400 sites to determine the intensity of segregation where a pressed pellet was used to minimize the effect of sample topology when using EDS-SEM. Next, an

elemental mapping of alumina was obtained through EDS-SEM analysis to determine the scale of segregation, which was introduce here for nanopowders mixtures and can be correlated to the size of the agglomerate, and thus an improvement over the elemental ratio reported in previous studies[16, 17] that does not provide any physical interpretation of the mixing quality.

In addition to enhanced experimental and characterization procedures performed during this REHPS mixing investigation, the first REHPS deagglomeration experiments were also performed where two characterization methods that were capable of measuring the size of the deagglomerated nanopowders fragments were used. These methods included online characterization of the agglomerate sizes by the SMPS and collection of the agglomerates by diffusion onto a silicon substrate and subsequent imaging and analysis via electron microscopy. These deagglomeration experiments show that the REHPS process was capable of producing the sub-micron fragments of nanoparticle agglomerates. Additionally these agglomerate sizes increased significantly with nozzle diameter and less significantly with a decrease in inlet diameter, nozzle length and expansion pressure. These results agreed qualitatively with the mixing results and showed that conditions that led to enhanced deagglomeration also typically led to higher quality mixtures, however this effect could be obscured by inhomogeneities introduced by the feed mixtures.

Preliminary results were also presented for two practical applications of REHPS for creating nano-composites. Results for the use of REHPS for formation of mullite, an alumino-silicate valued for its refractory properties, indicate that the mixing quality has direct effect on degree of mullite formation. Second, composites containing complex

materials such as carbon nanotubes, which have not been previously explored with the REHPS process, were considered and it was shown that REHPS can not only deagglomerate carbon nanotube bundles but also mix them at sub-micron scale with nano-powders of alumina, silica and titania.

The deagglomeration and mixing experiments were coupled with complementary modeling was performed to elucidate the primary deagglomeration mechanism responsible for the agglomerate breakage and subsequent mixing. Previous authors have suggested that the primary deagglomeration mechanism is the explosive expansion of the carbon dioxide from within the agglomerate as it transitions from a high pressure to an ambient environment. Two deagglomeration mechanisms were proposed during this study, namely intense turbulent shear stress imparted by the fluid in the nozzle and impaction with the Mach disc near the exit of the nozzle. Explosive expansion was observed to have almost no effect on nozzle deagglomeration and subsequent mixing. This was shown by the estimation of the length scale of the maximum energy eddies, which increased nearly linearly with the nozzle diameter and corresponded closely to the scale of the scale of segregation results. The turbulent shear stress was also estimated and qualitatively agreed with this length scale. Impaction with the Mach disc has played a minimal role.

REFERENCES

1. Imanaka N, Kohler J, Masui T, Adachi G, Taguchi E, Mori H. Inclusion of nanometer-sized Al2O3 particles in a crystalline (Sc,Lu)2(WO4)3 matrix *Journal of American Ceramic Society.* 2000; 83: 427-429

2. MG L. Nanomaterials for practical functional uses *Journal of Alloys Compounds.* 2008; 449: 242-245

3. Roco M. Nanoparticles and nanotechnology research *Journal of Nanoparticle Research.* 1999; 1: 1-6

4. Friedlander S. Smoke, Dust, and Haze: Fundamentals of Aerosol Dynamics. New York, NY: Oxford University Press, 2000

5. Nam CH, Pfeffer RR, Dave RN, Sundaresan S. Aerated vibrofluidization of silica nanoparticles *AIChE Journal.* 2004; 50: 1776-1785

6. Yu Q, Dave RN, Zhu C, Quevedo J, Pfeffer RR. Enhanced fluidization of nanoparticles in an oscillating magnetic field *AIChE Journal.* 2005; 51: 1971-1979

7. Kurkela J, Brown D, Raula J, Kauppinen E. New Apparatus for Studying Powder Deagglomeration *Powder Technology.* 2008; 180: 164-171

8. Yao W, Suangshen G, Fei W, Jun W. Fluidization and agglomerate structure of SiO2 nanoparticles *Powder Technology.* 2002; 124: 152-159

9. Iwasaki T, Satoh M. Characterization of powder mixers based on mechanical energy using soft dye granules *Advanced Powder Technology.* 2002; 13: 395-409

10. Van der Wel PGJ. Powder Mixing *Powder Handling Processing.* 1999; 11: 83-86

11. Fan LT, Chen YM, Lai FS. Recent developments in solids mixing *Powder Technology.* 1990; 61: 255-287

12. Vaizoglu O. Assessment of the degree of mixing of powder mixtures *Turkey Journal of Physics.* 1999; 23: 97-104

13. Barrow R, Yang J, Dave RN, Pfeffer RR. Dry-Mixing of Sub-micron Size B and BaCrO4 Particles for Use in T-10 Delay Composition *Proceedings (CD-ROM) of Fifth World Congress on Particle Technology*. 2006; Disk 2: 1-6

14. Marioth E, Kroeber H, Loebbecke S, Fuhr I, H. K. Deagglomeration and mixing of nanoparticles using the rapid expansion of supercritical dispersions *Proceedings of Partec 2007 Meeting.* 2007; S31_1

15. Scicolone JV, Sangawar GP, To D, Ermoline A, Dave RN, Gupta RB, Pfeffer R. Deagglomeration and Mixing of Nanoparticles *Proceedings of Partec 2007 Meeting.* 2007; P08_10

16. Wei D, Dave RN, Pfeffer R. Mixing and Characterization of Nanosized Powders: An Assessment of Different Techniques *Journal of Nanoparticle Research.* 2002; 4: 21-41

17. Yang J, Wang Y, Dave RN, Pfeffer RR. Mixing of Nanoparticles by Rapid Expansion of High Pressure Suspensions *Advanced Powder Technology*. 2003; 14: 471-493

18. Nelson K, Deng Y. Effect of polycrystalline structure of TiO2 particles on the light scattering efficiency *Journal of Colloid and Interface Science.* 2008; 319: 130-139

19. Seekkuarachchi IN, Kumazawa H. Aggregation and Disruption Mechanisms of Nanoparticulate Aggregates. 2. Dispersion of Aggregates Using a Motionless Mixer *Industrial Engineering and Chemical Research.* 2008; 47: 2401-2413

20. Ding P, Pacek A. Effect of pH on deagglomeration and rehology/morphology of aqueous suspension of geothite nanopowder *Journal of Colloid and Interface Science.* 2008; 325: 165-172

21. Shinohara N, Dabbs DM, Aksay IA. Infrared Transparent Mullite Through Densification of Monolithic Gels at 1250oC *Infrared and Optical Transmitting Materials.* 1986; 683: 19-24

22. Oliveira MILL, Chen K, Ferreira JMF. Influence of the Deagglomeration Procedure on Aqueous Dispersion, Slip Casting and Sintering of Si3N4-based Ceramics *Journal of the European Ceramic Society*. 2001; 22: 1601-1607

23. Ferkel H, Hellmig RJ. Effect of Nanopowder Deagglomeration on the Densities of Nanocrystalline Ceramic Green Bodies and their Sintering Behaviour *Nanostructured Materials.* 1999; 11: 617-622

24. Vol'khin VV, I.L. K, Pongratz P, Halwax E. Mullite Formation from Highly Homogeneous Mixtures of Al2O3 and SiO2 *Inorganic Materials.* 2000; 36: 375-379

25. Jinno J-I, Kamada N, Miyake M, Yamada K, Mukai T, Odomi M, Toguchi H, Kimura T. Effect of particle size reduction on dissolution and oral absorption of a poorly water-soluble durg, cilostazol, in beagle dogs *Journal of controlled Realse.* 2006; 111: 56-64

26. Smirnova I, Turk M, Wischumerski R, Wahl MA. Comparison of different methods for enhancing the dissolution rate of poorly soluble drugs: Case of griseofulvin *Engineering in Life Sciences.* 2005; 5: 277-280

27. Koybayashi Y. Theoretical Studies of Acid Gas Removal by Lime/Limestone Powder Intection *Kagaku-Kogaku Ronbunshu.* 1993; 19: 840

28. Koybayashi Y. Studies of Aggregation Effects on Sox Removal by Limestone Powder *AIChE Journal.* 1995; 41: 2642-2652

29. Weimar AW, Cochran GA, Eisman GA, Henley JP, Hook BD, Mills LK. Rapid Process for Manufacturing Aluminum Nitride Powder *Journal of American Ceramic Society.* 1994; 77: 3-18

30. Sun J, Gao L, Jin X. Reinforcement of alumina matrix with multi-walled carbon nanotubes *Ceramics International.* 2005; 31: 893-896

31. Kumari L, Zhang T, Du GH, Li WZ, Wang QW, Datye A, Wu KH. Thermal properties of CNT-Alumina nanocomposites *Composites Science and Technology.* 2008; 68: 2178-2183

32. Wei D, Dave RN, Pfeffer R. Mixing and Characterization of Nanosized Powders: An Assessment of Different Techniques. *Journal of Nanoparticle Research.* 2002; 4: 21-41

33. Nakamura H, Watano S. Fundamental particle fluidization behavior and handling of nano-particles in a rotating fluidized bed *Powder Technology.* 2008; 183: 324-332

34. Valverde JM, Quintanilla MA, Catellanos A, Lepek D, Quevedo J, Dave RN, Pfeffer RR. Fluidization of fine and ultrafine particles using nitrogen and neon as fluidizing gases *AIChE Journal.* 2008; 54: 86-103

35. To D, Yin X, Sundaresan S, Dave RN. Deagglomeration of Nano-particle Aggregates via Rapid Expansion of High-Pressure Suspensions *AIChE Journal.* 2009; 55: 2756-3032

36. Neimark AV, Koylu UO, Rosner DE. Extended Characteriztion of Combustion-Generated Aggregates: Self-Affinity and Lacunarities *Journal of Colloid and Interface Science.* 1996; 180: 590-597

37. Lee C, Kramer TA. Prediction of Three-dimensional Fractal Dimensions Using the Two-Dimensional Properties of Fractal Aggregates *Advances in Colloid and Interface Science.* 2004; 112: 49-57

38. Aoki M, Ring TA, Haggerty JS. Analysis and modeling of the ultrasonic comminution device *Advanced Ceramic Materials.* 1987; 2: 209-212

39. Ding P, Pacek A. De-agglomeration of goethite nanoparticles using ultrasonic comminution device *Powder Technology.* 2008; 187: 1-10

40. Uhland SA, Cima MJ, Sachs EM. Additive-enhanced redispersion of ceramic agglomerates *Journal of American Ceramic Society.* 2003; 86: 1487-1492

41. Le Bars N, Levitz P, Messier A, Francois M, Van Damme H. Deagglomeration and dispersion of barium titanate and alumina particles in an organic medium *Journal of Colloid and Interface Science.* 1995; 175: 400-410

42. Endo Y, Hasebe S, Kousaka Y. Dispersion of aggregates of the powder by acceleration in an air stream and its application to the evalucation of adhesion between particles *Powder Technology.* 1997; 91: 25-30

43. Voss A, Finlay W. Deagglomeration of dry powder pharmaceutical aerosols *International Journal of Pharmaceutics.* 2002; 248: 39-50

44. Kousaka Y, Okuyama K, Shimizu A, Yoshida T. Dispersion Mechanism of Aggregate Particles in Air *Journal of Chemical Engineering of Japan.* 1979; 12: 152-159

45. Brandt O, Rajahusmi AM, Roth P. First Observations on Break up of Particle Agglomerates in Shock Waves *Experiments in fluids.* 1987; 5: 86-94

46. Galinat S, Masbernat O, Guiraud C, Dalmazzone C, Noik C. Drop break up in turbulent pipe flow downstream of a restriction *Chemical Engineering Science.* 2005; 60: 6511-6528

47. Zumaeta N, Byrne EP, Fitzpatrick JJ. Predicting precipitate breakage during turbulent flow through different flow geometries *Colloids and Surfaces A: Physicochemical and engineering Aspects.* 2007; 292: 251-263

48. Zumaeta N, Cartland-Glover GM, Heffereman SP, Byrne EP, Fitzpatrick JJ. Breakage model development and application with CFD for predicting breakage of whey protein precipitate particles *Chemical Engineering Science.* 2005; 60: 3443-3452

49. Vankova N, Tcholakova S, Ivanov IB, Vulchev VD, Danner T. Emulsification in turbulent flow 1: Mean and maximum drop diameters in inertial and viscous regimes *Journal of Colloid and Interface Science.* 2007; 312: 363-380

50. Pope SB. Turbulent flows. Cambridge, EnglandNew York, NY: Cambridge University Press, 2000

51. Perry RH, Green DW. In: Perry's Chemical Engineers' Handbook, Eighth Edition New York, NY: McGraw-Hill, 2009

52. Sangawar GP, Gupta RB, Ermoline A, Scicolone JV, Dave RN. Environmentally Benign Nanomixing by Sonication in High Pressure Carbon Dioxide *Journal of Nanoparticle Research.* 2008; In Press:

53. Scicolone JV, Mujumdar A, Dave RN. Magnetically Assisted Impaction Mixing of Nano-particles *Powder Technology.* 2009; In Press:

54. Danckwerts PV. The Definition and Measurement of Some Characterisitics of Mixtures *Applications of Science Research.* 1952; 3: 279-296

55. Sanganwar GP, Gupta RB, Ermoline A, Scicolone JV, Dave RN. Environmentally Benign Nanomixing by Sonication in High Pressure Carbon Dioxide *Journal of Nanoparticle Research.* 2008; In Press:

56. Scicolone JV, Mujumdar A, Dave RN. Mixing of Nanosized Particle by Magnetically Assisted Impaction Mixing in Dry and Fluid Suspension *Proceedings of AIChE 2008 Annual Meeting* 2008;

57. Wang HW, John W. Particle density correction for the aerodynamic particle sizer *Aerosol Science and Technology.* 1987; 6: 191-198

58. Sun M, Hsu TJ. Flocculation Model of Cohesive Sediment Using Variable Fractal Dimension *Environmental Fluid Mechanics.* 2008; 8: 55-71

59. Khelifa A, Hill PS. Models for Effectived Density and Settling Velocities of Flocs *Journal of Hydraulic Research.* 2006; 44: 390-401

60. Maggi F, Mietta F, Winterwerp JC. Effect of variable fractal dimension on the floc size distribution of suspended cohesive sediment *Journal of Hydrology.* 2007; 343: 43-55

61. Lemmon EW, McLinden MO, Friend DG. *Themophysical Properties*. In: PJ Linstrom,WG Mallard. NIST Chemistry Webbook, NIST Standard Reference Database Number 69 Gaithersburg, MD: National Intitute of Standards and Technology, 2009

62. Shapiro A. The dynamics and thermodynamics of chempressible fluid flow. New York, NY: The Ronald Press Company, 1958

63. Lemmon EW, McLinden MO, Friend DG. In: NIST Chemistry Webbook, NIST Standard Reference Database Number 69 National Intitute of Standards and Technology, 2009

64. Kukukoya A, Aubin J, Kresta SM. A new definition of mixing and segregation: three dimensions of a key process variable *Chemical Engineering Research and Design.* 2009; 87: 633-647

65. Weber M, Thies M. *Supercritical Fluid Technology in Materials Science and Engineering: Syntheses, Properties, and Applications*. In: YP Sun. Understanding the RESS process 2002

66. Weber M, Thies M. A simplified and generalized model for the rapid expansion of supercritical solutions *Journal of Supercritical Fluids.* 2007; 40: 402-419

67. Span R, Wagner W. A new equation of state for carbon dioxide covering the fluid region from the triple-point temperature to 1100K at pressures up to 800 MPa *Journal of Physical Chemistry Reference Data.* 1996; 25: 1509-1596

68. Weiler C, Wolkenhauer M, Trunk M, Langguth P. New model describing the total dispersion of dry powder agglomerates *Powder Technology.* 2010; 203: 248-253

69. Wengeler R, Nirschl H. Turbulent hydrodynamic stress induced dispersion and fragmentation of nanoscale agglomerates *Journal of Colloid and Interface Science.* 2007; 306: 262-273

70. Baldyga J, Makowski L, Orciuch W, Sauter C, Schuchmann HP. Deagglomeration processes in high-shear devices *Chemical Engineering Research and Design.* 2008; 86: 1369-1381

71. Baldyga J, Orciuch W, Makowski L, Malik K, Ozcan-Taskin G, Eagles W, Pardon G. Dispersion of nanoparticle clusters in a rotor-stator mixer *Journal of Dispersion Science and Technology.* 2008; 29: 564-572

72. Baldyga J, Orciuch W, Makowski L, Malski-Brodzicki M, Malik K. Break up of nano-particle clusters in high-shear devices *Chemical Engineering and Processing: Process Intensification.* 2007; 46: 851-861

73. Xie L, Rielly CD, Ozcan-Taskin G. Break-up of Nanoparticle Agglomerates by Hydrodynamically Limited Processes *Journal of Dispersion Science and Technology.* 2008; 29: 573-579

74. Bar-Meir G. In: Fundamentals of Compressible Fluid Mechanics Minneapolis, MN: 2009

75. Debenedetti PG, Tom JW, Kwauk X, Yeo SD. Rapid expansion of supercritical solutions (RESS): fundamentals and applications *Fluid Phase Equilibria.* 1993; 82: 311-321

76. Reverchon E, Pallado P. Hydrodynamic modeling of the RESS process *Journal of Supercritical Fluids.* 1996; 9: 216-221

77. Franklin RK, Edwards JR, Chernyak Y, Gould RD, Henon F, Carbonell RG. Formation of perfluoropolyether coatings by the rapid expansion of supercritical solutions (RESS) process. Part 2: Numberical modeling *Industrial and Engineering Chemistry Research.* 2001; 40: 6127-6139

78. Hirunsit P, Huang Z, Srinophakun T, Charoenchaitrakool M, Kawi S. Particle formation of ibuprofen-supercritical CO2 system from rapid expansion of supercritical solutions (RESS): a mathematical model *Powder Technology.* 2005; 154: 83-94

79. Khalil I, Miller DR. The structure of supercritical fluid free-jet expansions *AIChE Journal.* 2004; 50: 2697-2704

80. Hodge BK, Koenig K. Compressible Fluid Dynamics: With Personal Computer Applications. Englewood Cliffs: Prentice Hall, 1995

81. Lide DR. In: CRC Handbook of Chemistry and Physics, 88th ed. Cleveland, OH: CRC Press, 2007

82. Strecker J, Roth P. Particle Breakup in Shock Waves Studied by Single particle light scattering *Particle and Particle System Characterization.* 1994; 11: 222-226

83. Weber M, Russell LM, Debenedetti PG. Mathematical modeling of nucleation and growth of particles formed by the rapid expansion of a supercritical solution under subsonic conditions *Journal of Supercritical Fluids.* 2002; 23: 65-80

84. Chernyak Y, Henon F, Harris RD, Gould RD, Franklin RK, Edwards JR, DeSimone JM, Carbonell RG. Formation of perfluoropolyether coatings by the rapid expansion of supercritical solutions (RESS) process. Part 1: Experimental results *Industrial and Engineering Chemistry Research.* 2001; 40: 6118-6126

85. Debenedetti PG. Homogeneous nucleation in supercritical fluids *AIChE Journal.* 1990; 36: 1289-1298

86. Lele AK, Shine AD. Morphology of polymers precipitated from a supercritical solvent *AIChE Journal.* 1992; 38: 742

87. Domingo C, Berends E, van Rosmalen GM. Precipitation of ultrafine organic crystals from the rapids expansion of supercritical solutions over a capillary and a frit nozzle *Journal of Supercritical Fluids.* 1997; 10: 39-55

88. Li J, Matos HA, de Azevedo EG. Two-phase homogeneous model for particle formation from gas-saturated solution processes *Journal of Supercritical Fluids.* 2004; 32: 275-286

89. Sparlart PR, Allmaras SR. A one-equation turbulence model for aerodynamic flows *Recherche Aerospatiale.* 1994; 1: 5-21

90. Tam CKW. Supersonic jet noise *Annual Review of Fluid Mechanics.* 1995; 27: 17-43

91. Panda J, Seasholtz RG. Measurement of shock structure and shock-vortex interaction in underexpanded jets using Rayleigh scattering. *Physics of Fluids.* 2005; 11: 3761-3777

92. Berland J, Bogey C, Bailly C. Numerical study of screech generation in a planar supersonic jet *Physics of Fluids.* 2007; 19: 075105

93. Aksay IA, Dabbs DM, Sarikaya M. Mullite for Structural, Electronic and Optical Applications *Journal of American Ceramic Society.* 1991; 74: 2343-2358

94. Gerardin C, Sundaresan S, Berziger J, Navrotsky A. Structural Investigation and Energetics of Mullite Formation from Sol-Gel Precursors *Chemical Materials.* 1994; 6: 160-170

95. Kara F, Sener O. Improvement of sintering and microstructural homogenity of a diphasic mullite *Journal of the European Ceramic Society.* 2001; 21: 901-905

96. Fielitz P, Borchardt G, Schmucker M, Schneider H. Aluminum grain boundary diffusion in polycrystalline mullite ceramics *Physcial Chemical Minerals.* 2007; 34: 431-436

97. Venables HJ, Wells JI. Powder Mixing *Drug Development and Industrial Pharmacy.* 2001; 27: 599-612

98. Weinekotter R, Gericke H. Mixing of Solids. *Particle Technology Series*. Dordrecht, The Netherlands Kluwer Academic Publishers, 2000

APPENDIX A

ADDITIONAL FIGURES FROM CHAPTER 2

This appendix contains the size distributions of alumina and titania nanopowders deagglomerated via the REHPS process. These figures are supplemental to the work described in Chapter 2.

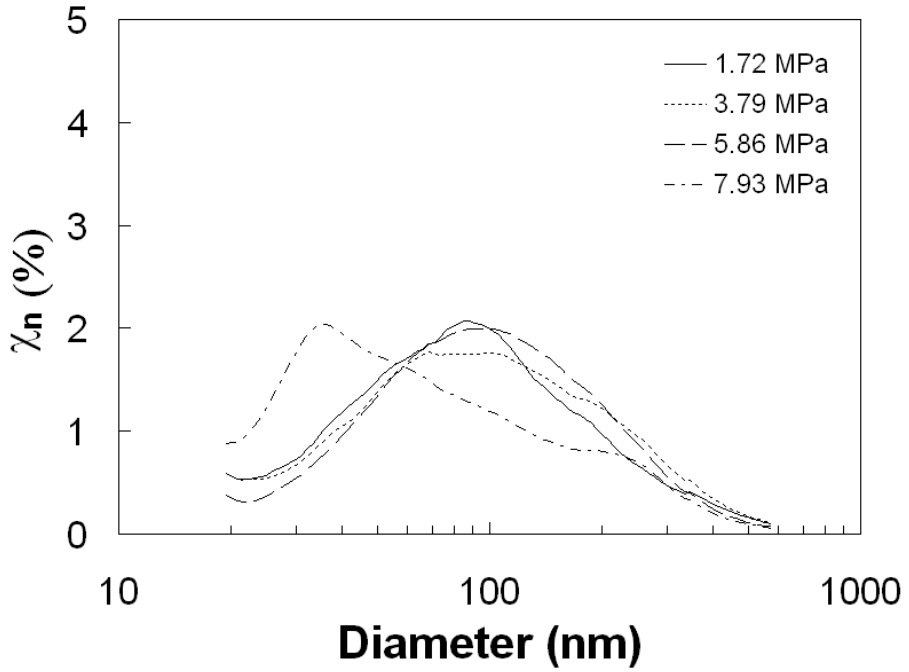

Figure A.1a Number weighted distributions of alumina nanopowders expanded at various pressures through a 254 μm x 10 cm nozzle; measured by the SMPS and summed over multiple runs.

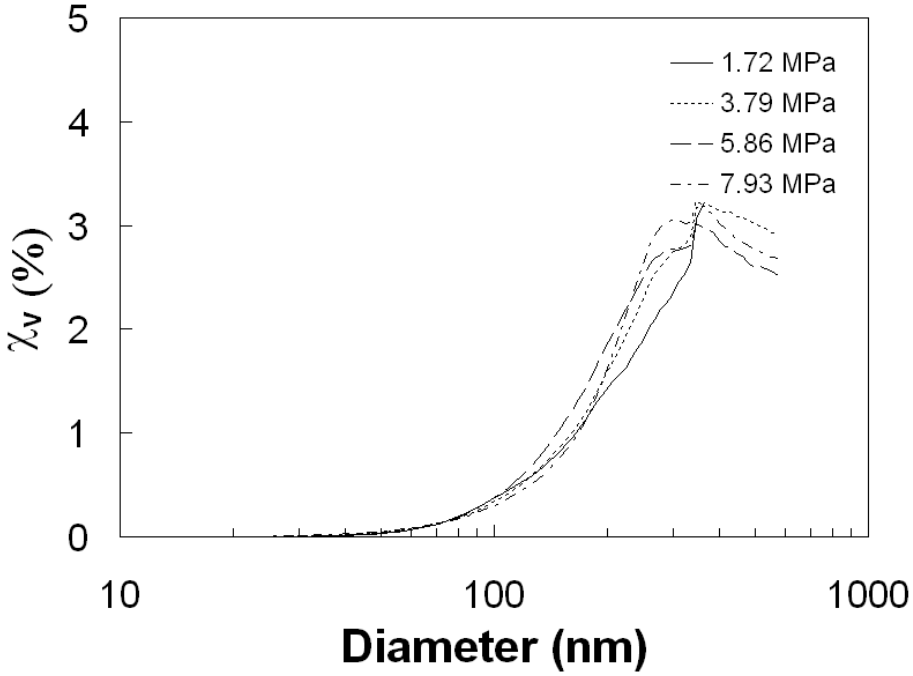

Figure A.1b Volume weighted distributions of alumina nanopowders expanded at various pressures through a 254 μm x 10 cm nozzle; measured by the SMPS and summed over multiple runs.

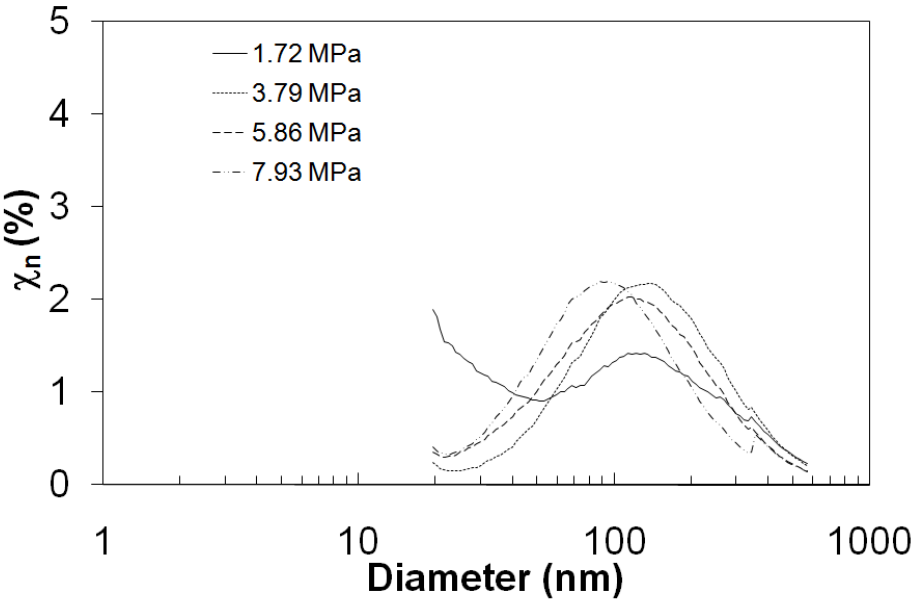

Figure A.2a Number weighted distributions of alumina nanopowders expanded at various pressures through a 254 μm x 10 cm nozzle; measured by the SMPS and summed over multiple runs.

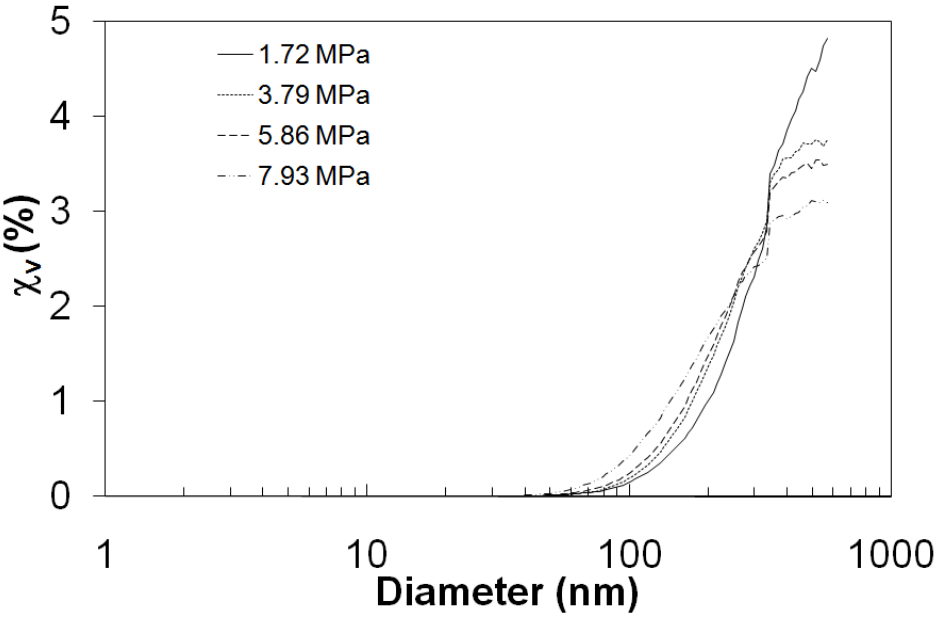

Figure A.2b Volume weighted distributions of alumina nanopowders expanded at various pressures through a 254 μm x 10 cm nozzle; measured by the SMPS and summed over multiple runs.

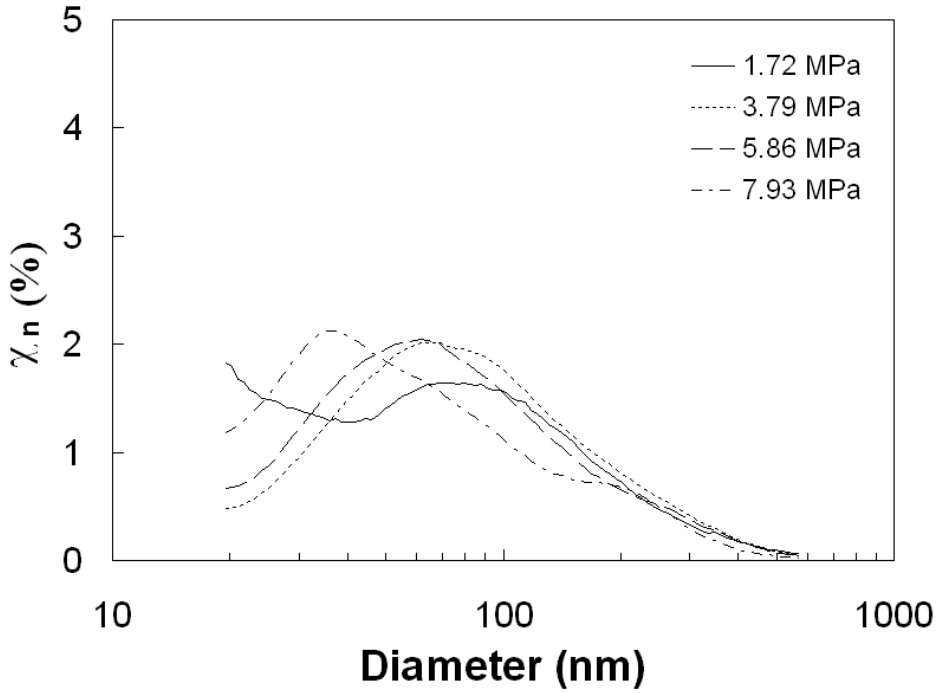

Figure A.3a Number weighted distributions of titania nanopowders expanded at various pressures through a 254 μm x 10 cm nozzle; measured by the SMPS and summed over multiple runs.

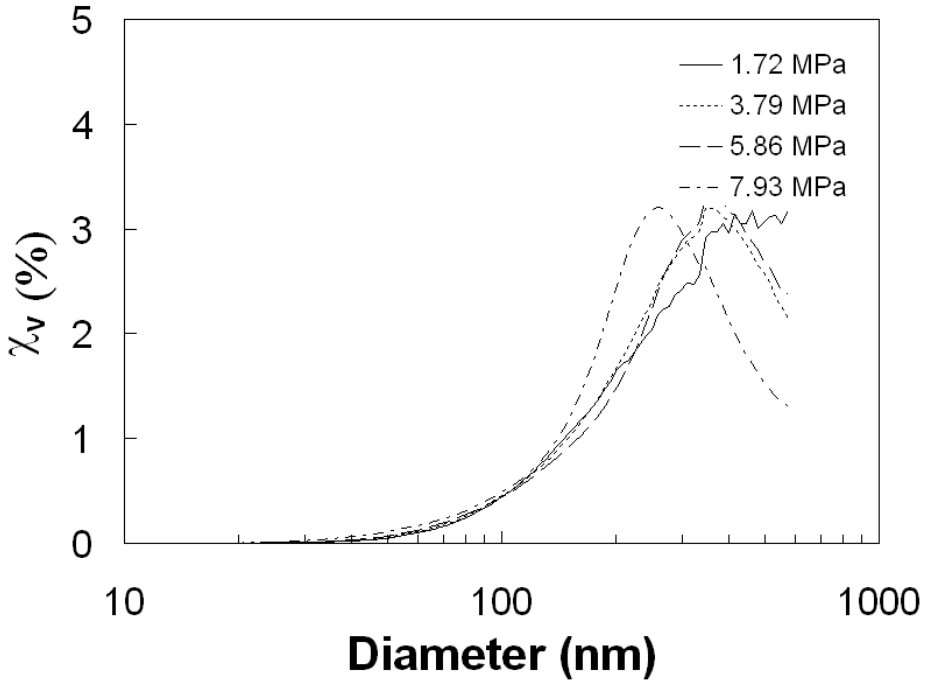

Figure A.3b Volume weighted distributions of titania nanopowders expanded at various pressures through a 254 μm x 10 cm nozzle; measured by the SMPS and summed over multiple runs.

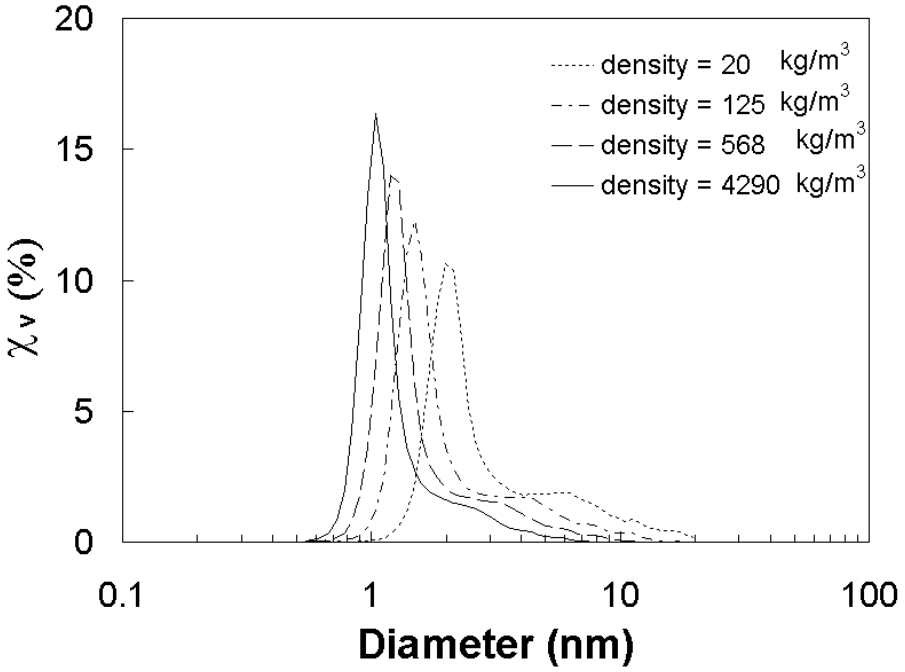

Figure A.4a Number weighted distributions of titania nanopowders expanded at 5.86 MPa through a 254 μm x 10 cm nozzle; measured by the APS. The Stokes Correction of size with respect to density was used at 4290, 568, 125, 20 kg/m^3.

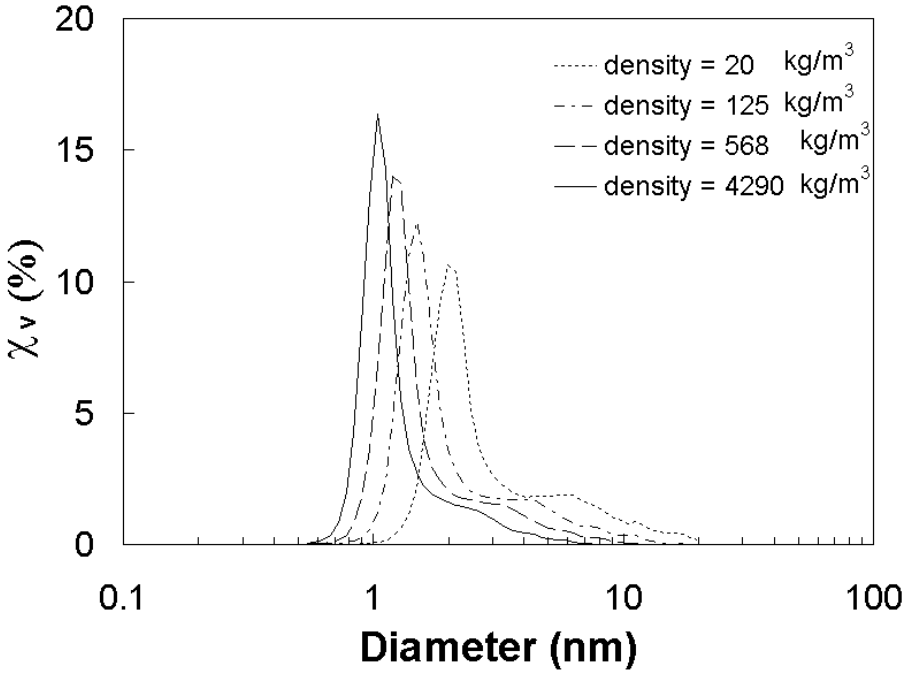

Figure A.4b Volume weighted distributions of titania nanopowders expanded at 5.86 MPa through a 254 μm x 10 cm nozzle; measured by the APS. The Stokes Correction of size with respect to density was used at 4290, 568, 125, 20 kg/m^3.

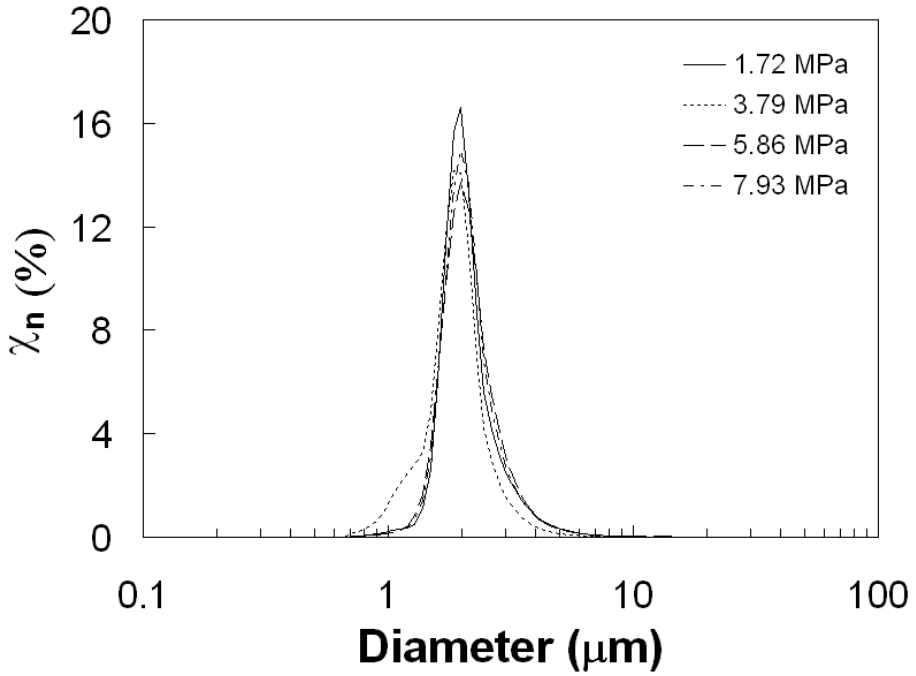

Figure A.5a Number weighted distributions of alumina nanopowders expanded at various pressures through a 254 μm x 10 cm nozzle; measured by the APS and summed over multiple runs. Agglomerate density is approximated at 48 kg/m^3.

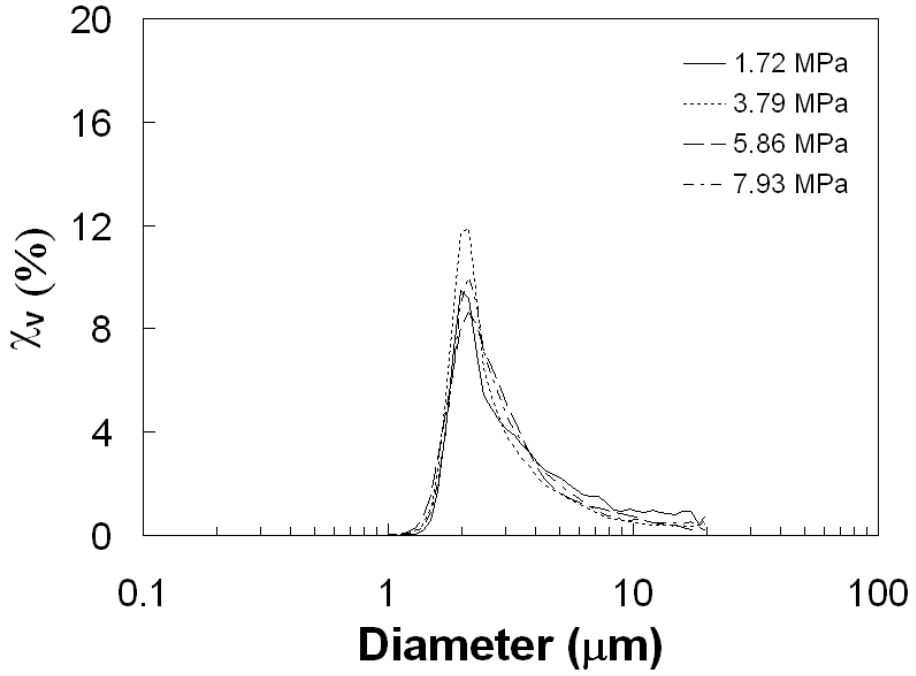

Figure A.5b Volume weighted distributions of alumina nanopowders expanded at various pressures through a 254 μm x 10 cm nozzle; measured by the APS and summed over multiple runs. Agglomerate density is approximated at 48 kg/m^3.

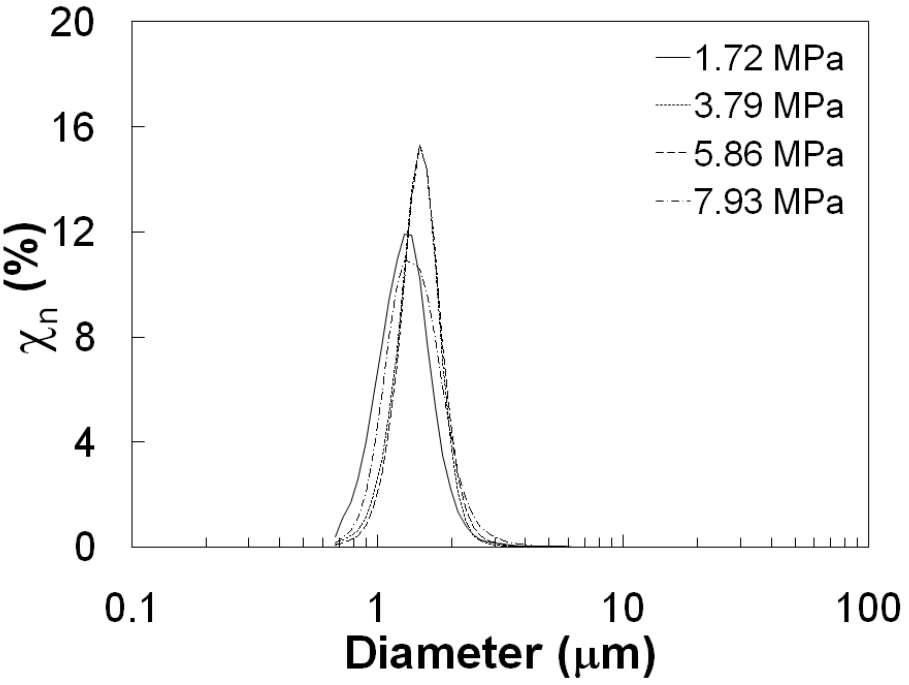

Figure A.6a Number weighted distributions of silica nanopowders expanded at various pressures through a 254 μm x 10 cm nozzle; measured by the APS and summed over multiple runs. Agglomerate density is approximated at 50 kg/m^3.

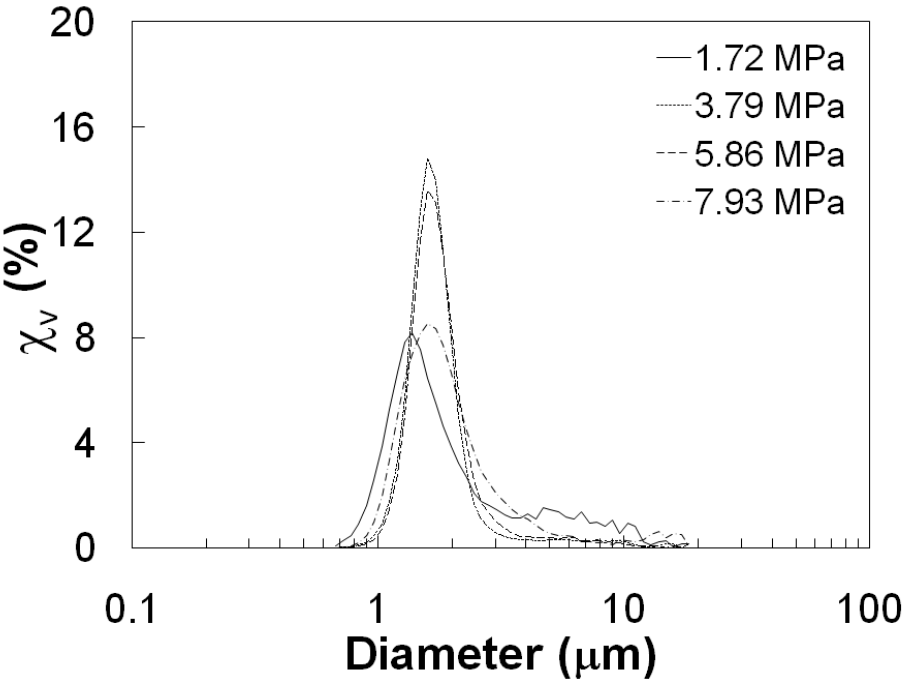

Figure A.6b Volume weighted distributions of silica nanopowders expanded at various pressures through a 254 μm x 10 cm nozzle; measured by the APS and summed over multiple runs. Agglomerate density is approximated at 50 kg/m^3.

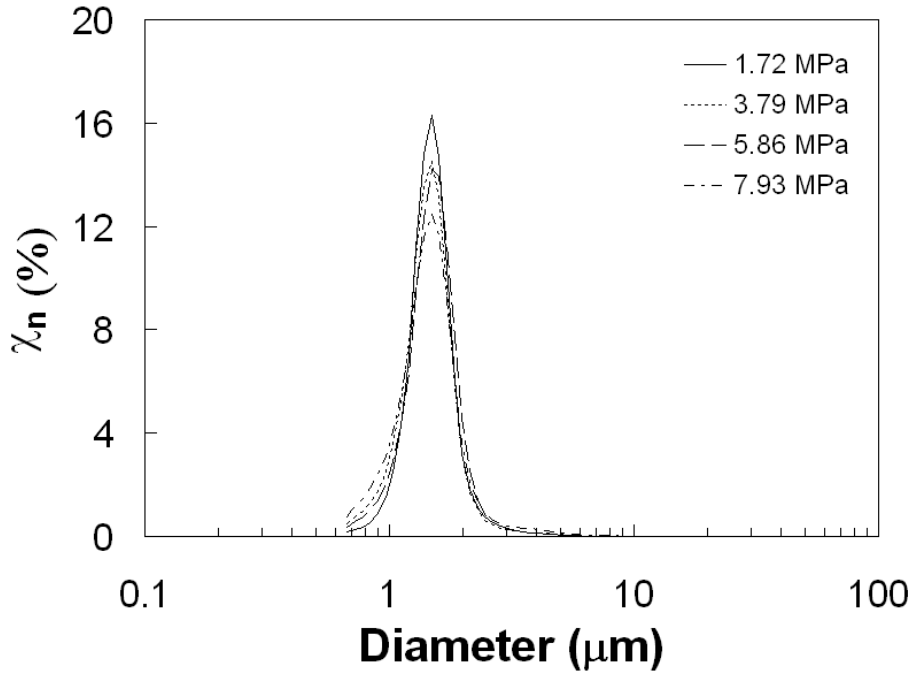

Figure A.7a Number weighted distributions of titania nanopowders expanded at various pressures through a 254 μm x 10 cm nozzle; measured by the APS and summed over multiple runs. Agglomerate density is approximated at 125 kg/m^3.

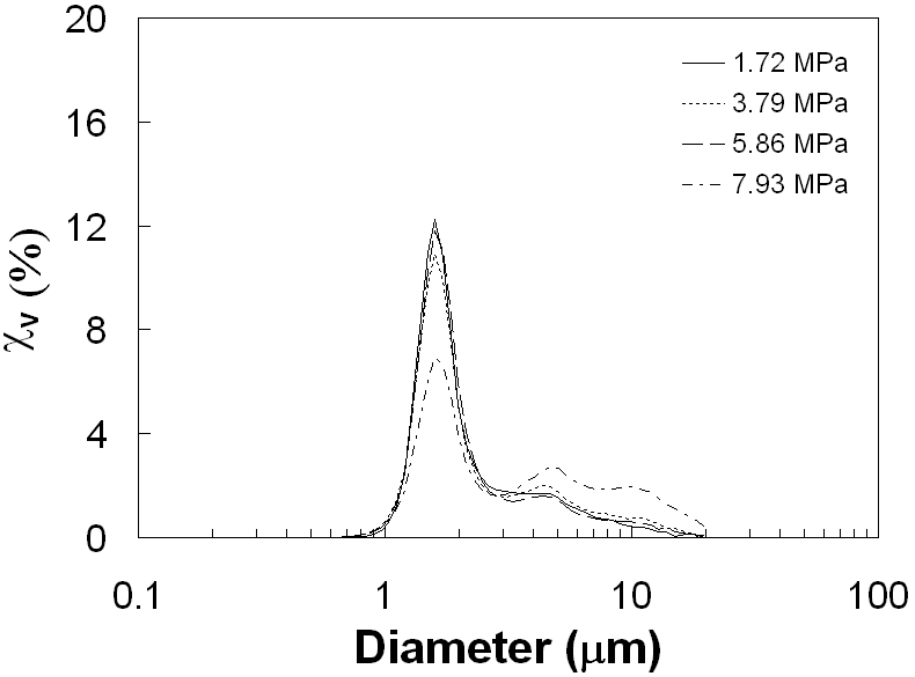

Figure A.7b Volume weighted distributions of titania nanopowders expanded at various pressures through a 254 μm x 10 cm nozzle; measured by the APS and summed over multiple runs. Agglomerate density is approximated at 125 kg/m^3.

APPENDIX B

MODELING OF REHPS DEAGGLOMERATION

It is clear from the experimental data presented above that rapid expansion of the gas through a fine nozzle led to breakup of the agglomerates of nanoparticles. The mechanisms through which these size reductions occur are now analyzed. In this appendix, a one-dimensional compressible flow model was applied to predict the change in CO_2 properties in the nozzle, and use empirical formulas to estimate the strength and position of the Mach disc – an abrupt supersonic-subsonic flow transition that is often featured in the free expansion. The analysis, described below, suggests that the shear flow in the nozzle and the subsequent impact of the agglomerates with the Mach disc in the free expansion region can both lead to micron or sub-micron level deagglomeration. Complementary two-dimensional numerical simulations, conducted to validate the one-dimensional solutions and to better understand the role of the Mach disc in the deagglomeration process are briefly outlined in the Appendix.

The RESS/REHPS process has been modeled by many researchers in the literature; for example, see Debenedetti et al.[75], Reverchon and Pallado[76], Franklin et al.[77], Hirunsit et al.[78], Khalil and Miller[79], Weber and Thies[65, 66]. Therefore, only a skeletal description of the model is presented here and the analysis is limited to conditions close to those employed in these experiments.

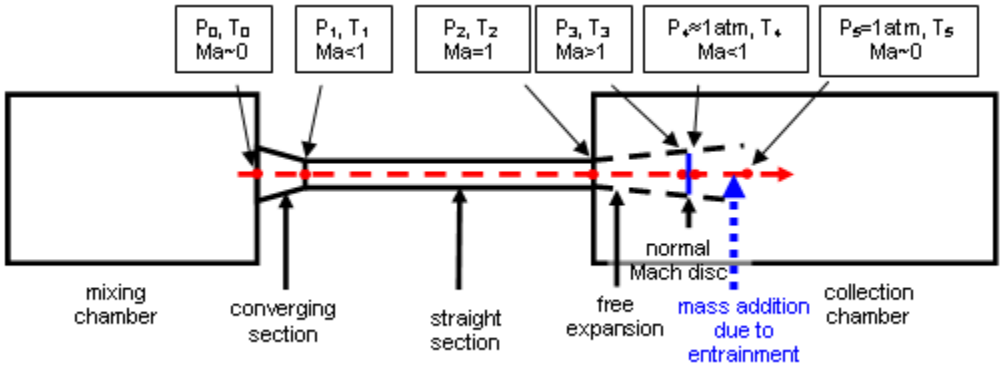

Figure B.1 Schematic of the RESS device considered in this study.

Figure B.1 shows the system considered in this study, which consists of a mixing chamber (the mixing vessel in Figure 2.1) filled with CO_2 maintained at specified temperature and pressure, a collection chamber (the expansion tube in Figure 2.1) that is open to the atmosphere, and a converging section and a straight nozzle connecting the two chambers to expand CO_2 to atmospheric conditions. To facilitate this discussion, six reference points (0-5) are used to separate this system into sections. As the CO_2 leaves the mixing chamber (point 0), it begins to expand first due to the change in the cross-sectional area (from 0 to 1), and then expand under the combined influence of heat transfer and friction (from 1 to 2). Here, "expand" only means that the density of CO_2 is decreasing. Due to the extreme pressure difference between the mixing and collection chambers, the flow in the straight nozzle is choked, i.e., the flow velocity is limited by the speed of sound at the end of the straight nozzle (point 2). Once CO_2 exits the straight nozzle, it undergoes a free expansion, where the temperature and pressure decrease very rapidly in the direction of flow while the velocity turns supersonic. When the pressure drops below collection chamber pressure, a Mach disc is formed (between points 3 and 4). Across this Mach disc, the thermodynamic properties experience step changes: the

pressure will increase abruptly to a value slightly lower than the collection chamber pressure, and the gas velocity will drop abruptly from supersonic to subsonic. After that, the pressure rises through deceleration and mixing with the ambient fluid, and reaches the collection chamber pressure at point 5.

B.1 Expansion in the Converging and Straight Sections (Point 0 to Point 2)

To model the flow in the converging and the straight sections (point 0 to point 2), a one-dimensional model identical to that in Weber and Thies[65, 66] was used, which contains the following mass, momentum, and energy conservation equations.

$$\begin{aligned} \frac{\mathrm{d}\rho}{\rho} + \frac{1}{2}\frac{\mathrm{d}a^2}{a^2} &= -\frac{1}{A}\frac{\mathrm{d}A}{\mathrm{d}x}\mathrm{d}x \\ \frac{\mathrm{d}P}{\rho a^2} + \frac{1}{2}\frac{\mathrm{d}a^2}{a^2} &= -\frac{2f}{D}\mathrm{d}x \\ \mathrm{d}h + \frac{1}{2}\mathrm{d}a^2 &= \frac{w\pi D}{\dot{m}}\mathrm{d}x \end{aligned} \qquad \text{(B.1)}$$

Here, x is the distance from point 0 to the point of interest, A is the cross-sectional area of the flow device which depends on x, a is the flow velocity, f is the Fanning friction factor of a round pipe, D is the diameter, w is a source term representing heat transfer into the fluid from the walls with a unit of watt per unit area, ρ is the density, P is the pressure, h is the specific enthalpy, and $\dot{m} = \rho A a$ is the mass flow rate. The Fanning friction factor f is a function of the Reynolds number and surface roughness. In this work, f = 0.005 was assumed in most of the calculations because this was the value used in all the other one-dimensional REHPS calculations. According to Perry's Chemical Engineer's Handbook, f = 0.005 when Re is about 10^5 and surface roughness λ/D is 0.0008.[51] A sensitivity analysis using another assumed value f = 0.008 is included in Table B.5.

These equations must be supplemented with a proper equation of state (EOS) so that h can be determined as a function of P and ρ. The EOS proposed by Span and Wagner[67] for CO_2, available in the form of dynamically linkable libraries, was used in the one-dimensional model. This EOS is limited to temperature above 216 K, the triple point of CO_2. If condensation of CO_2 occurs in the expansion process, the model equations would require some modification; however, for the limited objective of the present modeling study, it is sufficient to restrict it to those cases where condensation does not occur.

Table B.1 Conditions at the Tip of the Nozzle Corresponding to Various Inlet Pressures As Predicted By the 1D Model

	Inlet pressure P_0		
	1.72 MPa	3.79 MPa	5.86 MPa
Pressure P_2	0.42 MPa	0.91 MPa	1.43 MPa
Temperature T_2	270 K	257 K	244 K
Density ρ_2	8.47 kg/m^3	20.4 kg/m^3	37.0 kg/m^3
Velocity V_2	248 m/s	238 m/s	219 m/s
Mass flow rate $\dot{m}$	0.106 gm/s	0.246 gm/s	0.410 gm/s
Kinematic Viscosity ν_2	0.016 cm^2/s	0.0064 cm^2/s	0.0034 cm^2/s

Table B.1 lists the conditions at point 2, the tip of the straight nozzle corresponding to different inlet pressures, obtained by integrating the conservation equations (see eq. B.1) from point 0, the mixing chamber. The numbers in this Table were generated by using the actual size of the expansion device used in the experiments

discussed in Chapter 2. The inlet diameter D_0, outlet diameter D_1 and the length of the converging section $L_{0\text{-}1}$ are 5 mm, 254 μm and 5 mm, respectively. The diameter $D_{1/2}$ and the length $L_{1\text{-}2}$ of the straight nozzle section are 254 μm and 102 mm, respectively. The temperature of the CO_2 at the inlet is 318K, while its pressure is allowed to assume different values as indicated in the Table. As the friction term in eq. (B.1) is of the form *f/D*, it is only important in the straight section where *D* is at minimum. Thus, friction was only considered in the straight section and neglected in the converging section. Such a simplification was also made in some earlier RESS/REHPS modeling work, e.g., Reverchon and Pallad[43]. In these calculations, the heat transfer term *w* was set to zero. Note that results are presented only for inlet pressures at or below 5.86 MPa; when the upstream pressure exceeded 5.86 MPa, the analysis predicted that CO_2 condensation can occur in the nozzle. (As aforementioned, this study was limited to cases where such condensation did not occur.) This is entirely consistent with the experiments which found evidence for condensation at the highest inlet pressure employed (7.93 MPa), but not at the lower inlet pressures (which were below 5.86 MPa).

Figure B.2 shows the variation of pressure, temperature, and density of CO_2 in the RESS device from the mixing chamber (point 0) to the tip of the straight nozzle (point 2) and the Mach number. The initial drop in pressure, temperature, and density from $x = 0$ to $x = 0.005$ (m) is due to the cross-sectional area change in the converging section, and the Mach number reaches about 0.2 at point 1. The subsequent expansion in the straight nozzle (resulting from friction) is more significant than that in the converging section. As x approaches 0.107 m, the end of the nozzle, the dependence of gas properties on x

becomes nearly singular due to the subsonic-supersonic transition. The Mach number variations are independent of the initial pressure.

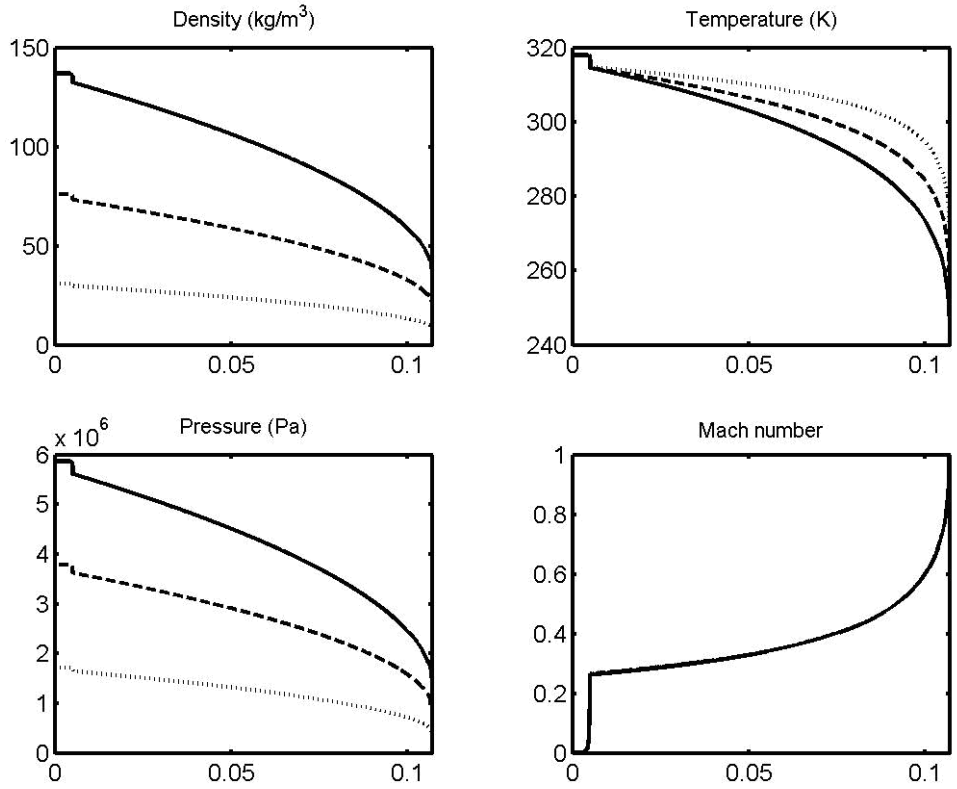

Figure B.2 Changes in density, temperature, pressure, and Mach number along the path of expansion (from point 0 to point 2). The horizontal axis is the distance from point 0 measured in meters. Upstream pressure P_0 = 5.86 MPa (solid line), 3.79 MPa (dashed line), and 1.72 MPa (dotted line).

Figure B.3 shows the variation of CO_2 velocity and kinematic viscosity as functions of distance in the RESS/REHPS device from point 0 to point 2. The increase in the upstream pressure from 1.72 MPa to 5.86 MPa has little effect on the velocities and average shear rates $\dot{\gamma} = V/d$; it, however, reduces the kinematic viscosity, resulting in an increase in the Reynolds number.

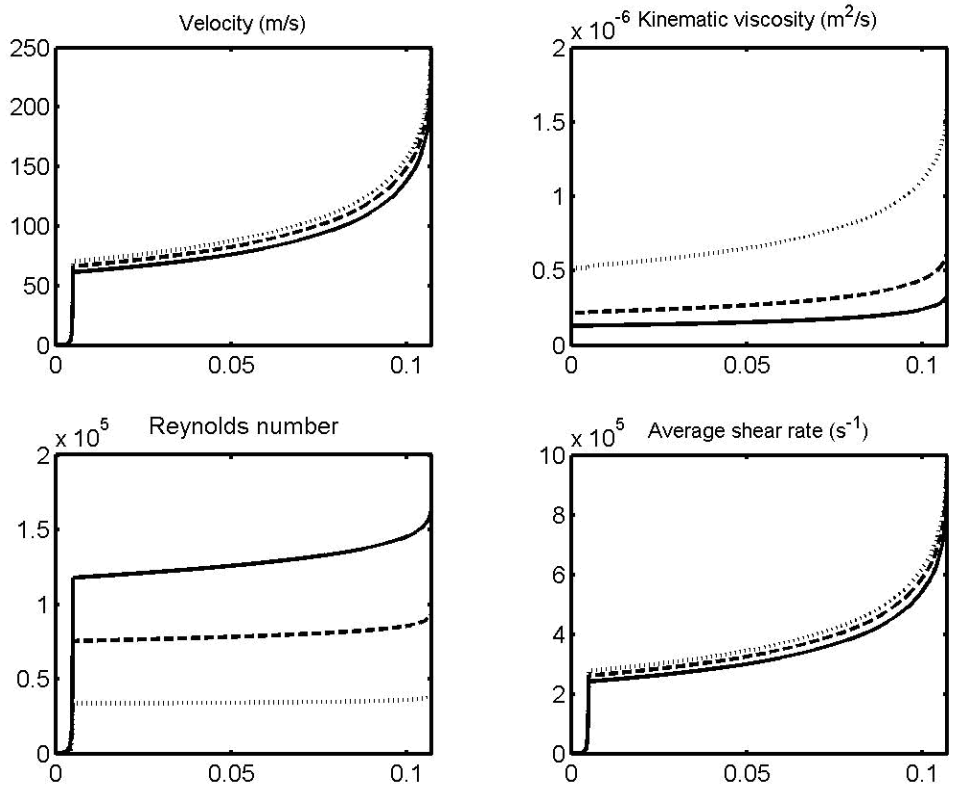

Figure B.3 Velocity, kinematic viscosity, average shear rate, and Reynolds number as functions of distance from point 0. Upstream pressure P_0 = 5.86 MPa (solid line), 3.79 MPa (dashed line), and 1.72 MPa (dotted line).

It is interesting to note from Table B.1 that the velocity V_2 decreases with increasing P_0, contrary to what is expected of incompressible flows. This is because in a choked flow the Mach number at the nozzle tip is always one. As the speed of sound decreases with decreasing temperature and the temperature T_2 drops as one increases P_0, V_2 has to decrease with increasing P_0 to satisfy the choked condition. The mass flow rate increased with increasing pressure in a nonlinear manner. The pressure reduction from point 0 to 2 was approximately a factor of 4 and was nearly independent of P_0.

4.5 B.2 Free Expansion From Point 2 to Point 3

The supersonic free expansion from point 2 to point 3 and the supersonic-subsonic transition from point 3 to point 5, were analyzed as follows:

a) An empirical relation for position of the Mach disc away from the tip of the nozzle x_M is given by[65, 66]:

$$\frac{x_M}{D_2} = 0.67\sqrt{\frac{\tilde{P}_2}{P_4}}, \tag{B.2}$$

where $\tilde{P}_2$ is the stagnant pressure corresponding to pressure P_2 which, for ideal gas, equals 1.853 P_2 (assuming C_P/C_V = 1.33). As the flow after the Mach disc is of low speed, it is safe to assume that $P_4 \approx P_5$ = 0.1 MPa.

b) An empirical relation for the diameter of the Mach disc D_M is given by:

$$\frac{D_M}{D_2} = 0.42\left(1 + K_M\right)\frac{x_M}{D_2}, \tag{B.3}$$

where $K_M \sim 0.2$ [65, 66] for CO_2 at the ideal-gas state.

c) The Mach number immediately before the Mach disc (point 3) is given by[65, 66]:

$$Ma_3 = \left(\frac{D_M}{D_2}\right)^2. \tag{B.4}$$

d) The Mach number immediately after the Mach disc (point 4) and the pressure drop across the Mach disc can be obtained using standard normal shock wave tables[80] for ideal gases. (Unlike in the converging section and in the straight nozzle, the supersonic expansion before the Mach disc generally involves very low pressure, temperature, and density of CO_2. Therefore, it is valid to apply equations based on the ideal-gas approximation for CO_2 in this region.)

Table B.2 Estimates of Location, Size, and Strength of the Mach Disc and the Associated Pressure Changes Across the Mach Disc Assuming $P_4 \approx P_5 = 0.1$ MPa

Inlet Pressure P_0	3.79 MPa	5.86 MPa
Position of the Mach disc (from nozzle tip)	0.69 mm	0.87 mm
Diameter of the Mach disc	0.35 mm	0.44 mm
Mach number before and after the Mach disc	1.94 / 0.59	2.99 / 0.48
Pressure before the Mach disc P_3	0.178 MPa	0.192 MPa
Pressure change across the Mach disc	0.077 MPa	0.091 MPa

Table B.2 presents the values of x_M, D_M, $Ma_{3/4}$, and the pressure change across the Mach disc corresponding to two different inlet pressures considered earlier in Table B.2. At the upstream (inlet) pressure of 1.72 MPa, eqns. (B.1)-(B.3) do not apply as they predict that $Ma_3 < 1$, which implies absence of the Mach disc. (Indeed, the 2D simulations discussed in the Appendix revealed a Mach disc for $P_0 = 2.07$ MPa but not for $P_0 = 1.03$ MPa. Thus, Mach disc is only present when P_0 is sufficiently high.) The data in Table B.2 indicate that the distance from the nozzle, diameter, and strength of the Mach disc all increase with increasing inlet pressure.

B.3 Shear and Impact Deagglomeration Mechanisms

As hydrodynamic fragmentation of nanoparticle agglomerates is most likely to occur in regions with high velocity gradients and/or rapid property changes, it is expected that the deagglomeration observed in the experiments was primarily due to the intense shear in the straight nozzle and the step changes in pressure, density, and temperature associated with the Mach disc.

In a simple model for shear-induced deagglomeration, one can imagine two spherical "blobs" of size *L*, each of which is a fractal ensemble of many primary particles stuck together by the van der Waals force. The blobs will experience a velocity difference of $\dot{\gamma}L$ in a shear flow with shear rate $\dot{\gamma}$ (see an illustration in Figure B.4) that leads to a drag differential between the two blobs

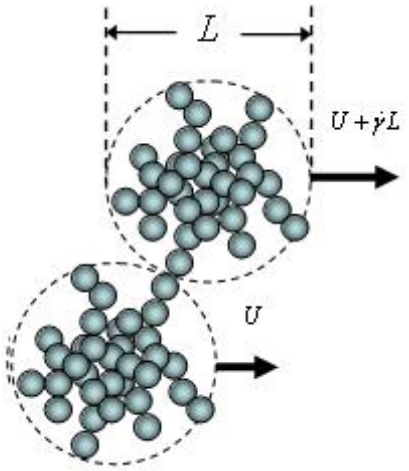

Figure B.4 The viscous drag differential acting on two agglomerates of size L in a simple shear flow.

$$F_{shear} = 3\pi\mu\dot{\gamma}L^2 \tag{B.5}$$

An estimate of the van der Waals force between two primary alumina particles of diameter L_P (assuming the particles are spherical) is given by.

$$F_{VdW} = \frac{L_P}{24}\frac{H}{\Delta^2}. \tag{B.6}$$

Here, *H* is the Hamaker constant, which is typically 10^{-19} J between metal oxide spheres submerged in a non-polar solvent[81], and Δ is a parameter controlling the maximum cohesive strength between primary particles that can be understood as the closest approach between two primary particles. On the macroscopic level, a higher Δ generally

leads to a lower surface energy of the material. In the illustrative calculations below, tow different values were consider for Δ: 1 nm and 0.5 nm representing different level of cohesion, and use L_P ~ 13 nm and 21 nm (alumina and titania primary particles). Letting $F_{shear} = F_{VdW}$ and substituting $\dot{\gamma} = V_2 / D_2$ into eq. (B.5), one can obtain L to be approximately 700 nm for alumina and 800-900 nm for titania when Δ = 1 nm, and 1300-1400 nm (alumina) and 1700-1800 nm (titania) when Δ = 0.5 nm (Table B.3). The order of magnitude of these numbers are in good agreement with the average size of agglomerates observed in the experiments described in Chapter 2, and suggest that the shear in the straight nozzle does play an important role in the deagglomeration process. Interestingly, due to the drastic reduction in the kinematic viscosity of the fluid at elevated pressures, L increases slightly with increasing inlet pressure P_0.

Table B.3 Estimates for the Average Size of Agglomerates After Passing Through the Nozzle, as Determined by Equating the Shear-Induced Viscous Drag Differential (eq. 5) and the Van Der Waals Force (eq. 6)

Pressure P_0	L_P = 13 nm Δ = 1 nm	L_P = 13 nm Δ = 0.5 nm	L_P = 21 nm Δ = 1 nm	L_P = 21 nm Δ = 0.5 nm
1.72 MPa	0.66 μm	1.32 μm	0.84 μm	1.68 μm
3.79 MPa	0.69 μm	1.38 μm	0.88 μm	1.76 μm
5.86 MPa	0.73 μm	1.46 μm	0.93 μm	1.85 μm

Impact deagglomeration may also be an important aspect of the REHPS process. As an agglomerate of nanoparticles passes through the Mach disc, the rapid changes in pressure, density and velocity across the Mach disc produce an impulse that may shatter the agglomerate into many smaller pieces. The experimental studies by Brandt et al.[34]

and by Strecker and Roth[60] showed that normal shock waves were very effective in reducing the average agglomerate size in a shock tube. In Brandt et al.[45], the reduction in agglomerate size was correlated to the pressure drop across the normal shock, and agglomerates consisting of 40 nm SiO_2 primary particles were fragmented to an average size of 400-500 nm when the pressure drop across the normal shock was about 0.1 MPa. In Strecker and Roth[82], as the primary particles were of a larger size (325 nm), the agglomerates were primarily in the form of dimers and trimers. After a normal shock wave passed through, the fractions of dimers and trimers were significantly reduced.

The effect of the Mach disc on the deagglomeration was modeled by setting the force acting on an agglomerate of size L due to the sudden pressure increase across the Mach disc to be proportional to the van der Waals binding force between a pair of primary particles

$$\frac{\Delta P \pi L^2}{4} \propto \frac{L_p H}{24\Delta^2} \tag{B.7}$$

Rearranging,

$$L = \alpha \sqrt{\frac{L_p H}{6\pi \Delta P \Delta^2}} \tag{B.8}$$

where α is a proportionality constant. The experimental data of Brandt et al.[45] for agglomerates containing spherical SiO_2 primary particles conform reasonably well to this formula and yield $\alpha \sim 5$ (assuming $\Delta = 0.5$ nm in their experiments). (If one assumes that $\Delta = 1.0$ nm in their experiments, then the estimated value of α would be ~10.) The average agglomerate size L after the suspension passes through the Mach disc, estimated by substituting the ΔP across the Mach disc listed in Table 5, $\alpha = 5$, and $\Delta = 0.5$ nm into

eq. (B.8), are presented in Table B.4; it can be seen that the values of *L* are about 300 nm for alumina agglomerates, and 350-400 nm for titania agglomerates. The order-of-magnitude agreement between these numbers and the average sizes observed in these experiments suggests that impact with the Mach disc may also be an effective deagglomeration mechanism in the RESS/REHPS process. In contrast with Table B.3, here *L* decreases slightly with increasing inlet pressure.

Table B.4 Estimated Average Agglomerate Size *L* After the Suspension Passes Through the Mach Disc (eq. 9)

Collection chamber pressure P_4	Mixing chamber pressure P_0	Mach number and pressure change across the Mach disc	Alumina (Δ = 0.5 nm)	Titania (Δ = 0.5 nm)
0.1 MPa	3.79 MPa	Ma = 1.94 ΔP = 0.077 MPa	0.30 μm	0.38 μm
	5.83 MPa	Ma = 2.98 ΔP = 0.091 MPa	0.28 μm	0.35 μm

The data in Table B.3 and B.4 suggest that the effect of inlet pressure P_0 on deagglomeration is complex. On one hand, an elevated P_0 increases the strength of the Mach disc; on the other hand, it reduces the viscosity of the fluid and the shear stresses in the nozzle. Therefore, when the two mechanisms work together, the agglomerate size may become insensitive to the change in $P_{0.}$ Indeed, in the experiments, the size of neither alumina nor titania powders changed significantly in the pressure range of 1.72–5.86 MPa.

Using the flow models for RESS/REHPS and the deagglomeration analyses presented above, the sensitivity of the final agglomerate sizes resulting from shear and impact, respectively, to various experimental parameters such as the inlet temperature, nozzle diameter, length, Fanning friction factor *f*, and heat transfer rate *w* were tested. Table B.5 summarizes some illustrative examples.

The Fanning friction factor *f* is largely an unknown parameter because it is a function of the Reynolds number, which varies with position in the nozzle and depends on the upstream conditions, and the roughness of the inner surface, which is difficult to measure for a thin nozzle. While it is not known what *f* is for the RESS/REHPS system, it is possible to substitute a different *f* into the 1D model and study its influence on the model predictions. In Table B.5, it can be observed that raising *f* from 0.005 to 0.008 reduces the pressure and density at nozzle exit and the flow rate. However, due to the increase in the kinematic viscosity, L_{shear} is not significantly changed. The influence on the free expansion and L_{impact} is also very small. This calculation shows that deagglomeration is not very sensitive to the friction factor.

Raising the inlet temperature T_0 from 318 K to 370 K decreases the mass flow rate through the nozzle (in agreement with Reverchon and Pallado[76]), but increases the velocity and kinematic viscosity at the exit. As a result, the shear in the straight nozzle becomes more effective in reducing the size of the agglomerates – the estimated agglomerate size is reduced by 13% from 1.37 μm to 1.19 μm. The change in inlet temperature, however, does not have any significant influence on the free expansion – the changes in the position and Mach number of the Mach disc are marginal and have no effect on deagglomeration.

Table B.5 Effect of Inlet Condition and Nozzle Diameter & Length On the State of CO_2 at the Tip of the Nozzle and Near the Mach Disc

Initial condition / Nozzle dimension	Properties at the tip of the nozzle	Properties of the Mach disc
Reference system: P_0 = 3.79 MPa, T_0 =318 K, $L_{0\text{-}1}$ = 5mm No heat transfer $D_{1/2}$ = 254 μm,$L_{1\text{-}2}$ = 102 mm	P_2 = 0.91 MPa, T_2 = 257 K, ρ_2 = 20.4 kg/m^3, V_2 = 238 m/s, $\dot{m}$ = 0.246 gm/s, ν = 0.0064 cm^2/s, L_{shear} = 0.69 μm	x_M = 0.69 mm, D_M = 0.35 mm Ma_3 = 1.94, Ma_4 = 0.59 ΔP = 0.077 MPa, L_{impact} = 0.30 μm
Same as the reference system except T_0 = 370 K	P_2 = 0.94 MPa, T_2 = 314 K, ρ_2 = 16.5 kg/m^3, V_2 = 262 m/s, $\dot{m}$ = 0.220 gm/s, ν = 0.0095 cm^2/s, L_{shear} = 0.60 μm	x_M = 0.70 mm, D_M = 0.36 mm Ma_3 = 1.95, Ma_4 = 0.59 ΔP = 0.077 MPa L_{impact} = 0.30 μm
Same as the reference system except heat transfer w = 10^5 watt/m^2	P_2 = 0.95 MPa, T_2 = 291 K, ρ_2 = 18.4 kg/m^3, V_2 = 252 m/s, $\dot{m}$ = 0.234 gm/s, ν = 0.0080 cm^2/s, L_{shear} = 0.63 μm	x_M = 0.71 mm, D_M = 0.36 mm Ma_3 = 1.98, Ma_4 = 0.58 ΔP = 0.078 MPa L_{impact} = 0.30 μm
Same as the reference system except $D_{1/2}$ = 350 μm	P_2 = 1.03 MPa, T_2 = 259 K, ρ_2 = 23.0 kg/m^3, V_2 = 236 m/s, $\dot{m}$ = 0.524 gm/s, ν = 0.0057 cm^2/s, L_{shear} = 0.81 μm	x_M = 1.02 mm, D_M = 0.51 mm Ma_3 = 2.14, Ma_4 = 0.56 ΔP = 0.082 MPa L_{impact} = 0.29 μm
Same as the reference system except $L_{1\text{-}2}$ = 50 mm	P_2 = 1.16 MPa, T_2 = 261 K, ρ_2 = 26.1 kg/m^3, V_2 = 236 m/s, $\dot{m}$ = 0.313 gm/s, ν = 0.0051 cm^2/s, L_{shear} = 0.68 μm	x_M = 0.78 mm, D_M = 0.40 mm Ma_3 = 2.43, Ma_4 = 0.52 ΔP = 0.086 MPa L_{impact} = 0.28 μm
Same as the reference system except $L_{1\text{-}2}$ = 2.6 mm	P_2 = 1.93 MPa, T_2 = 273 K, ρ_2 = 43.8 kg/m^3, V_2 = 236 m/s, $\dot{m}$ = 0.523 gm/s, ν = 0.0032 cm^2/s, L_{shear} = 0.66 μm	x_M = 1.01 mm (0.72 mm) D_M = 0.51 mm (0.36 mm) Ma_3 = 4.02 (2.04) Ma_4 = 0.43 (0.57) ΔP = 0.095 MPa (0.157 MPa) L_{impact} = 0.27 μm (0.21 μm)

As rapid expansion of supercritical CO_2 is always accompanied by strong reduction in temperature, heat transfer from the ambient to the nozzle is bound to occur in a REHPS process. Even though the rate of heat transfer in these experiments are not

known quantitatively, its effect can be studied in a qualitative manner by assigning a non-zero value to the heat source term w in eq. (B.1). As shown in Table B.5, the effect of supplying heat to the nozzle is very similar to that of raising the inlet temperature. It increases the temperature, velocity, and kinematic viscosity of CO_2 at the tip of the nozzle, and has a positive influence on deagglomeration. Note that $w = 10^5$ watt/m^2 is a very high rate of heat transfer; yet, this calculation indicates only small effects on L_{shear} and L_{impact}. Thus, in practical RESS systems the heating of the nozzle, while important in keeping dry ice from forming, does not play a major role in deagglomeration.

Table B.5 then lists the conditions one would expect at the tip of the nozzle and near the Mach disc when the nozzle diameter is increased from 254 μm to 350 μm. Increasing nozzle diameter reduces the shear and the flow resistance and raises the flow rate of CO_2 significantly. This decreases the efficiency of deagglomeration in the nozzle, but increases the Mach number and pressure change across of the Mach disc.

Finally, it is shown in Table B.5 that a shorter nozzle leads to a higher shear rate in the nozzle and a higher Mach number in the free expansion, thus helping to reduce the agglomerate size. It is interesting to note that even though the Mach number reaches a very high value of 4.02 and P_3 drops down to 1/18 of P_4 for the shortest nozzle (2.6 mm in length), the pressure change across the Mach disc $P_4 - P_3$ is only 0.095 MPa. This observation suggests that in order to exploit the pressure change across the Mach disc to fragment the agglomerates, one could increase P_4 and P_5 to achieve higher ΔP and better deagglomeration. For example, if CO_2 is expanded into a pressurized chamber with P_4 = 0.2 MPa using the short nozzle (0.26 cm), while Ma_3 is reduced from 4.02 to 2.03, the

pressure drop across the Mach disc is increased from 0.095 MPa to 0.157 MPa and eq. (B.8) predicts a decrease in the agglomerate size from 270 nm to 210 nm.

The above sensitivity analysis reveals that while there is room for optimizing the RESS process design, the typical agglomerate sizes undergo only incremental changes with changes in the process conditions; in other words, the agglomerate size estimates obtained in the above analysis are robust.

In this section, the free expansion zone was treated empirically and some concerns remain about the reliability of the Mach disc properties and deagglomeration at this location. In general, not all the gas issuing out of the orifice will pass through the Mach disc, and only a fraction of the agglomerates coming out of the nozzle will experience the impact force. Many experiments and two-dimensional simulations indicate that in a RESS process only about 50% of the mass would pass through the Mach disc[65, 78, 83, 84]. To check the flow behavior in the free expansion zone, steady 2D (axisymmetric) computational fluid dynamics (CFD) simulations were performed using a commercial software Fluent®. The results of these CFD simulations are presented in the next section. These simulations suggest that only about 50% of the mass would pass through the Mach disc for P_0 = 5.86 MPa, while for the lower pressures the fraction of agglomerates passing through the Mach disc is even less. Furthermore, Mach disc was only present when P_0 is sufficiently high, consistent with the predictions of the empirical formulas; deagglomeration occurred even in the cases where the Mach disc was absent. These considerations suggest that shattering at the Mach disc alone is not likely to be the dominant mechanism and that shear in the nozzle must be contributing appreciably to the deagglomeration observed in the experiments.

B.4 Two-Dimensional Numerical Simulations of CO_2 Flow in the REHPS Device

The 1D model discussed in the main text is based on the assumption that average properties of CO_2, e.g., pressure, density, temperature, velocity, do not vary rapidly in the direction of the mean flow, and the streamlines are nearly parallel. Additionally, a constant value was assumed for the friction factor in the momentum equation, as has been done in many studies[76, 77, 83, 85-88]. In reality, however, the friction factor would depend on the flow rate, and thus would be a function of position. Moreover, in the free expansion the 1D flow approximation would not be applicable. In order to overcome these shortcomings, several 2D axisymmetric, steady-state CFD simulations were carried out using Fluent®. In these 2D simulations, as the friction occurs naturally through the interaction between the fluid and the wall, there is no need to specify the friction factor. Moreover, 2D simulations allow us to characterize the structure of the freely expanding jet and examine the role of the Mach disc in deagglomeration in more detail.

Figure B5 shows the computational mesh of the RESS device that includes a 5 mm converging section, a 102 mm long, 254 μm diameter nozzle, and a 300 mm long, 12.5 mm diameter tube. The mesh density was increased near the walls, near the inlet and the exit to capture the rapid change in CO_2 properties in those regions (see Figure B5 for an enlargement near the tip of the nozzle). These simulations employed the density-based solver option with second-order upwind scheme (available in Fluent®), and applied constant-pressure boundary conditions at the inlet of the converging section (5.86, 3.45, and 2.07 MPa) and at the exit of the tube (0.1 MPa). The analysis is limited to cases where condensation of CO_2 does not occur and as pressures are low in the free expansion, an ideal gas approximation was deemed sufficient. The Sparlart-Allmaras

turbulent model (available in Fluent®), a common choice for compressible flow simulations[50, 89] was included.

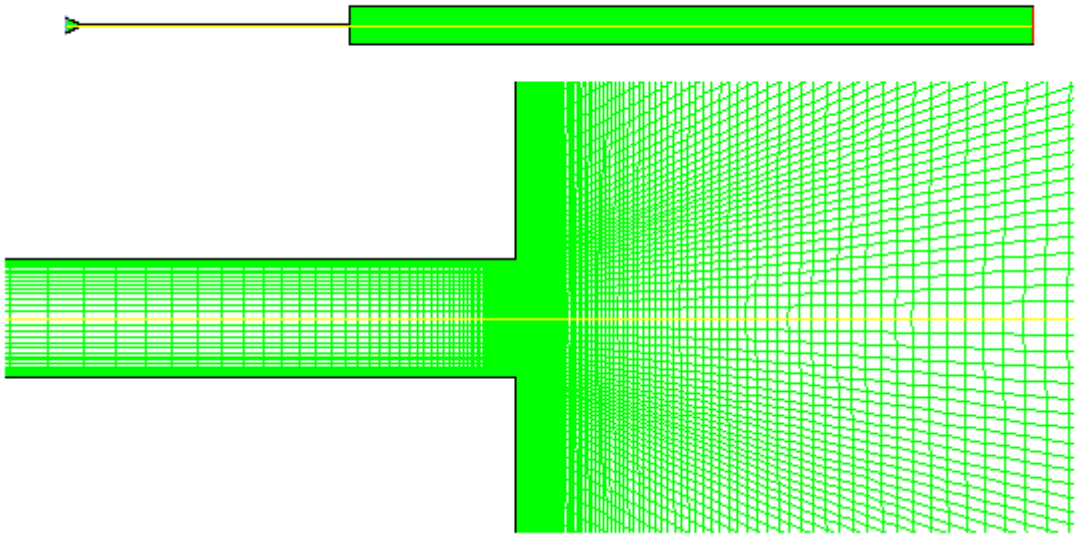

Figure B.5 The axisymmetric RESS geometry used in the Fluent simulations. The mesh resolution near the walls and near the exit of the nozzle is increased to capture the strong velocity gradients in those areas.

Figure B.6 shows the variation of the centerline pressure as a function of distance from the inlet of the converging section to the tip of the nozzle. The shapes of the profiles are very similar to that in 11, indicating that the flow from point 0 to 2 can be described well by the 1D model even though it assumes a constant friction factor. P_2 obtained from Fluent® simulations are very close to those obtained from 1D model calculations using the more accurate Span-Wagner EOS[67].

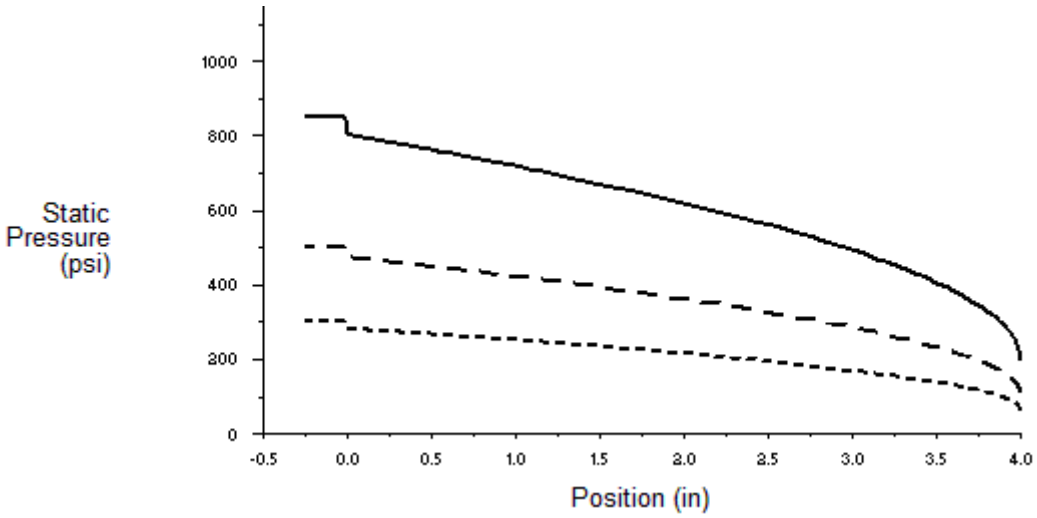

Figure B.6 The variation of centerline pressure as a function of x from the inlet of the converging section (point 0) to the tip of the nozzle (point 2). The solid line corresponds to P_0 = 5.86 MPa, the long-dashed line 3.45 MPa, and the short-dashed line 2.07 MPa.

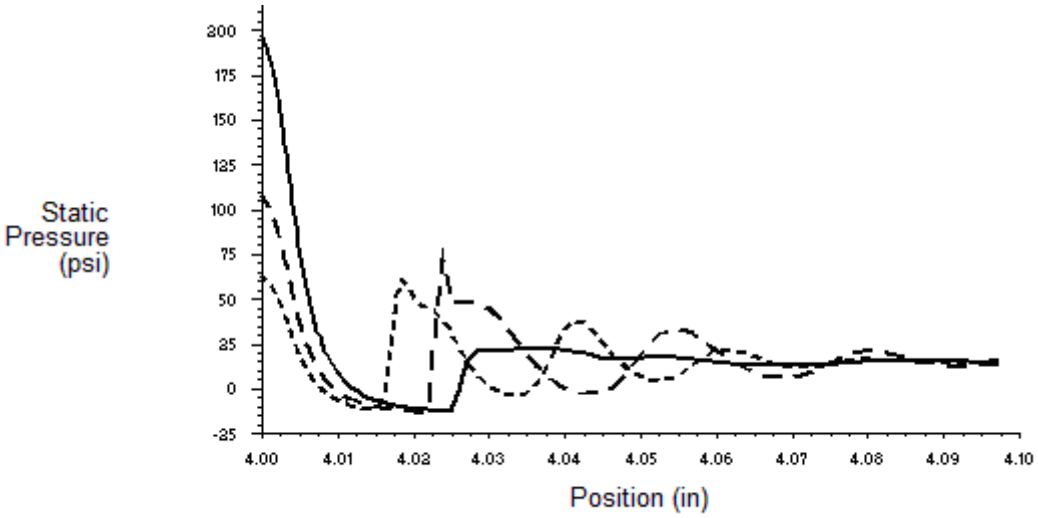

Figure B.7 The variation of centerline pressure as a function of x from the tip of the nozzle (point 2) into the tube. The solid line corresponds to P_0 = 5.86 MPa, the long-dashed line 3.45 MPa, and the short-dashed line 2.07 MPa.

Figure B.7 shows the variation of centerline pressure as a function of distance away from the tip of the nozzle. For P_0 = 5.86 MPa, there is an abrupt increase in pressure about 0.64 mm (0.025 inch) away from the tip of the nozzle that is associated to a Mach disc. As the pressure after the abrupt change is only slightly higher than the

atmospheric pressure 0.1 MPa, it is reasonable in the 1D model to assume $P_4 \approx P_5 = 0.1$ MPa. As the pressure drops (3.45 MPa then 2.07 MPa), the abrupt change moves closer to the nozzle. For the lowest pressure 1.03 MPa, the abrupt change became more gradual, and there were fluctuations in the pressure that extended to about 2 mm away from the nozzle – they are pulses that are typical of a freely expanding supersonic jet when the pressure of the jet is not very high[90-92].

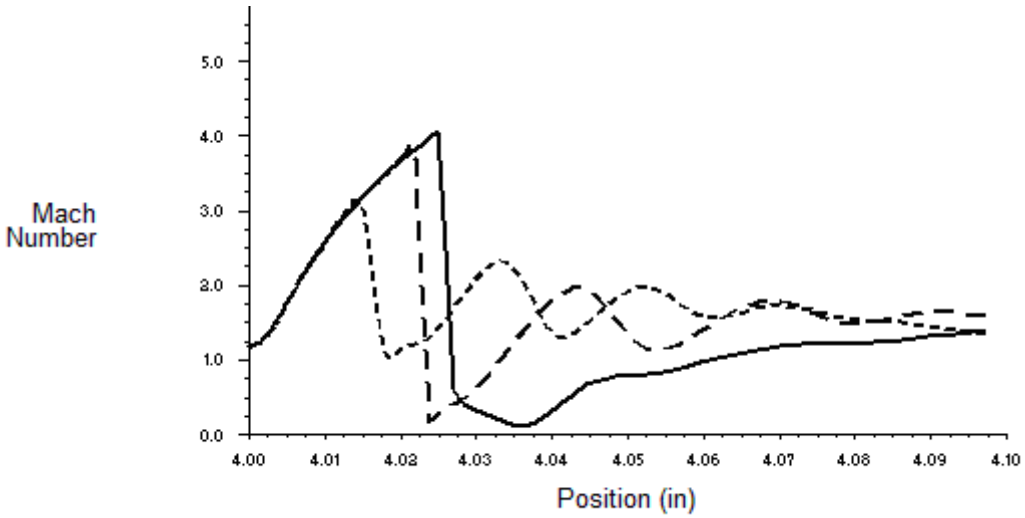

Figure B.8 The variation of centerline Mach number as a function of x from the tip of the nozzle (point 2) into the tube. The solid line corresponds to $P_0 = 5.86$ MPa, the long-dashed line 3.45 MPa, and the short-dashed line 2.07 MPa.

The presence of a Mach disc is also evident in Figure B.8 where the centerline Mach number as a function of distance is plotted. The Mach number for the highest pressure 5.86 MPa reached 5, which is higher than the prediction of eqs. (B.1)-(B.3). Again, at the lowest pressure, there were variations in the Mach number profile that suggest pulsating flow patterns.

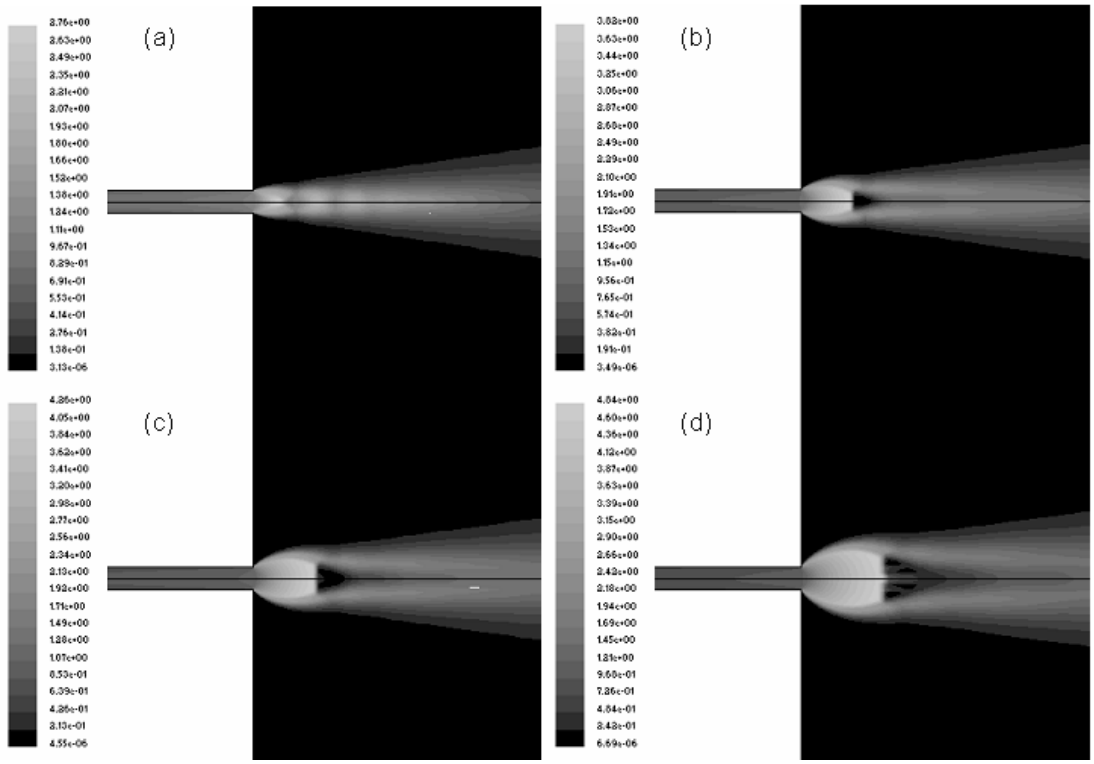

Figure B.9 Mach number distribution near the exit of the nozzle. From top to bottom: P_0 = 5.86 MPa, 3.45 MPa, and 2.07 MPa.

Figure B.9 contains three contour plots showing the Mach number distribution near the tip of the nozzle. It is clear that Mach discs were present at the three higher pressures P_0 = 5.86 MPa, 3.45 MPa, and 2.07 MPa. The size of the Mach disc decreases with decreasing pressure. As the inlet pressure was reduced to 1.03 MPa, the Mach disc disappeared and pulses started to form. Figure B.9 also shows that, in the free expansion, not all material will pass through the Mach disc.

B.5 Summary

The mechanisms through which a reduction in the size of the agglomerates occurs via the RESS/REHPS process were also analyzed using a one-dimensional compressible flow

model to predict the change in CO_2 properties in the nozzle, along with the use of empirical formulas to estimate the strength and position of the Mach disc in the free expansion region. The one-dimensional model used in this analysis is identical to that used by Weber and Thies[45,46], and is utilized for the purpose of understanding the mechanisms of agglomerate break-up. This analysis examined both the shear-induced break-up in the nozzle and the impact break-up at the Mach disc. While all of the agglomerates in the flow experience the break-up due to shear, it is estimated through 2D simulations of flow in the free jet that only about half would pass through the Mach disc. The results suggest that the shear flow in the nozzle and the subsequent impact of the agglomerates with the Mach disc in the free expansion can both lead to micron or sub-micron level deagglomeration. These results are supported by the experimental observations. Furthermore, sensitivity analysis based on this model revealed that the characteristic fragment size was robust, changing only modestly with operating conditions such as the mixing chamber pressure; thus, deagglomeration by RESS can indeed be achieved over a broad range of operating conditions.

As dry nanoparticles are invariably present as large fractal agglomerates that are tens or hundreds of microns in size, dry mixing of the individual nanoparticle constituents at the sub-micron scale is not easily achieved unless an effective deagglomeration step is included in the process. The RESS/REHPS process discussed in this paper achieves such fragmentation and is therefore of value in mixing nanoparticle agglomerates, which can subsequently be processed to make nanocomposites of superior properties than feasible otherwise.

APPENDIX C

APPLICATION OF NANO-MIXING VIA MULLITE FORMATION

C.1 Introduction

One of the benefits of producing high quality nanopowders mixtures is that they can significantly improve solid state reaction rates[27-29]. This is because the rate limiting step of this reaction is often the solid state diffusion of the reactant material through the reactant materials itself, the interface and or the product material. The effect of this limitation can be minimized by simultaneously decreasing the domain sizes of the reactant material and increasing the interfacial surface area, which can be achieved via nano-mixing[24]. This has been investigated here by mixing alumina and silica nanopowders together with a weight ratio of 72:28, using various mixing methods for the purpose of producing mullite. Mullite, a naturally occurring refractory material, which is valued for its high creep resistance at very high temperatures[93]. Because of its rarity it is often produced synthetically by reacting alumina and silica powders at temperatures greater than 1600^{o}C. It had previously been shown that the rate limiting step for mullite formation is the diffusion of Al^{3+} ions through mullite[94]. It should be noted that the mixing of alumina and silica nanopowders is not a common method of producing mullite, because it tends to form mullite too rapidly and ultimately prevents densification via viscous deformation due to its large creep resistance at high temperatures[95]. The experimental method employed in this study is solely a measure of mixing quality via the extent of reaction and not for material formation.

C.2 Experimental

Two different environmentally benign dry mixing methods were utilized to produce high quality nano-powder mixtures of alumina (Alu C, d_p = 13 nm) and silica (R972, d_p = 16 nm), supplied by Evonik Degussa. These methods include the Magnetically Assisted Impact Mixing (MAIM) and the Rapid Expansion of High Pressure and Supercritical Suspensions (REHPS).

The MAIM mixing method uses millimeter sized barium ferrite magnetic granules (supplied by Aveka) propelled by an oscillating magnetic field to promote mixing of the nanopowders as shown in Figure C.1. Mixing of the nanopowders occurs due to the collisions and rotational motions of the magnets and their interactions with the powders. 4.0 g of alumina and silica powders were loaded into a 240 mL glass vessel at mullite stoichiometry. The mixing quality of MAIM mixed powders can be tuned by varying both processing times and the magnet to sample weight ratio, where longer processing times and increased magnets improve mixing quality. Three different experimental conditions were investigated, each with significantly different expected mixing qualities, which are shown below in Table C.1. 2-pass REHPS mixtures were prepared at mullite stoichiometry using the same methodology described in the Chapter 3.

Table C.1 MAIM Operating Conditions for Producing Mixtures of Different Mixing Qualities

Experiment	Mag/Sample (g/g)	Time (min)
1	1 / 2	10
2	2 / 1	30
3	5 / 1	60

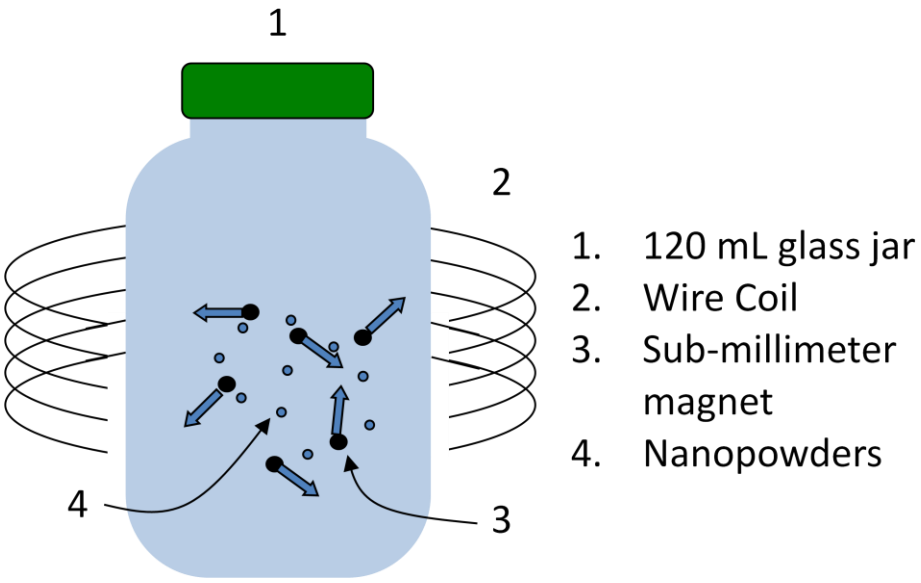

Figure C.1 Schematic of Magnetically Assisted Impact Mixing (MAIM) apparatus.

The intensity of segregation values of the MAIM and REHPS mixtures was determined using the same methodology as described in the REHPS mixing Chapter 3. The IOS values were then sintered at either 1400 or 1550^{o}C for 1 hour at a heating rate of 20^{o}C/min for the purpose of producing mullite. The sintered pellets were ground with a mortar and pestle and mixed with 40 mg of calcium fluoride (CaF_2), which was used as an internal standard. The degree of mullitization was determined via quantitative X-ray diffraction analysis using an X-ray Powder Diffractor (XRD, PW3040, Philips). This was achieved by comparing the ratio of the peak area for the mullite peak at 25.9 2θ to the CaF_2 peak at 47.0 2θ to a previously prepared calibration curve. The calibration curve was prepared by comparing the peak area ratio to the mass ratio of the mullite to CaF_2. The mullite used for the calibration curve was purchased from Sigma Aldrich. The calibration curve was prepared by mixing increasing amounts of mullite with 40 mg

of CaF_2 and comparing the ratio of the specified peak areas to the weight ratio and is shown in Figure C.2.

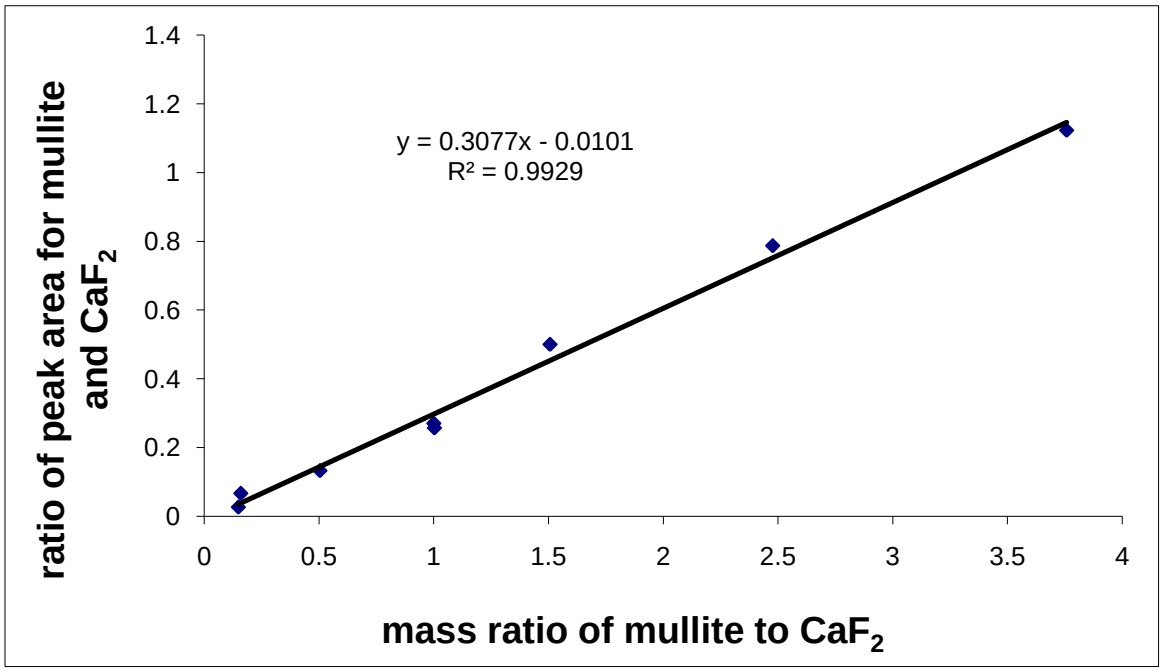

Figure C.2 Calibration curve to determine mullitization form XRD patterns. Mullitization is determined by comparing the mass ratio of mullite to CaF_2 to the peak area ratio of mullite to CaF_2.

C.3 Results

A typical XRD pattern of the mixed unsintered nano-powders is shown in Figure 5.3a. This pattern identifies an amorphous peak, which indicates the presence of the amorphous silica. It also identifies peaks that coincide with γ-phase alumina powder. The poor resolution of the pattern is indicative of nano-sized particles. Figure C.3b shows the XRD pattern of the mixed sintered nano powders.

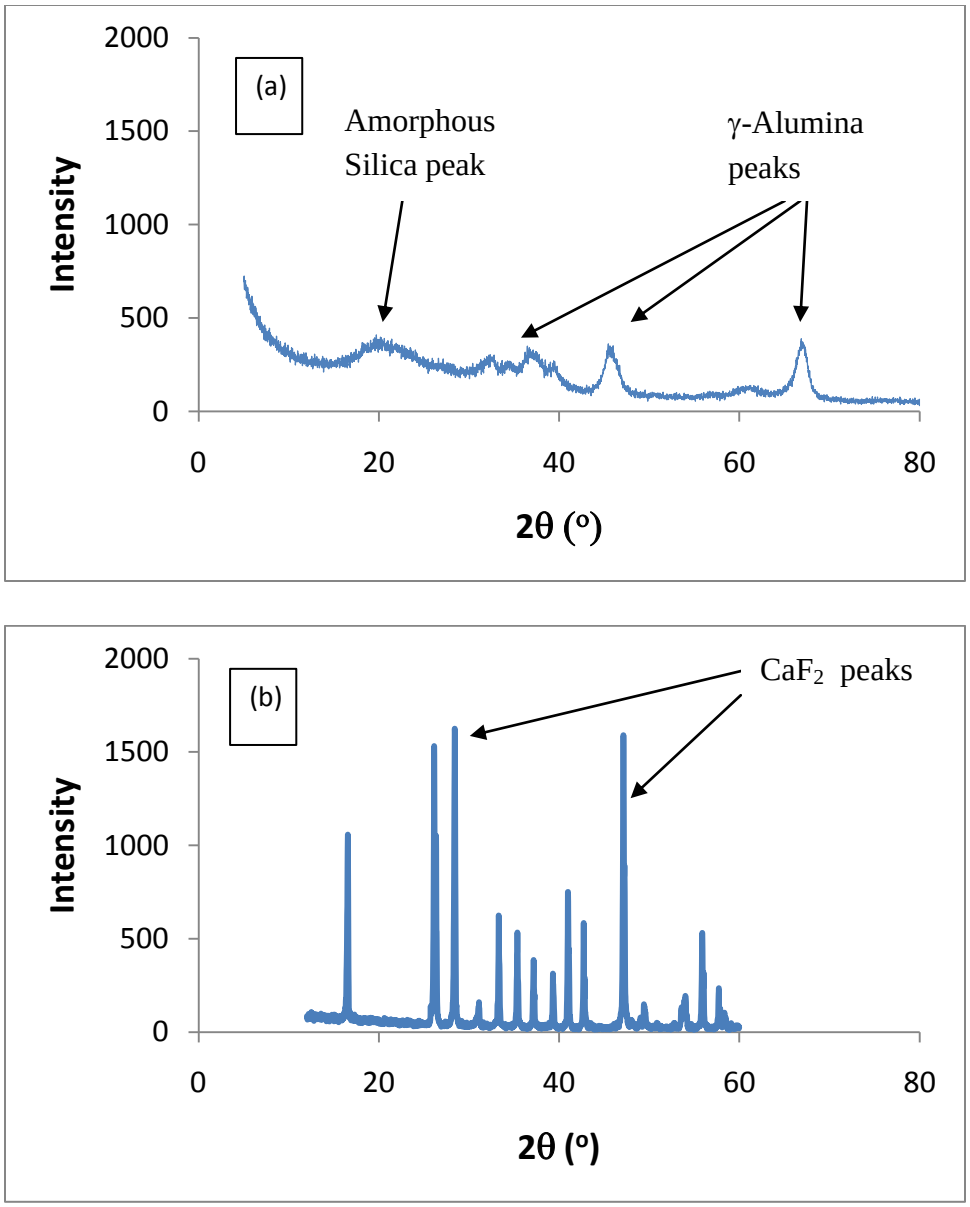

Figure C.3 XRD pattern of mixed alumina and silica powders (a) before sintering and (b) after sintering combined with CaF_2.

The extent of mullitization was then compared to the intensity of segregation for each of the 3 experiments in Figure C.4a, which shows that the extent of mullitization corresponds relatively well with mixing quality, as indicated by its slight logarithmic dependence of intensity of segregation. Some variability may be introduced due to the

low reproducibility in the intensity of segregation measurement for poor mixtures. This makes sense, as the intensity of segregation is believed to vary with a weak quadratic dependence on constituents' domain size. The 2-pass REHPS mixed powders expanded from 7.93 MPa showed comparable mullitization percentages to the REHPS method at values of 74.9 and 68.4%.

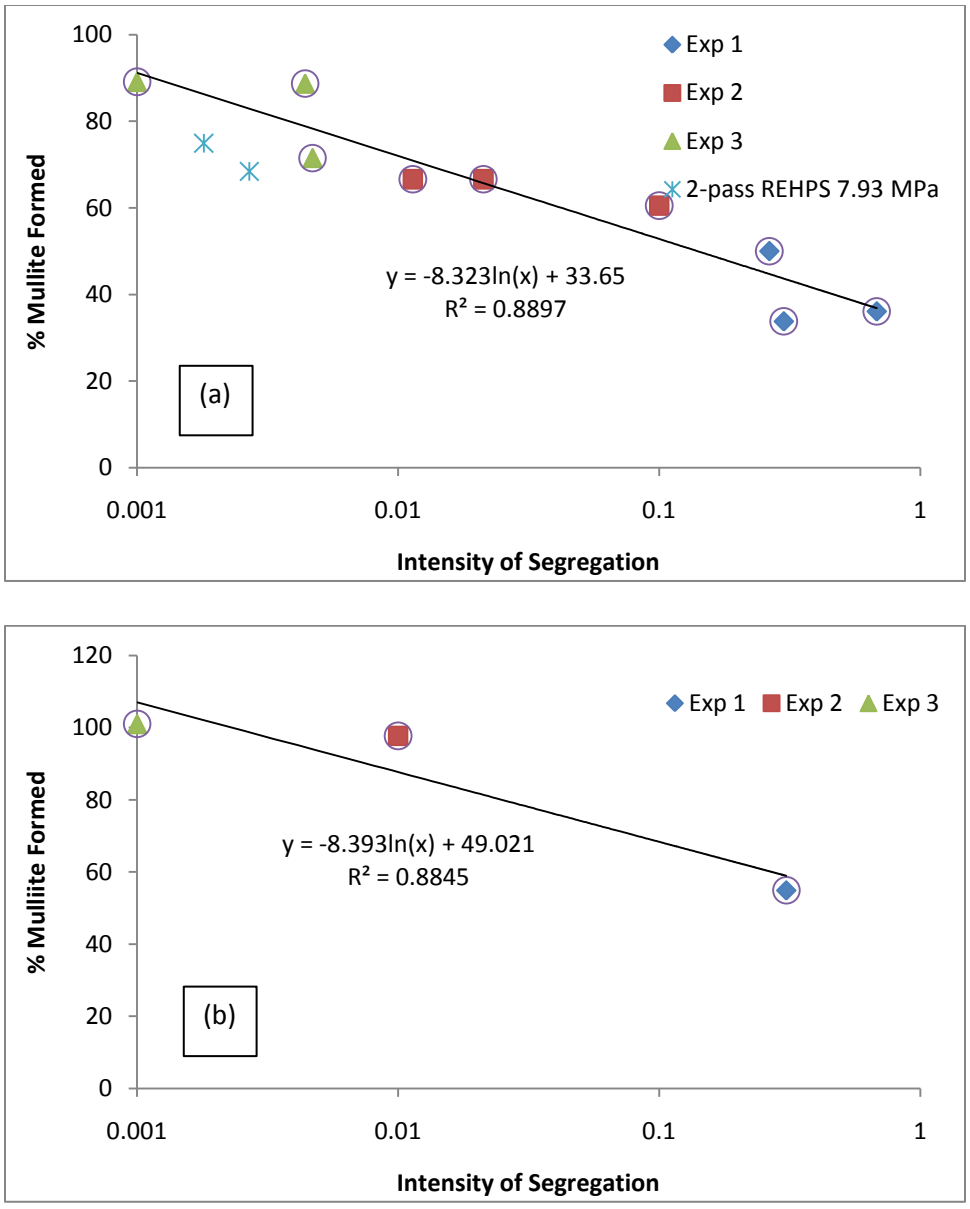

Figure C.4 Extent of mullitization with respect to intensity of segregation for MAIM and REHPS mixtures when sintered at (a) 1400°C for 1 hour and (b) 1550°C for 1 hour.

When fired at 1550^{o}C for 1 hour a similar general trend is observed, however at significantly increased extents of mullization. This agrees with the reaction mechanism proposed by Benzinger et al., as the diffusion rate of Al^{3+} through mullite follows an Arrhenius law dependent on temperature and increases by about 2 orders of magnitude at this elevated temperature[94, 96]. At the best mixing condition (Experiment 3) mullization reached 100%. At poorer mixing conditions the mullitization was still significantly increased over those sintered at 1400^{o}C.

C.4 Conclusions

Mixtures of alumina and silica nanopowders were prepared by Magnetically Assisted Impact Mixing (MAIM) and the Rapid Expansion of High Pressure and Supercritical Suspensions (REHPS). These mixtures were reacted at high temperatures to form mullite. It was shown that percentage of mullite formed significantly increased with increasing mixing quality or decreasing intensity of segregation due to the higher interfacial surface area.

APPENDIX D

STIRRING IN SUPERCRITICAL FLUIDS

D.1 Introduction

Mixing of nanoparticles is primarily performed in liquid solvents and surfactants, which are often capable of imparting the necessary forces to break up and stabilize agglomerated structures. The solvents, however, can be hazardous to the environment and require costly and time consuming post processing steps to remove. Additionally, the removal process can lead to density and electrostatic based segregation and caking. Supercritical fluids like supercritical CO_2 offer a unique opportunity because they can exhibit both liquid-like and gas-like properties at moderate temperatures, which can be tuned simply by adjusting the pressure. Specifically the liquid-like density and viscosity can transfer the necessary shearing forces to break up agglomerates. The gas-like nature allows it to be removed from the mixture simply by releasing the pressure without the potential segregation or drying issues mentioned above. It has been shown that supercritical fluids can replace organic solvents as an environmentally benign mixing medium[16, 17, 35, 55]. One example is the Rapid Expansion of High Pressure and Supercritical Suspension (REHPS, discussed in detail in Chapters 2-4), where a nanopowder suspension is expanded through capillary nozzle on the order of 100 microns to simultaneously break the nanoparticle agglomerates and achieve intimate mixing of two or more constituents[16, 17, 35]. It has been suggested that this technique takes advantage of the highly tunable nature of supercritical fluids by applying intense shearing forces inside the nozzle (see Chapter 4). It should be mentioned that this technique

requires deagglomeration and mixing to be simultaneous; a poor pre-mixing condition may introduce different constituents into the deagglomeration zone at different times and therefore not meet that criteria. Therefore a method to produce high quality premixes is required.

In the stirring process agglomerates are broken by shear introduced by the stirring actions. The fragments are then mixed via three mixing mechanisms: convective, shear and diffusive mixing. Convective mixing is controlled by mechanical movement, such as physical interaction with the impeller. Shear mixing is controlled by interactions with shear forces produced by the agitation of a fluid medium by the impellers stirring actions. Diffusive mixing is controlled by random exchanges of particles between the different constituents at their interfaces[97, 98]. In general both convective and shear type mixing can be characterized by the scale of segregation, as large scale inhomogeneities (segregations) are expected. Diffusive mixing is typically described by the intensity of segregation, because it describes small scale concentration deviations.

High pressure and supercritical carbon dioxide was investigated as an environmentally benign medium for the mixing of nanopowders via stirring. It will be shown that stirring in high density carbon dioxide (i.e. liquid and liquid-like conditions) is capable of producing mixtures comparable to those produced in more conventional solvents.

D.2. Experimental

D.2.1 Materials and Equipment

Alumina (Alu C, d_p = 13 nm) and hydrophobically coated silica (R972, d_p = 16 nm), provided by Evonik Degussa GmbH (Germany) were stirred in atmospheric air, high pressure carbon dioxide (99.9% pure), acetone (99.5%) or hexane (99.5%), in a 300-mL high pressure stirred vessel. A 4-blade flat blade impeller, with a width to diameter ratio of 1/3.5 was used. The pressure was controlled by a liquid CO_2 Thar pump (model 350, USA). Materials were used as received without any further modification or purification.

D.2.2 Experimental Set-up and Procedure

An equal weight mixture (1:1 weight ratio, 3-g total) of alumina and silica were stirred in a 300-mL high pressure vessel in high pressure or supercritical carbon dioxide and is shown schematically in Figure D.1. The mixture was stirred with a 4-blade flat blade impeller with a blade width of 1cm and a total width of 3.5 cm. The suspension was stirred at a rotation speed of 2000 RPM for mixing times up to 80 min.

The operating pressure and temperature of the high pressure vessel remained constant for the duration of the stirring experiment. The pressure of the CO_2 was maintained using a Thar liquid CO_2 pump. Upon leaving the pump the CO_2 was heated in a stainless steel heat exchange coil immersed in a hot water bath, which was in thermal equilibrium with the stirred vessel. The operating pressure ranged from 2.72 – 14.63 MPa and the temperature ranged from 20 – 45^{o}C. These conditions include the gas, liquid and supercritical phases. To compare this process to a more typical nano-mixing

experiment the nanopowders were also mixed in air, acetone or hexane at ambient conditions. Once the experiment was completed the vessel was slowly depressurized through an expansion valve and the mixture was removed for characterization. When acetone or hexane was used the solvent was filtered through an 11-μm paper filter and then dried.

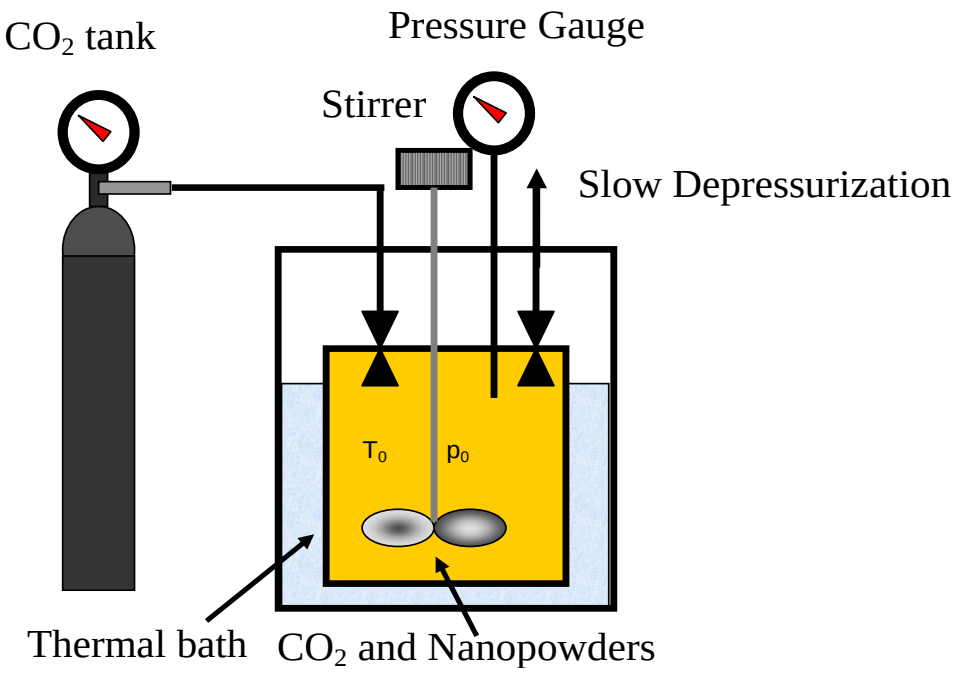

Figure D.1 Schematic of stirring apparatus used to mix nanopowders.

D.2.3 Characterization of Mixed Powders

The powder mixtures prepared by stirring and REHPS were uni-axially pressed into a 13-mm tablet at 600 MPa and characterized using a Field Emission Scanning Electron Microscope (FESEM) (LEO 1530VP FE-SEM) and Energy Dispersive X-ray Spectroscopy (EDS). SEM in conjunction with EDS is capable of quantifying the elemental composition of sample areas on the micro-scale.

SOS values were experimentally determined by evaluating the elemental concentrations with respect to spatial locations utilizing EDS analysis. EDS scans of 750 x 400 μm^2 sites on the tablet surface were producing using a magnification of 500x. EDS scans were also produced at a higher magnification of 5000x, representing an area of 75 x 40 μm^2. Brightness values in the map were considered to be proportional to the concentration. The brightness values were used to calculate $R(r)$ and *SOS* that were described in Chapter 3.2. A minimum of 3 pellets were analyzed from each powder mixture in this way, and the *SOS* values were averaged. For a detailed description of the SOS and its determination please refer to To et al. (Ref: mixing paper). Intensity of segregation is typically offers limited mixing quality information for mixtures with large scale inhomogeneities due to the lack of spatial information in the measurement. As a result the intensity of segregation was not considered in this study.

D.3. Results and Discussion

Mixtures of alumina and silica nanopowders were prepared in a stirred vessel in a high pressure CO_2 environment. Experiments were performed by varying two major parameters, namely the mixing time, and mixing fluid.

The mixing quality of alumina and silica nanopowders afforded by the stirring process in different fluids was characterized by the scale of segregation and is listed in Table D.1. The temperature, pressure (gauge pressure with respect to the atmosphere, i.e. atmospheric pressure is 0 MPa) and phase of the fluid are also listed in Table D.1. It can be seen that the scale of segregation values of the nanopowders stirred in air at atmospheric conditions are all greater than 9, indicating that this stirring condition is

incapable of sufficiently mixing the agglomerates. Additionally, the scale of segregation does not decrease with stirring time, suggesting that further breakage or mixing of the nano-particle agglomerates is unlikely at these conditions.

Table D.1 Scale of Segregation of Nanopowder Mixtures Prepared in Different Solvents and at Different Mixing Times Measured at a Magnification of 500x

	Mixing Fluid				
	Air	CO2		Organic Solvent	
				Acetone	Hexane
Time (min)	0 MPa 25°C Gas	14.8 MPa 35°C SCF	9.7 MPa 20°C Liquid	0 MPa 25°C Liquid	0 MPa 25°C Liquid
5	9.4 ± 5.7	8.5 ± 3.6	--	8.0 ± 4.7	--
20	9.9 ± 6.7	8.1 ± 0.7	--	6.4 ± 3.0	--
40	16.1 ± 3.2	4.8 ± 0.9	6.0 ±2.4	5.5 ± 2.2	4.9 ± 1.0
80	9.3 ± 2.2	--	--	--	--
Density (kg/m^3)	1.2	812	853	793	655

Upon comparing the SOS values of the nanopowders stirred in air to those stirred in the other solvents (CO_2 or organic solvents); a considerable improvement in mixing quality can be observed when other solvents are used. In the case of stirring in acetone or supercritical carbon dioxide (P= 14.8 MPa, T=35°C), a general trend of improving mixing quality can be observed with increasing mixing time as shown by the decreasing scale of segregation. It can also be seen that the site-to-site variability decreases with increasing stirring times. This indicates that stirring in a dense fluid is capable of imparting sufficient shear to break up the agglomerates and enhance mixing quality.

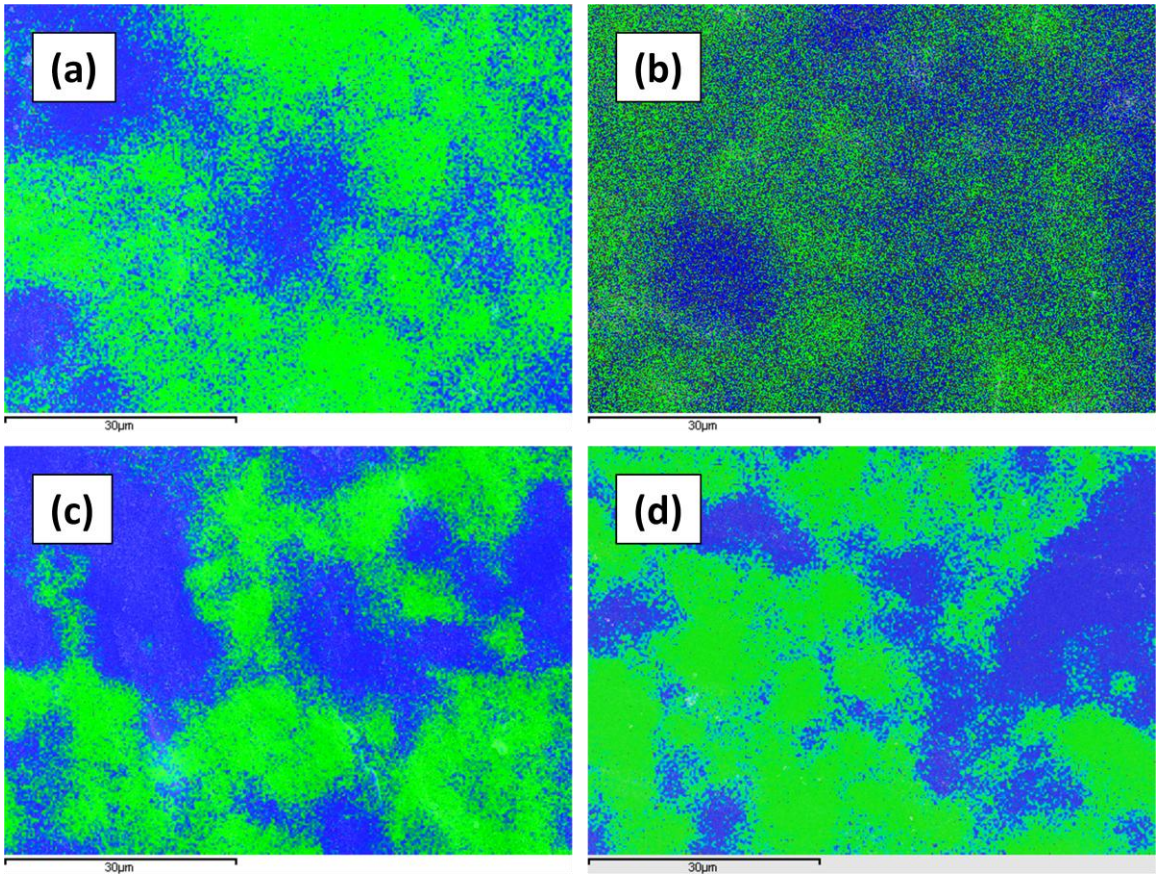

Figure D.2 Overlaid EDS elemental maps of alumina (green) and silica (blue) mixtures stirring in (a) liquid CO_2, (b) supercritical CO_2, (c) acetone and (d) hexane at 2000 RPM for 40 minutes

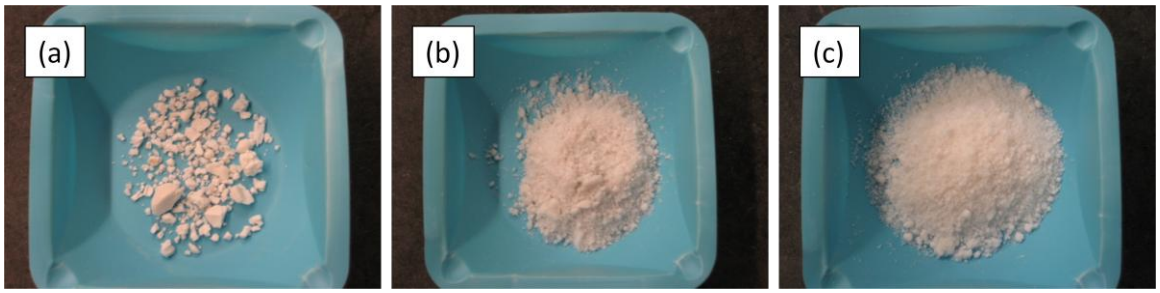

Figure D.3 0.5g of dried nanopowders after stirring in (a) hexane, (b) supercritical CO_2 and (c) liquid CO_2

The mixing qualities of the nanopowders stirred in each of the dense solvents for 40 minutes are similar, as shown by SOS values listed in Table D.1. This finding is

supported by the typical EDS scans (measured at 5000x) shown in Figure D.2, which depicts comparable coarse scale mixtures of alumina (green) and silica (blue) nanopowders. One notable difference between processing in carbon dioxide as opposed to the more traditional organic solvents is the requirement of filtration and drying to remove the organic solvents and ultimately results in powder caking. The effect of the powder caking can be seen in Figure D.3, where 0.5 g of the dry sample after stirring in hexane, supercritical CO_2 and liquid CO_2 is depicted. It can be seen that powders stirred in hexane, which required filtration and drying, led to significant caking of the nanopowders and significant reduction in the powder porosity. When carbon dioxide (supercritical or liquid) was used the powders retain their high porosity, without sacrificing the mixing quality.

D.4 Conclusions

Mixtures of alumina and silica powders were prepared by stirring in air, carbon dioxide, acetone or hexane. It was shown that stirring in CO_2 yielded similar mixing qualities, however did not result in the caking that was observed to occur when the organic solvents were removed.